Study on Physical Properties and Its Application Relating to the Band Gap Generation in Bilayer Graphene with Ionic Liquid

A dissertation submitted to

THE GRADUATE SCHOOL OF ENGINEERING SCIENCE

OSAKA UNIVERSITY

in partial fulfillment of the requirements for the degree of

DOCTOR OF PHILOSOPHY IN ENGINEERING

BY

YUSUKE YAMASHIRO

MARCH 2014

Abstract

A band gap was created in bilayer graphene field-effect transistor (FET) by using ionic liquid gate structure. The band gap in bilayer graphene is attractive object of research for both a material physics and an application because a size of the band gap can be controlled by applying an electric field in FETs. Purposes of the present study are investigation of physical properties relating to band gap generation in bilayer graphene with ionic liquid and its application to transistors. The electrical measurements of ionic liquid gated FET shows that an increase in the resistance of the bilayer graphene was clearly observed as the magnitude of the electric-field intensity was increased, owing to the creation of the band gap. Measurements of temperature dependence of channel conductance derived a band gap of 235 meV was created in bilayer graphene.

Electronic states and phonon energies in the bilayer graphene were investigated by electrical and optical measurements under an external electric field applied by using bottom and ionic liquid gates. Although top gate insulator and electrode in conventional structure prevent optical investigation, the transparent ionic liquid gate makes possible the optical measurements under an external electric field. Moreover, the potential of graphene is controllable in wide gate range owing to high electrical strength of the ionic liquid. In Raman spectra, symmetric and antisymmetric optical phonons were observed in the Raman scattering spectra. Their behaviors as a function of electric field was explained by a Kohn anomaly. The mixing of symmetric and antisymmetric optical phonons was reduced by the external electric field, owing to the enhancement of electron-phonon interactions that accompanied the band gap opening.

Continuously, experiments for practical use of ionic liquid gated graphene FETs are investigated. The transfer characteristics of the G-FETs revealed that the transconductance when using the ionic-liquid gate was significantly higher than that when using the back gate, because an electrical double layer formed in the ionic liquid with 200-fold the capacitance of a 300-nm-thick SiO_2 layer. The result indicates that the ionic-liquid-gate structure enables application of an effective electric field. Moreover, floating-bridge structures of graphene with ionic-liquid gate was fabricated to improve mobility and on/off ratio. After removing the SiO_2 layer under the graphene channel and introduction of ionic liquid, the ionic liquid under the suspended-graphene channel contacts with an exposed back-gate electrode, resulting in formation of the floating-bridge structures. Owing to elimination of the interaction with SiO_2 layers and the electrical double layer in the ionic liquid, the floating-bridge bilayer graphene devices have the on/off ratio of 20 in a conductance when the back-gate voltage of only 2 V was applied.

Chapter 1 General Introduction

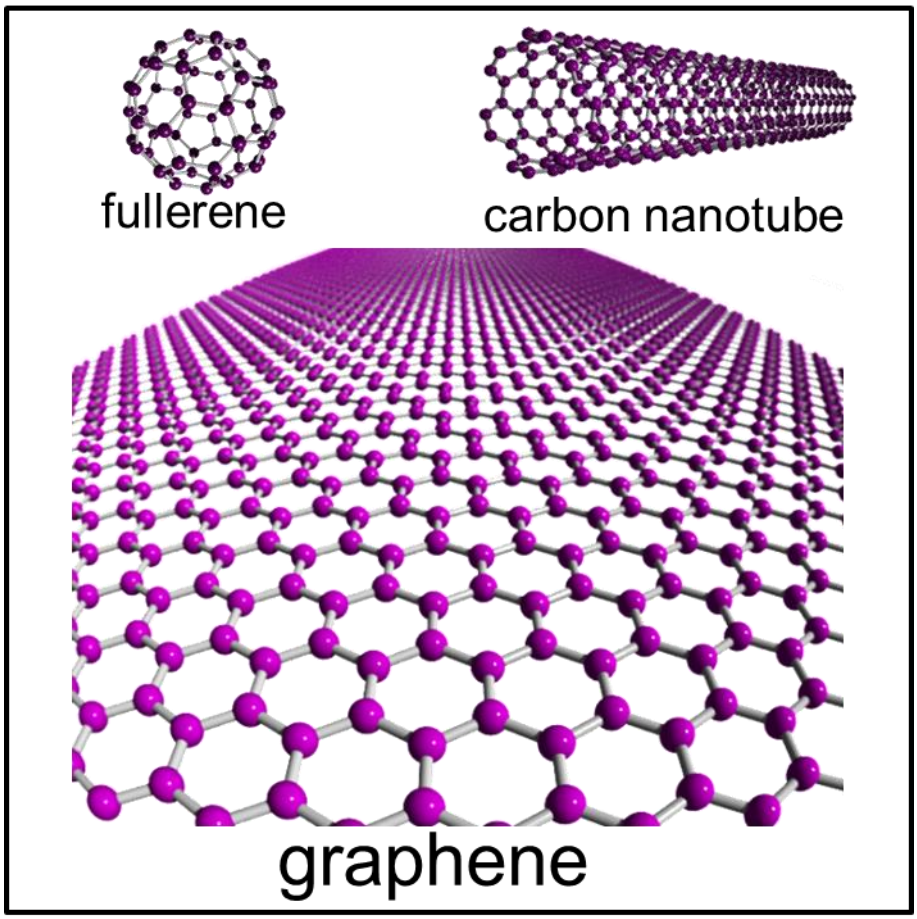

1.1 Introduction

In this chapter, a background and a purpose of present thesis concerning graphene field-effect transistor will be described.

1.2 Graphene

1.2.1 Attractive properties of graphene

Graphene, two-dimensional sheet consisted of only carbon atoms, was reported and opened its easy fabrication process in 2004 by Andre Geim and Konstantin Novoselov. It is assumed that such an ideal two-dimensional material with a one atom thickness

sheet is impossible to exist. Thus, graphene had not been discovered and studied, although graphite, CNT and fullerene are well investigated in experimental for a long time. The easy method to prepare graphene results that many investigations were tried in experimental by researchers around the world.

Excellent properties such as massless charge carriers make graphene one of the most intriguing targets of study in material physics.[1)] Graphene is also expected to find use as a building block in next-generation electronics such as field-effect transistors[2-3)] high-frequency electronics[4-5)], transparent electrodes[6-7)], and high-sensitivity sensors[8-10)] because of its mechanical strength, chemically stability, and extraordinary high mobility[11-13)] (shown in Fig.1-1). In particular, it is attractive that the mobility reached 20,000 cm^2/Vs, which is approximately 100-fold that of Si. Because the miniaturization of Si LSI is close to the limitation, graphene attracts increasing attention as a new material to improve LSI performance.

The highly successful progress of CMOS-based LSI technology has been achieved for many years by miniaturizing the process rule. The miniaturization of process rule and, at the same time, lowering the operation voltage of the transistors made it possible to integrate a larger number of transistors in LSI and to make operation of LSI faster without increasing power consumption (“Scaling Law”). The Scaling Law led a tremendous progress in Si LSI technology; the number of transistors in LSI has grown 100,000 times larger, and the operation speed has increased 30,000 times in thirty years from the early 1970s. As a result, research on compound semiconductors which were expected to replace Si has not been performed intensively as expected at the beginning. However, the scaling down of the process rule of Si LSI is now thought to have come close to its limits. Therefore utilization of materials, such as CNT or graphene which exhibits much higher mobility than Si, has attracted attention as a key to improve LSI performance without scaling down the process rule.

Thickness		one atom
Mechanical strength	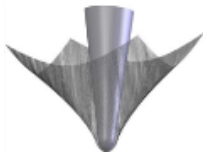	more than diamond
Mobility	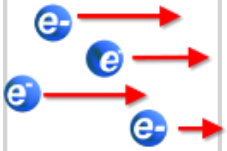	200,000 [cm^2/Vs] 100−fold of Si

Figure 1-1. Attractive properties of graphene for an application.

1.2.2 Electronic band structure

Graphene has a honeycomb-like structure consisted with carbon atoms. Primitive translation vectors ($\boldsymbol{a}_1$, $\boldsymbol{a}_2$) shape unit-cell parallelogram in which two carbon atoms exist. Tentatively, they are labeled as A-site and B-site atoms. Each atom respectively consist triangle lattice and they make an angle of 180º, resulting structure of graphene (Fig.1-2). One A-site atoms forms three sp^3 hybrid orbits and are linked to three B-site atoms by a strong σ bond. Because the strong σ bond splits the energies of sp^3 orbits into very high or deep, energy dispersion near the charge point of graphene is not mainly determined by the sp^3 orbit but p_z orbit. Around charge neutrality point, a wave function of π band, which is almost consisted with p_z orbit, can be described by

$$\psi_{\boldsymbol{k}}(\mathbf{r}) = \frac{1}{\sqrt{N}}\sum_{l}\Big[e^{-i\boldsymbol{k}\cdot\boldsymbol{R}_l}C_1(\boldsymbol{k})\varphi_{2pz}(\boldsymbol{r}-\boldsymbol{R}_l) + e^{-i\boldsymbol{k}\cdot(\boldsymbol{R}_l-\boldsymbol{u})}C_2(\boldsymbol{k})\varphi_{2pz}(\boldsymbol{r}-\boldsymbol{R}_l-\boldsymbol{u})\Big] \tag{1.1}$$

where, $\boldsymbol{u}$ is a vector between A-site and B-site atom. $\boldsymbol{R}_l$ is a position of l-th atom.

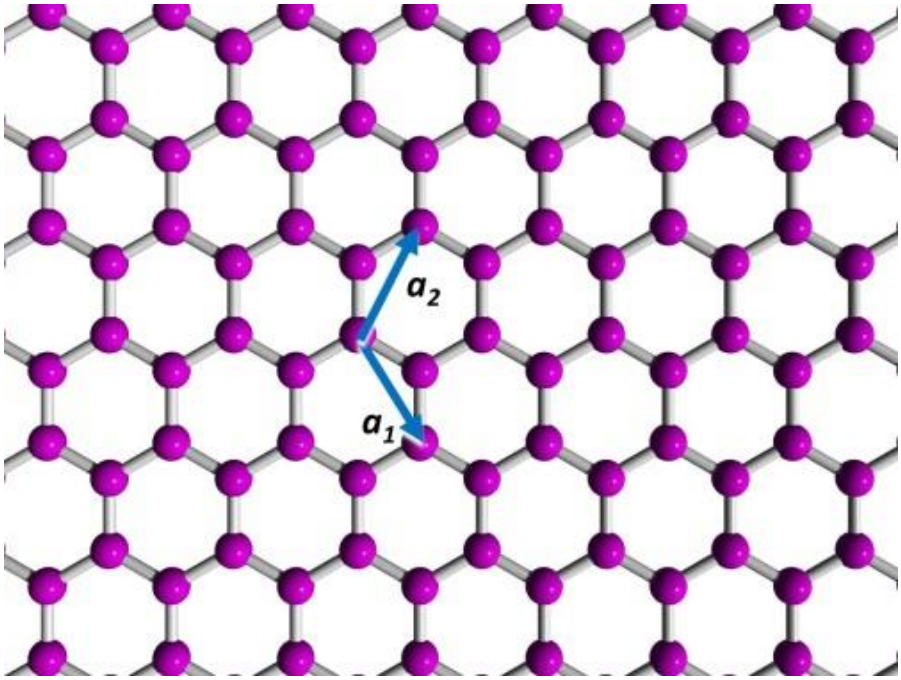

Figure 1-2. Crystal structure of graphene and its primitive translation vectors.

Tight binding approximation well describe the state and derive the coefficients $C_1(\boldsymbol{k})$ and $C_2(\boldsymbol{k})$, and the Eigen energy ε.

$$\begin{pmatrix} \varepsilon_0 & tf(\boldsymbol{k}) \\ tf^*(\boldsymbol{k}) & \varepsilon_0 \end{pmatrix} \begin{pmatrix} C_1(\boldsymbol{k}) \\ C_2(\boldsymbol{k}) \end{pmatrix} = \varepsilon \begin{pmatrix} C_1(\boldsymbol{k}) \\ C_2(\boldsymbol{k}) \end{pmatrix}$$

$$\varepsilon_{\pm}(\boldsymbol{k}) = \varepsilon_0 \pm w(\boldsymbol{k})t \tag{1.2}$$

where ε_0 is an eigenenergy of φ_{2pz}, t is transition energy.

$$f(\boldsymbol{k}) = e^{-i\boldsymbol{k}\cdot\boldsymbol{u}} + e^{-i\boldsymbol{k}\cdot(\boldsymbol{u}-\boldsymbol{a_1})} + e^{-i\boldsymbol{k}\cdot(\boldsymbol{u}-\boldsymbol{a_1}-\boldsymbol{a_2})}$$

$$w(\boldsymbol{k}) \equiv |f(\boldsymbol{k})|$$

$$= \sqrt{3 + 2\cos(2\pi\boldsymbol{k}\cdot\boldsymbol{a_1}) + 2\cos(2\pi\boldsymbol{k}\cdot\boldsymbol{a_2}) + 2\cos[2\pi\boldsymbol{k}(\boldsymbol{a_1}+\boldsymbol{a_2})]} \tag{1.3}$$

In Eq. (1.2), $\varepsilon_{\pm}$ indicates energy levels of conduction and valence bands, respectively.

Figure 1-3 shows visualized energy dispersion of mono layer graphene, corresponding to Eq. (1.2). The band structure is similar to that of typical semiconductors, however, graphene has no gap between valence and conduction band as graphene is called zero gap semiconductor. In addition, the valence and conduction bands are shaped of cones contacted each other at one point. The one-point contact and liner dispersion are same with a dispersion predicted in Dirac particle. That is why, the electronic band structure and the contact point are called Dirac cone and Dirac point, respectively. Carriers near the Dirac point in mono layer graphene acts as Dirac particle due to the band structure. On the other hand, bilayer graphene doesn't have the liner dispersion but quadratic function dispersion contacted with one point. In bilayer graphene, author calls the no longer Dirac point as "charge neutrality point". Carriers are not like Dirac particle. Band gaps don't exist in both monolayer and bilayer (and multilayer) graphene. The symmetric between A-site and B-site atoms are caused by the no band gap in mono layer graphene. Bilayer graphene has the symmetric atoms between upper layer atom and lower layer atom, resulting zero band gap.

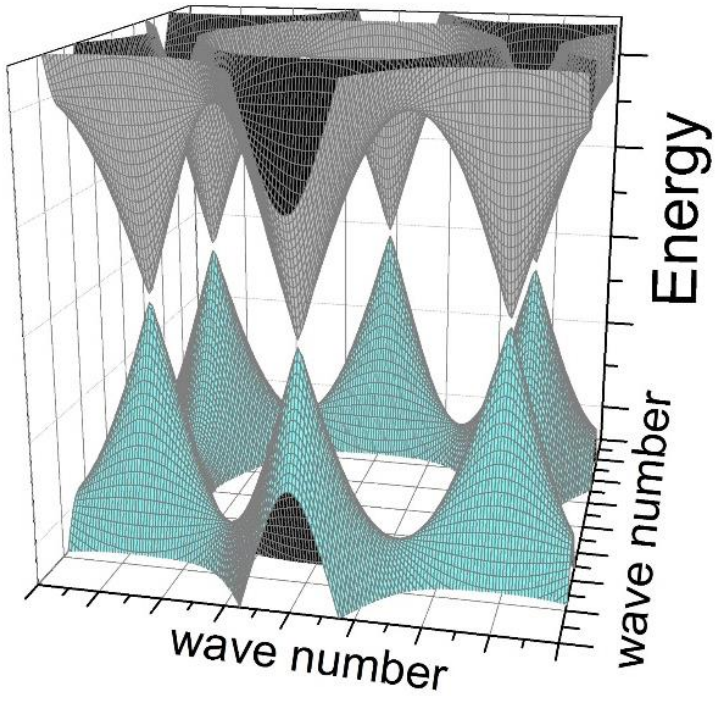

Figure 1-3. Electrical band structure of monolayer graphene. Kohn-shaped valence band and conduction band are contacted at Dirac point.

1.2.3 Unique features in the transport property

1. Anomalous quantum Hall effect

In general quantum Hall Effect, a conductivity σ is expressed in

$$\sigma = -ne^2/h. \qquad (1.4)$$

Where *n*, *e* and *h* are an integer value, elementary charge and Planck's constant, respectively.

However, in mono layer graphene, the quantum Hall Effect is expressed in

$$\sigma = 4(n + 1/2)\frac{e^2}{h}. \qquad (1.5)$$

The coefficient of 4 is obtained for the product of the orbit- and spin- number. Unlike normal metals, the conductivity is shifted 1/2 from integer value. The shift arises due to the zero effective carrier mass near the Dirac points.

Bilayer graphene also shows the quantum Hall effect described by different equation.

$$\sigma = 4n\frac{e^2}{h} \quad (n \neq 0) \qquad (1.6)$$

2. Minimum conductivity

As previously mentioned, the density state of graphene become zero at Dirac point. Simple notion expect that conductivity become zero when the potential is adjusted to coincide with the Dirac point. The resistance of graphene become the most high at the Dirac point, however, the resistance remains a conductivity of ~$4e^2/h$.

The cause of the minimum conductivity seems to be carrier doping from environmental, for example substrate, water and oxygen molecular, however, it is not entirely clear.

1.2.4 Method of preparing graphene sample

There are several methods to prepare graphene. High crystal quality, large size, low cost, and suitable to Si are needed for practical use. Famous methods are shown in Fig. 1-4.

1. Mechanical exfoliation

Mechanically exfoliating graphene from graphite with an adhesive tape is very simply method to obtain high quality graphene. Graphene size, amount, and quality are affected with the type of bulk graphite as source of graphene. Author prefer to use Kish graphite because larger graphene are obtained than HOPG and Natural graphite. Despite its primitive method, mechanical exfoliated graphene has the highest quality of all methods. The high quality and simple process are attractive for researcher in material physics. Thus most measurements of graphene in material physics have been prepared by the mechanical exfoliation method. One of disadvantages are that the graphene size is less than 20 micro meter. At least 100 mm are needed for practical use. Additionally, the position on the substrate, shape of graphene, and the number of graphene are random. The process with random never realize high-volume production.

2. CVD growth with catalyst

Catalyst metal (Ni, Cu) which deposited on a substrate grows graphene layers in hydrocarbon gas at high temperature. The method is called Chemical Vapor Deposition (CVD) method. The size and position of graphene accompanies to that of catalyst metal which can be controled. Resent years, a crystal quality of the CVD graphene become as high as that of Mechanical exfoliated graphene. However, transfer process from catalyst metal to Si/SiO_2 substrate generates defects and decreases the quality of graphene.

3. Epitaxial growth on silicon carbide (SiC)

Annealing of SiC substrate in vacuum takes Si atoms away. Then remained carbon atoms construct graphene. The epitaxial growth can also prepare large-scale graphene. A difficulty of transfer from SiC to other substrate is a challenge in this method.

4. Reduced Graphene Oxide (rGO)

Graphene oxide can be elaborated in large amounts from bulk graphite. Although graphene oxide is not conductor, reduced graphene oxide (rGO) has similar electrical characteristics to graphene. Its carrier mobility is not extremely high because of defects, oxidation, and inhomogeneous construction of layer.

5. Growth using amorphous carbon source

Graphene can be synthesized from amorphous carbon instead of the hydrocarbon gas source. After deposition of amorphous carbon and catalyst, graphene are synthesized at

high temperature. The synthesis without gas flow process makes equipment simple.

6. Other method

Several methods to prepare graphene are suggested. For example, a growth of mechanical exfoliated graphene flake, unzipping of carbon nanotube and so on.

method / properties	Mechanical exfoliation	rGO	SiC	CVD
size	×	◎	○	◎
mobility	◎	×	○	○
for application	×	○	△	◎
image			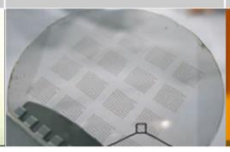	

Figure 1-4. Comparative table of methods to prepare graphene.

1.2.5 Identification of the number of layers

Electrical and optical characteristics strongly depend on the number of graphene layers because of interlayer interaction. That is why, we should determine the number of layer at the start of fabrication process of graphene FETs and discussions. If we accustom to make graphene, identification of the layer number is easy by only looking at optical image. However, more quantitative methods will be introduced.

1. Raman spectrometric method

The number of layer composing graphene is easily distinguished with Raman spectra if the number is one, two or three. Raman spectrum of graphene shows G' (2D) peak at ~2500 cm^{-1}. In monolayer graphene, the shape of G' is single sharp peak. Bilayer graphene has shoulder peak consisted by four peaks. Trilayer graphene also consisted by several peaks but is not observed the shoulder. The G' shapes of monolayer and trilayer graphene are similar, however, the division between mono and trilayer is easy by compare their intensity ratio of G'/G. Because its intensity ratio of G'/G become small as the layer number increases.

2. Contrast differences of optical images

Graphene on Si/SiO_2 substrate is visible although one atom thickness. To identify accurate number, only a green component of RGB image of graphene are used. Because transparency of graphene is ~97.7 percent, the contrast of graphene decrease ~5 percent from SiO_2 region per one layer. The differences of contrast can determine the number of layer.

3. Atomic force microscopy (AFM)

AFM has high resolution along with vertical axis. The layer number of graphene can be estimated by measurement of the thickness. However, the thickness obtained by AFM is thicker than the thickness of 0.3 nm which is true thickness of graphene. The thicker value may be caused by adhesive on the substrate.

1.3 Devices with use of graphene

As described on previous section, bare graphene is not switched off due to zero gap band structure. This section introduces devices of graphene without the band gap.

1.3.1 Graphene FET

Figure 1-5(a) shows schematic of graphene FET and its experimental setup.

Basically graphene and electrodes are ohmic connection. Thus, the drain current is controlled by only the change of density state of graphene unlike schottky transistors. Figure 1-5(b) shows V_g versus I_d and band structures at each V_g. When Fermi level coincide to Dirac point, the density state become the smallest. When the positive (negative) gate voltage are applied, Fermi level rise (dip) and increase the density state, resulting to current enhancement. Graphene has enough high transconductance and on current. However, off current is not completely suppressed due to zero-gap between valence and conduction bands as shown in Fig.1-6(a). Although, a large on/off ratio of electrical currents is essential to operate digital devices, the ratio of graphene is ~5 on Si/SiO_2 substrate. Band gap generation in graphene is a critical challenge for fabricating high on/off ratio devices.

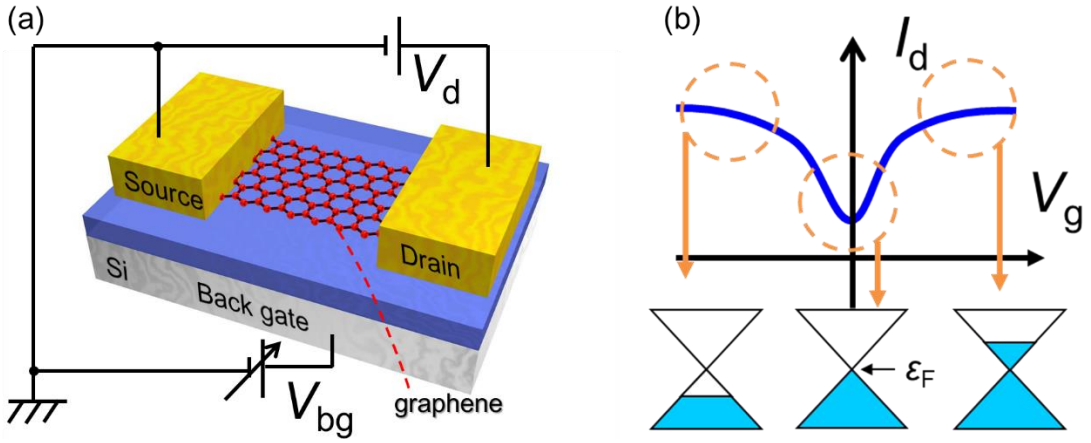

Figure 1-5. (a) Schematic of graphene FET and experimental set up. (b) Illustration of drain current and band structure which depends on gate voltage in graphene.

1.3.2 Graphene sensor

The low on/off ratio is large handicap for logic circuits and memory devices, however, sensor devices needs not very important the high on/off ratio but high transconductance for high sensitivity. Many researchers study graphene for gas or bio sensors without generating band gap. Molecular adsorption at surface of graphene often induce carriers to graphene because of charges of molecules. The induction of carrier in graphene change the drain current, resulting to detect the molecular adsorption. Graphene's high aspect ratio (width to thickness) also increases the sensitivity. Selective detection can be realize by antigen-antibody reaction.

1.4 Band gap generation in graphene

1.4.1 Graphene nanoribbon

Several methods to open a band gap in graphene are proposed. Recently, graphene nanoribbons have been intensively investigated because theoretical studies had predicted that a band gap of which energy depends on the ribbon width is generated (Fig. 1-6b).[14-17)]

$$\mathrm{E}_g = \frac{0.2}{W}\ [\mathrm{eV}], \qquad (1.7)$$

where W [nm] is width of the nanoribbon. As described by the equation, up to 10 nm of width are needed to generate band gap of several dozen meV. The fabrication of graphene nanoribbon within a tolerance of a few nanometers remains a daunting technological challenge.[15)] Actually, Eq. (1.7) are adjusted to a following equation in experiments.

$$\mathrm{E}_g \approx \frac{0.2}{W - 16\,nm}\ [\mathrm{eV}] \qquad (1.8)$$

The differences between theoretical and experimental equations are expected due to

roughness of edge of nanoribbon. Crystallographic orientation of graphene nanoribbons also important but not be controllable. Furthermore, devices with graphene nanoribbon channel do not have high carrier mobility as compared with conventional graphene-based device.[18)]

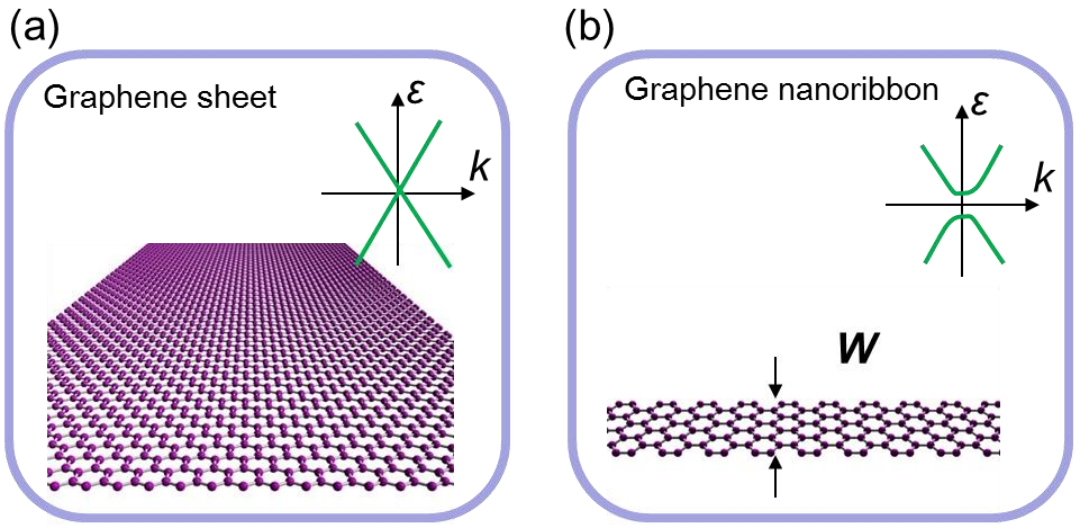

Figure 1-6. (a) Electronic dispersion of Graphene sheet is liner dispersion. (b) Electronic dispersion of graphene nanoribbon has gap between valence band and conduction band.

1.1.1 Bilayer graphene under the electric field

Alternatively, the band gap can be formed by applying a perpendicular electric field to bilayer graphene (Fig.1-7).[19-21)] Because zero gap are relating to symmetric atoms, a breaking of symmetry between upper and lower layer with electric field generate band gap.

The approach does not require etching or cutting graphene, and the band-gap energy can be controlled by changing the electric-field intensity. The change between metal-like and semiconductor-like state with only applying electric field is expected for writable logic circuit in the feature. The electric field is generally applied across solid insulators with top- and back-gate electrodes. The gate voltage change not only electric field but the Fermi level of bilayer graphene. Therefore, dual gates should be prepared to apply the electric field without rising or dipping of the Fermi level.

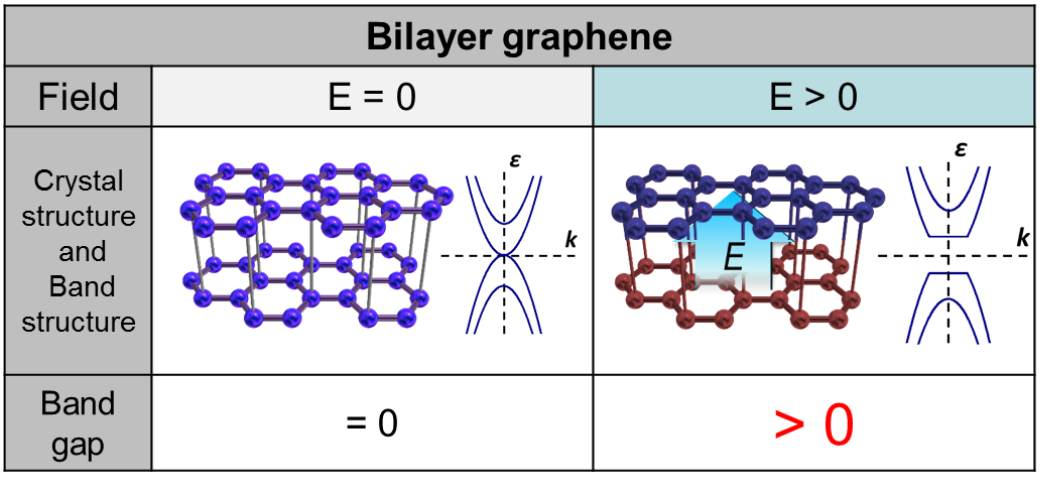

Figure 1-7. Electronic dispersion of bilayer graphene. Band gap is created by applying electric field.

Fig 1-8 shows a series of drain currents versus top-gate voltage at back-gate voltages from -120 to 60 V.[22] Resistance at V_b of 0 V is the smallest of all V_b. At $V_b > 0$ or $V_b < 0$, band gap are generated and increase the resistances.

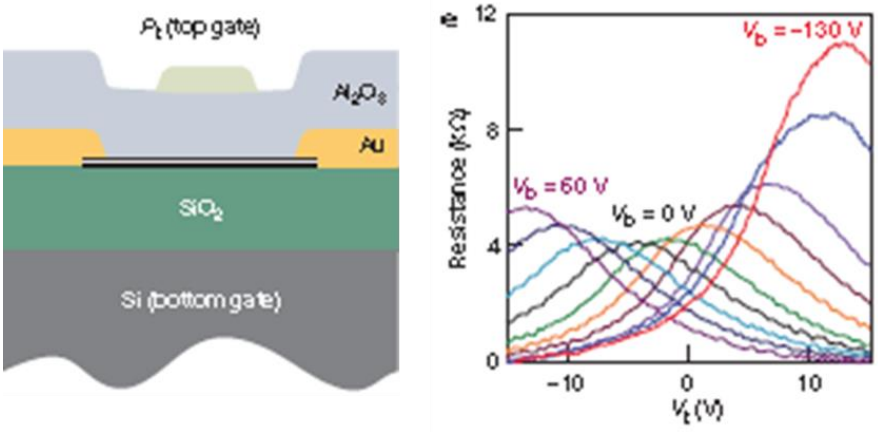

Figure 1-8. (a) Typical top-gate structure of bilayer graphene FET, which is reported by Y. Zhang et al. (b) Resistance of bilayer graphene increases at (V_b, V_t) = (60 V, -12 V), (-130 V, 12 V) caused by band gap opening.

1.5 Ionic liquid

An ionic liquid is a general term for salts in a liquid state under 100°C. Although depending to the kind of the ionic liquid, lots of them have lower melting point than 300 K. The ionic liquids are made of molecular positive ion and molecular negative ion pairs. Large molecular mass constituting the ionic liquid makes possible the low melting point.

1.5.1 Properties

An ionic liquid has unique properties. For example, vapor pressure of ionic liquid is very low. It allows the ionic liquid to be used in vacuum without evaporation. Second, its high relative permittivity and electrical double layer with high electrical strength are advantages for capacitor. Additionally, colorless and transparent in visible range. With the properties, the ionic liquid is used for secondary battery, high capacitance insulator, and so on.

1.6 Purpose of the present study

Band gap generation in bilayer graphene by broken symmetry under the electric field is interesting for both material physics and applications. The study of the band gap in bilayer graphene is not enough because graphene is experimentally revealed in recent years. Many challenges still remain for practical use too.

In this thesis, the author suggests new structure for band gap generation of bilayer graphene using ionic liquid. Physical properties of the ionic liquid gated bilayer graphene FETs with electrical and optical measurements will be researched. Additionally, very-low power-consumption devices for applications will be developed. In general, high gate voltage is needed to generate large band gap in bilayer graphene. We focus attention on ionic liquid which is used as electrolyte gate in a field of superconductivity. Ionic liquid electrolyte forms very thin insulator on the graphene surface and has very high electrical strength, resulting that high electric field can be applied with low gate voltage. The purpose of present study is development of extra low power consumption graphene device by using the ionic liquid after investigating the physical properties.

1.6.1 Outline of this thesis

Back ground, purpose, and properties of graphene were described in chapter 1. Chapter 2 shows fabrication of graphene field effect transistor without the ionic liquid, which are common procedures to all of chapters, for example fabrication process and characterization methods of graphene FETs. From the following chapter, the ionic liquid will be used. We fabricated ionic liquid gated structure on Si/SiO_2 substrate and investigated the band gap of bilayer graphene by electrical measurements in chapter 3. The electrical characteristics of ionic-liquid-gated bilayer G-FETs by applying an effective electric field shows different characteristics from monolayer and trilayer graphene because of a band gap creation. Furthermore, the band gap size was estimated by Arrhenius plots of a conduction.

On the other hand, in chapter 4, the physical properties relating to the band gap will be investigated by optical measurements. The electric field which controlled by applying bias voltage to a bottom-gate and a transparent ionic side-gate in a FET, opens band gap and affects Raman spectra. Peak energy of symmetric and antisymmetric optical phonons depends on band gap generation. Their behaviors were explained by a Kohn anomaly.

Chapter 3 and 4 are discussed about mainly material properties relating to the band gap. Chapter 5 pays attention to practical use or an application of the ionic liquid gated devices. In the device structure used in chapter 3 and 4 is affected from the substrate. In general, silicon dioxide layers have charged impurities on the surfaces, and thus the charge puddles will be created in the graphene channels. As a result, the doped charges will induce the degradation of the carrier mobility and on/off ratio of channel currents. Fabrication of the suspended structure is the most effective method for removing the influence from the substrate. We attempt to improve the mobility, on/off ratio of current and consumption power of graphene transistor by using suspended graphene and ionic liquid gate.

In chapter 6, conclusions of this work are given.

This work revealed that physical properties relating to band gap in bilayer graphene using ionic liquid and its excellent properties for an application to transistor.

Chapter 2 Fabrication of Graphene Field Effect Transistor

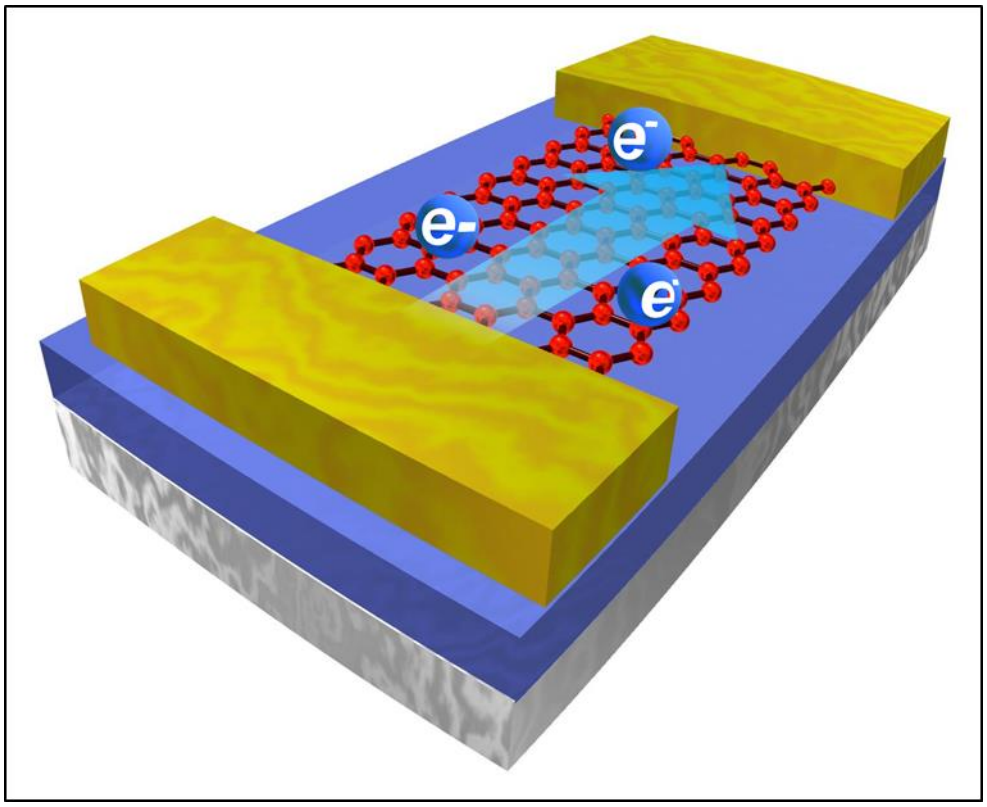

2.1 Introduction

In this chapter, fabrication process and characterization methods of graphene FETs without an ionic liquid will be described.

2.2 Fabrication process of graphene FET

2.2.1 Surface oxidation of Si substrate

Silicon substrates covered with dioxide layer are used for making graphene FETs. First, highly *n*-doped Si wafer is cut into a square 10 mm in height and width by using a diamond scriber (Fig.2-1a). Cutting scraps on the chip are blown away by N_2 gas. Second,

residues on the surface are removed by ultrasonic cleaning in acetone, alcohol and ultrapure water. Finally, annealing in oxygen atmosphere at 1050ºC for 300 minutes forms 300-nm-thick SiO_2 layer (Fig.2-1b). An interference color of Si/SiO_2 substrate is determined by the thickness of the SiO_2 layer and, then, the color affects viewable of graphene on the substrate. Figure 2-2 shows optical micrographs of graphene layers on the Si substrate covered with SiO_2 layer of 90, 270, 300 and 340 nm thickness. Most appropriate color for making a search for graphene, is when the thickness of 300 nm or 90 nm are formed.[23-24] All devices in this study are fabricated on 300-nm thickness because 300-nm thickness of SiO_2 layer have a large electrical strength and can be applied to up to 100 V of voltage without breakdown.

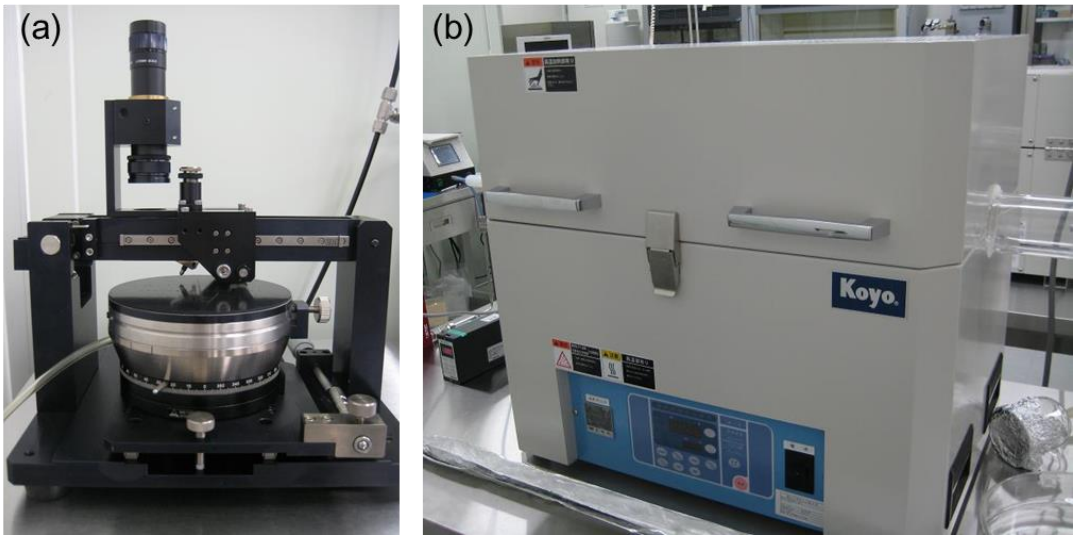

Figure 2-1. (a) A diamond scriber and (b) An electronic furnace.

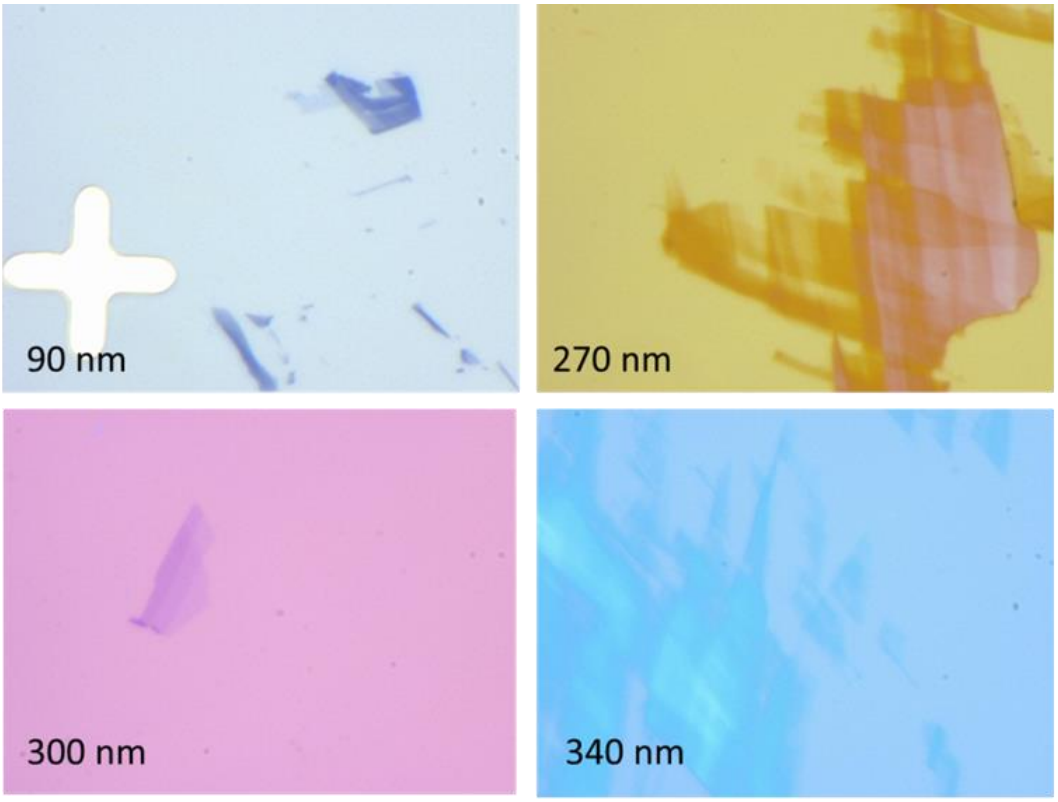

Figure 2-2. (a-d) Optical images of graphene on Si substrate covered with 90-, 270-, 300- and 340-nm thickness of SiO_2 layers.

2.2.1 Preparation of graphene by Mechanical exfoliation

Graphene layers are extracted from Kish graphite (Covalent Materials) by mechanical exfoliation using adhesive tape. Graphene layers were transferred onto highly *n*-doped Si substrates covered by a 300-nm-thick SiO_2 layer.[25)]

Providing further explanation.

1. Picking up one or two graphite flake by using adhesive tape.
2. Sandwiching the graphite particle between sticky sides of adhesive tape.
3. Exfoliating very slowly (Fig. 2-3a).
4. Repeating step 2-3 about 10 times until graphite become enough thin.
5. Attaching the tape on Si/SiO_2 substrate (Fig. 2-3b).
6. Removing air bubbles between the tape and substrate if needed.
7. Pressing and trace lightly the tape surface with soft tong for ~5 minutes.
8. Removing the tape very slowly. (spend ~1 min) (Fig. 2-3c).
9. Removing adhesive residues by ultrasonic cleaning in acetone for 2 seconds and rinsing the substrate in 1-methyl-2-propanol.

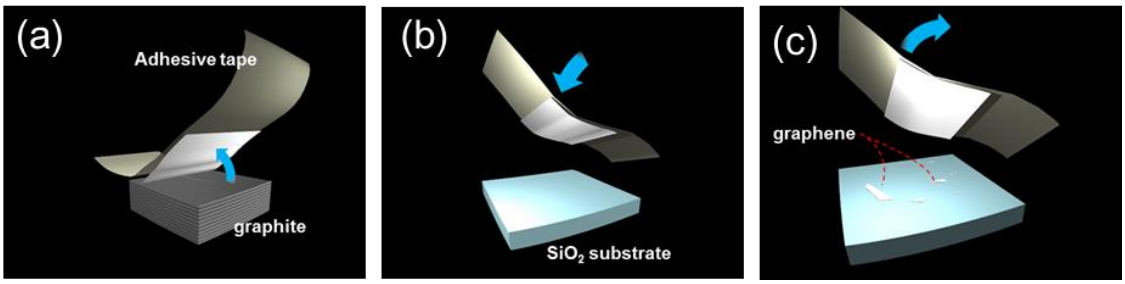

Figure 2-3 Procedure of mechanical exfoliation method. (a) Exfoliation of thin graphite from bulk graphite. (b) Pressing the tape lightly on the substrate and stroking surface for 5 minutes. (c) Removing the tape very slowly. Graphene and graphite flakes remain with random size and position.

Figure 2-4(a) and 2-4(b) show optical images of adhesive tape with thin graphite and graphene layers on Si substrate with 300-nm thickness of dioxide layer.

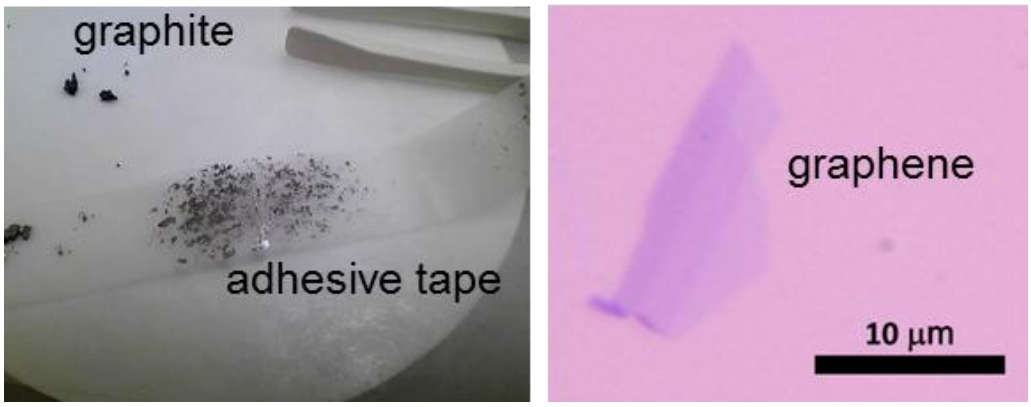

Figure 2-4 (a) Kish graphite and adhesive tape. (b) Few layer graphene on Si/SiO_2 substrate.

2.2.2 Marker patterning

Marker patterning is required before forming source and drain electrodes to determine coordinates of graphene on the substrate. Ti/Au markers are deposited on the whole of substrate surface at intervals of 1 mm by photolithography technique using mask aligner (Fig.2-5a). An Evaporation of 15 nm or more thickness metals (Au, Pd, Pt) are required by an evaporative apparatus (Fig.2-5b) to adjust the position in a process of electron beam lithography. In contrast, too thick metal prevent the formation of source and drain electrode.

Procedures of photolithography and metal deposition will be represented as follow.

1. Annealing the substrate on a hot plate at 150°C for 3 min for improving hydrophilicity.
2. Applying photo resist to the substrate (LOR), then resist spreads uniformly by using spin coater. As soon as spin coating finish, baking the substrate on the hot plate at 180°C for 3 min.
3. Applying again photo resist (OFPR) on the substrate and spreading with spin coater. Baking the substrate on the hot plate at 90°C for 1 min.
4. Exposing the substrate through a masking grass.
5. Rinsing the substrate in developing solution (NMD) for one minute. Exposed regions dissolve in the solution.
6. Confirming that the photolithographic patterns are well fabricated with a use of microscope and depositing Ti and Au electrode.
7. Lifting off in N-methylpyrrolidone for 1 hour.

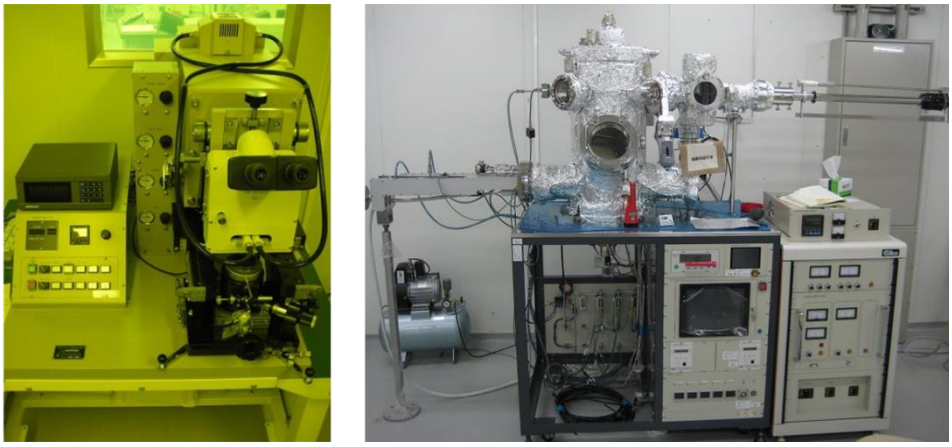

Figure 2-5 (a) Mask aligner and (b) evaporative apparatus.

2.2.3 Determination of graphene position

In this process, optical images of graphene are observed to identify the layer number, shape and accurate positions of graphene in the substrate surface. Author use two different scale images. One is taken a picture at 500-fold magnification for confirming the coordinates with reference to cross markers (Fig.2-6). The other is taken at 5000-fold magnification for identifying the shape and the layer number of graphene. The coordinates, the layer number and the shape of graphene are listed on excel files. Although much of your time and energy are consumed for searching graphene, this process should be tried carefully. Otherwise only a few available graphene will remain for fabricating graphene FETs.

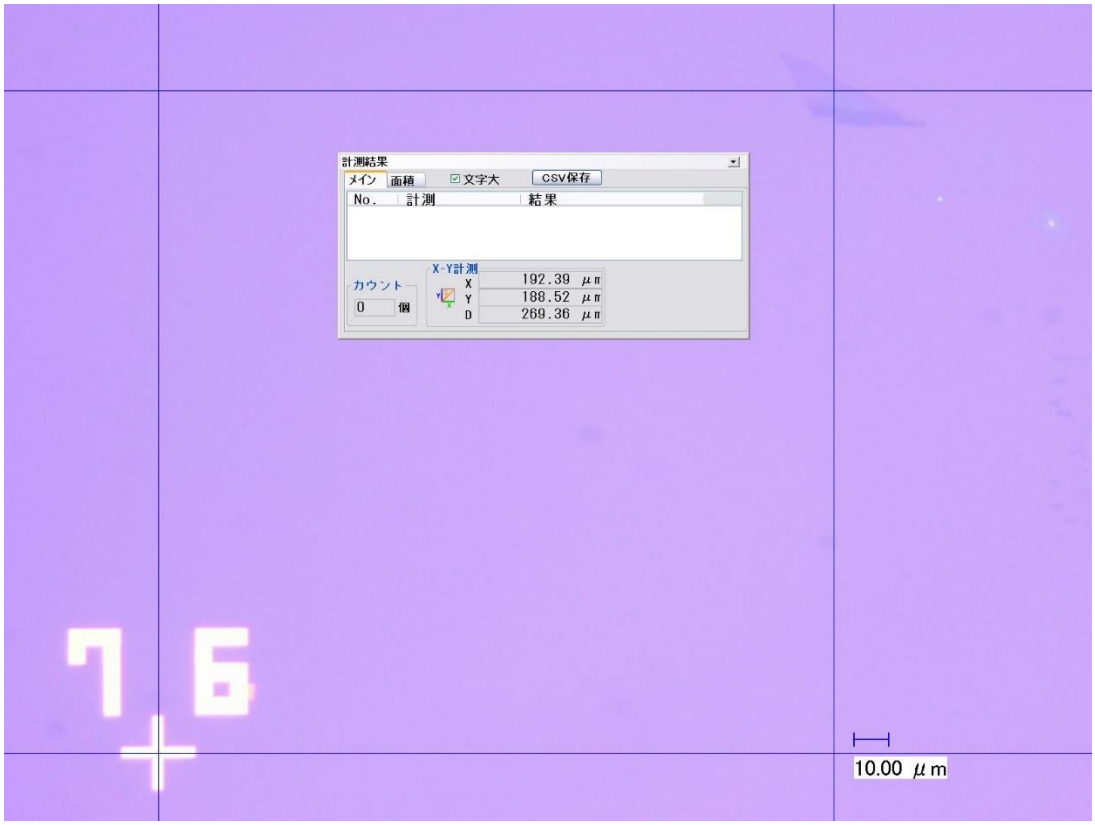

Figure 2-6 Optical image of substrate taken at 500-foldmagnification. The coordinates of graphene are measured with reference to cross markers.

2.2.4 Electrode Formation

In general, electrodes are patterned not by photo lithography but by electron beam lithography (Fig.2-7) because each exfoliated graphene has different shapes and size, and needs different patterns of electrodes. An Excel file about coordinates of graphene and CAD files of electrode patterns should be prepared in first. The procedure of electron beam lithography and that of metal deposition will be indicated as follow.

1. Annealing the substrate on a hot plate at 150°C for 3 min for improving its hydrophilicity.
2. Applying photo resist (LOR) to the substrate and making the thickness thin by using spin coater. Baking the substrate on the hot plate at 180°C for 3 min.
3. Applying electron beam resist (ZEP520A) on the substrate and spreading it by using the spin coater. Baking the substrate again on the hot plate at 150°C for 3 min.
4. Exposing the substrate by using electron beam lithography.
5. Rinsing the substrate in developing solution for 2 minutes.

6. Rinsing again the substrate in another developing solution (NMD) for 10 seconds.
7. Depositing Ti and Au electrode after confirming that the lithographic patterns are well fabricated.
8. Lifting off in N-methylpyrrolidone for 1 hour or more.

Figure 2-7 Electron beam lithography equipment.

2.2.5 Annealing in a hydrogen atmosphere

Residues of resist, adhesive, water and oxygen molecules on the graphene channel are unavoidable issue in fabrication procedure of graphene FET. They affect properties of graphene significantly because two-dimensional graphene which has high surface-volume ratio, is sensitive to an environmental change. The graphene devices should be cleaned by annealing before electrical measurements. There are two methods to annealing. One is annealing in hydrogen atmosphere at 300°C for 1 hour. The other is electrical annealing in vacuum. Applied High voltage increases the temperature of graphene and remove resist residues, water and oxygen molecules. Typical devices get ambipolar conduction of graphene's intrinsic property after the annealing.

2.3 Characterization method of graphene

2.3.1 Raman spectroscopy

Raman spectroscopic analysis is often used to characterize quality, stress, or band structure of graphene. Figure 2-8 shows Raman spectroscopy system, schematic of Raman setup and typical Raman spectra of monolayer graphene. Main peaks observed in graphene are D-band, G-band and G'-band.

G-band peak which is observed at ~1600 cm^{-1} where HeNe (λ = 633 nm) laser is used for excitation, indicates an optical phonon mode of six-membered ring at the Γ point. The intensity and vibration energy of G-band is influenced to the crystal quality, stress and electron-phonon interaction. G'-band (2D-band) observed at ~2700 cm^{-1} originates from an inter valley scattering of a second-order process consisted of two phonon. Because the inter valley scattering occurs in the band structure of graphene, carbon nanotube or graphite, amorphous carbon don't shows the G'-band peak. That is why, the observation of fine 2D-band become evidence of graphene in particular synthesis study. D-band peak observed at ~1350 cm^{-1} also originates from a second-order process. Its energy is approximately a half of that of G'-band because one phonon and one elastic scattering are contributed. D-band peak is not active when graphene forms fine honeycombs continuously because the elastic scattering occurs just when structure defects or edge of graphene sheet are irradiated by laser. Thus, the intensity of D-band is considered to be a measure of quantity of defects.

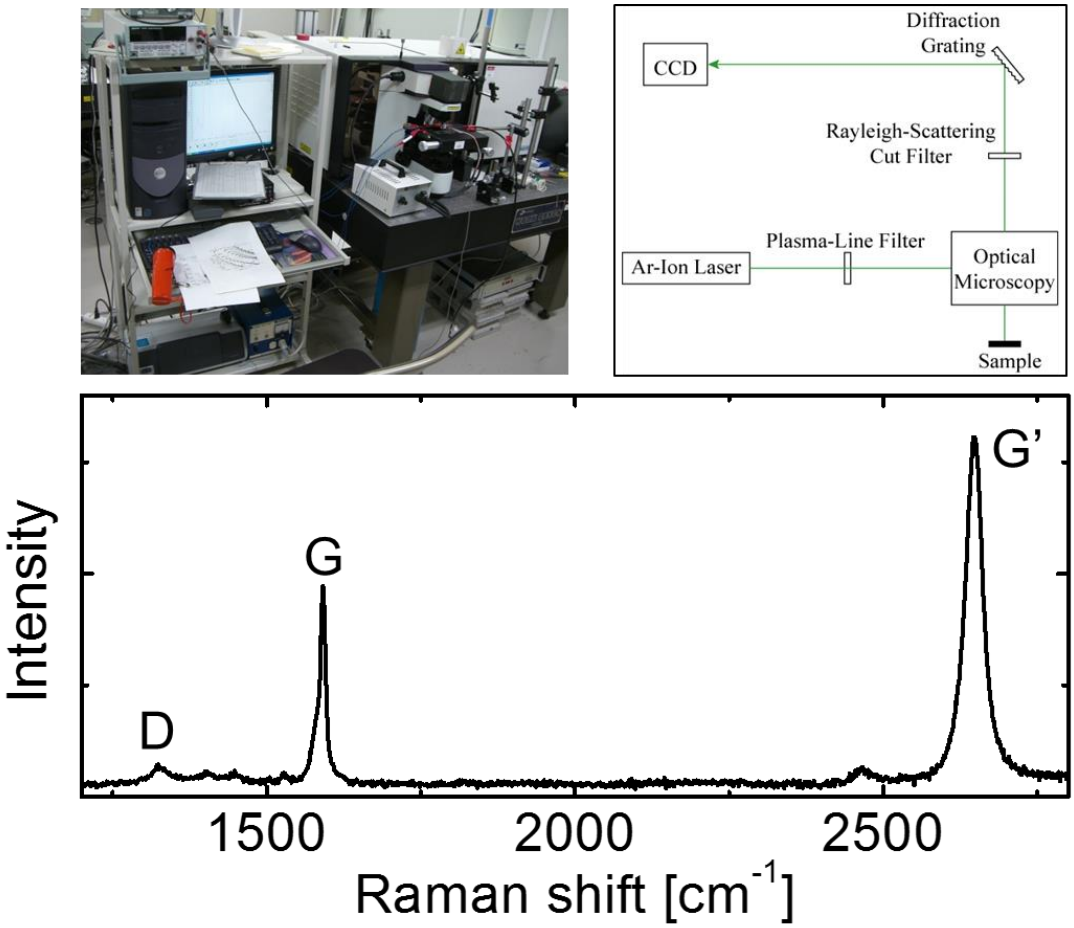

Figure 2-8 (a) Raman spectroscopy system. (b) Schematic of Raman Setup. (c) Raman spectra of monolayer graphene

2.3.2 Scanning electron microscopy (SEM)

A scanning electron microscopy (SEM) is not always necessary because optical microscope has enough high resolution for observation of the two dimensional graphene (Fig. 2-9).

In our study, SEM is used when the observation of suspended graphene shown in chapter 5. SEM observation is measured after all measurements (electrical or Raman measurements) due to adsorbed contaminations on the surface of graphene.

Figure 2-9 Scanning electron microscopy.

2.3.3 Electrical measurements

Figure 2-10 shows a stage of electrical measurements in chamber and an optical image of electrode pads. The devices are hold on the stage and contacted by needles connected to parameter analyzer by triaxial cable. The chamber can be vacuum and its temperature are variable from 10 K to 473 K.

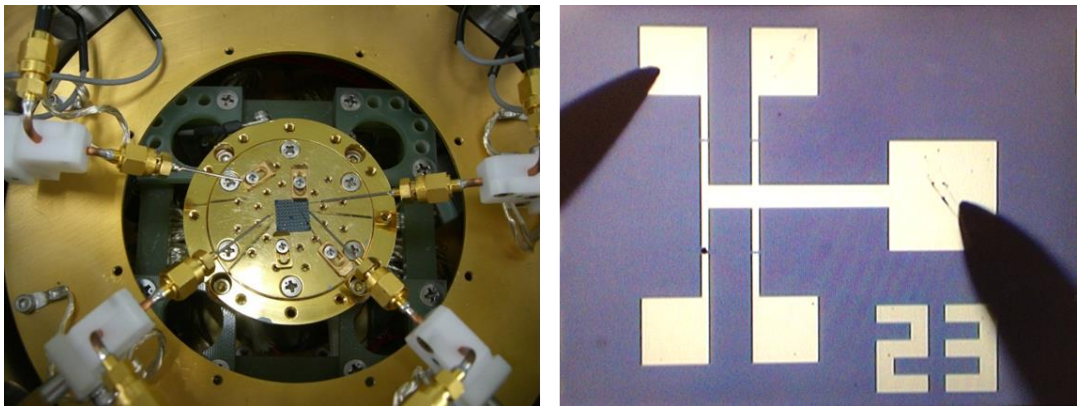

Figure 2-10 (a) Stage in chamber and (b) optical image of the device.

2.4 Results and Discussion in the characterization of the present study

2.4.1 Identification of the number of graphene layers by the optical images

The number of graphene can be identified without a specially equipment. Figure 2-11(a) shows an optical micrograph of graphene layers on Si substrate covered with 300-nm thickness dioxide layer. The brightest area corresponds to SiO_2 surface and the little dark color areas is graphene. The brightness decreases as the number of layer increases. Figure 2-11 (b) inset shows analysis result of Fig. 2-11(a). Horizontal axis corresponds to brightness of the image and vertical axis corresponds to the number of pixel area. Four peaks indicate brightness of SiO_2 surface, monolayer, bilayer and trilayer graphene areas. Their brightness are normalized based on the brightness of the SiO_2 and plotted on Fig. 2-11 (b) as a function of the number of layer. The plots are good fitted with a liner function.

$$[Brightness] = 1 - 0.056n, \qquad (2.1)$$

where *n* is the number of graphene layer. The results indicates that the number of graphene layer can be determined from the contrast between SiO_2 and graphene layers.

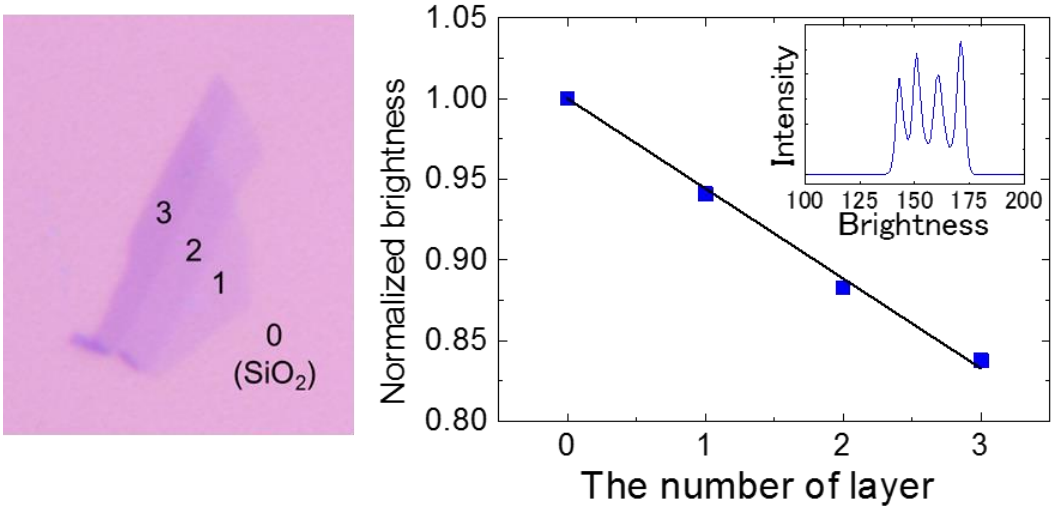

Figure 2-11 (a) Optical micrograph of mono- bi- tri-layer graphene on Si substrate with 300-nm thickness of dioxide layer. (b) Plots of normalized brightness vs the number of layer. Inset shows analysis result of the optical image of graphene. Vertical axis of the inset corresponds to the number of pixel.

2.4.1 Identification of the number of graphene layers by Raman spectroscopy

The most certain method to identify the number of graphene layers is observation of Raman spectra. One of the layer number dependences is shown in the intensities ratio of G' to G. Figure 2-12 shows Raman spectra of monolayer, bilayer and trilayer graphene. The intensity ratio of G'/G is decreased with increase in the layer number. In addition, shapes of G'-band peaks are different between monolayer, bilayer and trilayer graphene. The G'-band peak of monolayer graphene is good fitted with a single Lorentz function as shown in Fig.2-12(a). On the other hand, that of the bilayer graphene is not fitted with a single but a shoulder peak fitted with four Lorentz functions. The peak shape of trilayer graphene is also fitted with many Lorentz functions but similar to a single Lorentz function. Although the difference of shape between monolayer and trilayer is small, the intensities are largely different. The difference of the intensity ratio of G' to G and peak shape makes it possible to determination of the number of layer.

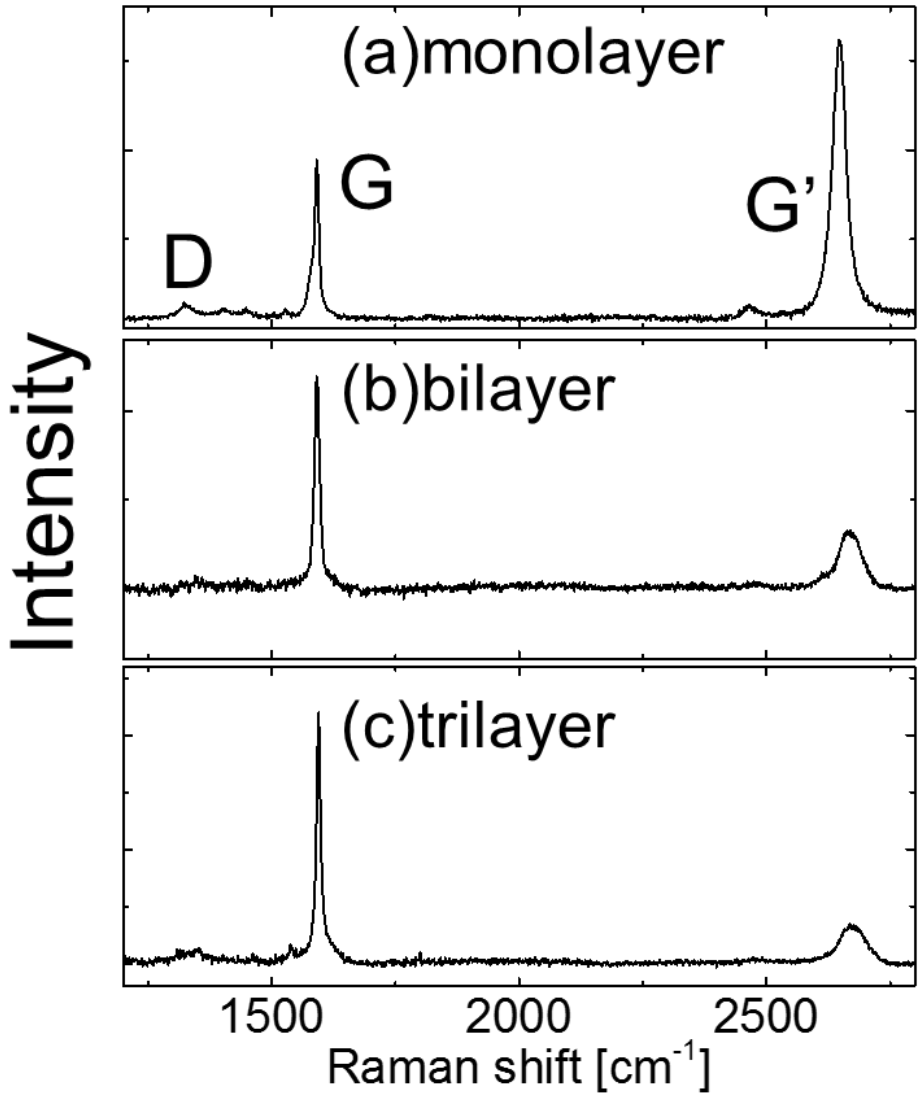

Figure 2-12 Rman spectra of monolayer (a), bilayer (b), and trilayer (c) graphene. The intensities and shape of peak depends on the number of layer.

2.4.2 Electrical characteristics of graphene FETs

Figure 2-13 shows schematic of experimental setup and optical micrograph of typical graphene FET. Applying back-gate voltage induces carriers into the graphene and Fermi level are changed. Figure 2-14 shows electrical characteristics of monolayer graphene FET at room temperature. The ambipolar conduction is unique characteristics of graphene. In our typical graphene FETs on the SiO_2 layer using mechanical exfoliation, mobility and on/off ratio are 3,000 – 5,000 cm^2/Vs and 3, respectively[26-27]. As described in experimental procedure, the electrical characteristics are measured after annealing for

improving the high properties. When exposed to air after annealing, the graphene absorbs oxygen and water molecules in atmosphere, results that charge neutrality point move to positive gate voltage and its mobility decreases as shown in Fig. 2-16. Thus, electrical characteristics should be measured in vacuum.

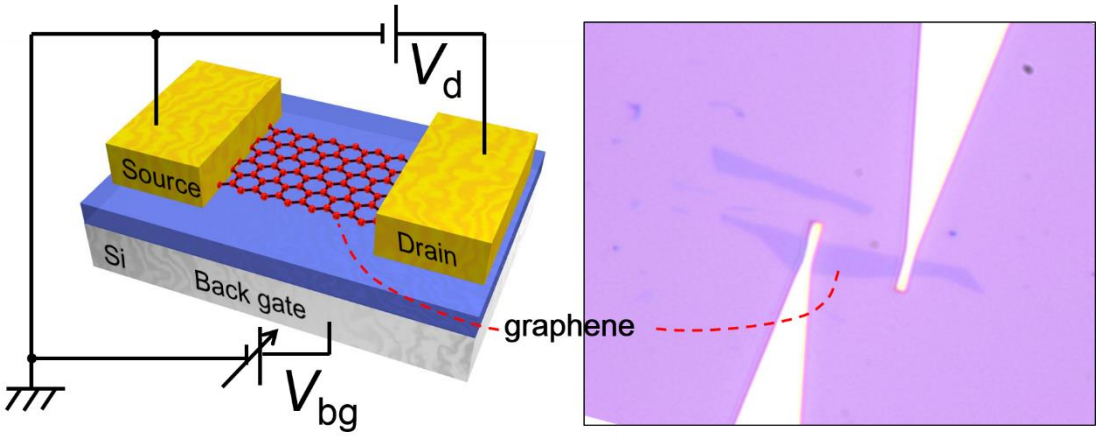

Figure 2-13 Schematic of experimental setup (a) and optical micrograph of typical graphene FET (b). Drain current can be controlled by the back gate electrode.

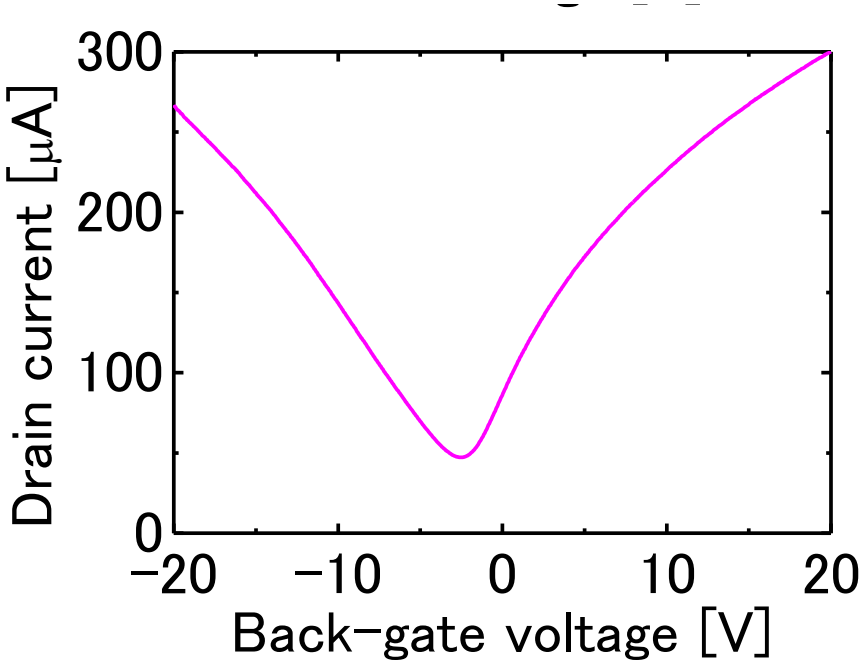

Figure 2-14 Typical back-gate dependence of drain current in monolayer graphene FET on Si/SiO_2.

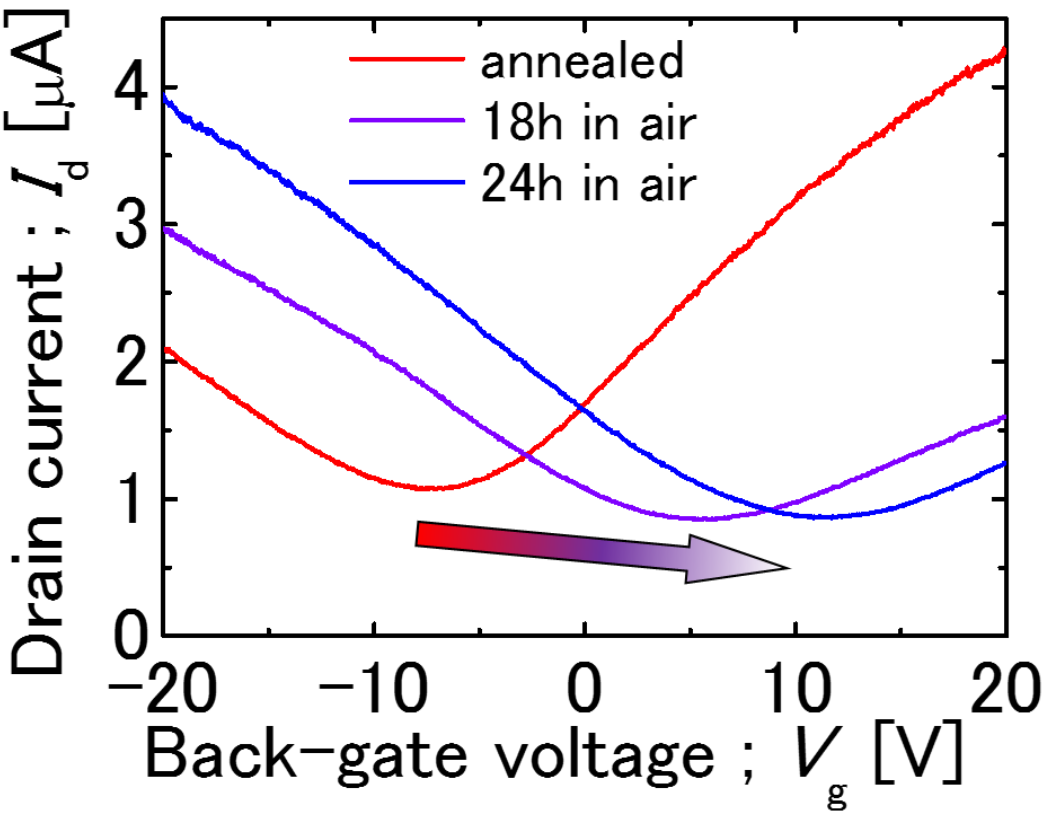

Figure 2-15 Electrical characteristics of monolayer graphene just after annealing, after 18h in air, and 24h in air.

2.5 Conclusions

We have prepared graphene layers on Si/SiO_2 substrate by mechanical exfoliated method and fabricated graphene FETs. The number of graphene layer was identified by optical images and Raman spectra. Mobility and on/off ratio of graphene FETs on the SiO_2 layer were 3,000 – 5,000 cm^2/Vs and 3, respectively. We confirmed that atmosphere exposure decreases mobility of graphene and shifts the charge neutrality point because of absorption of oxygen and water molecules.

Chapter 3 Electric-field-induced band gap of bilayer graphene in ionic liquid

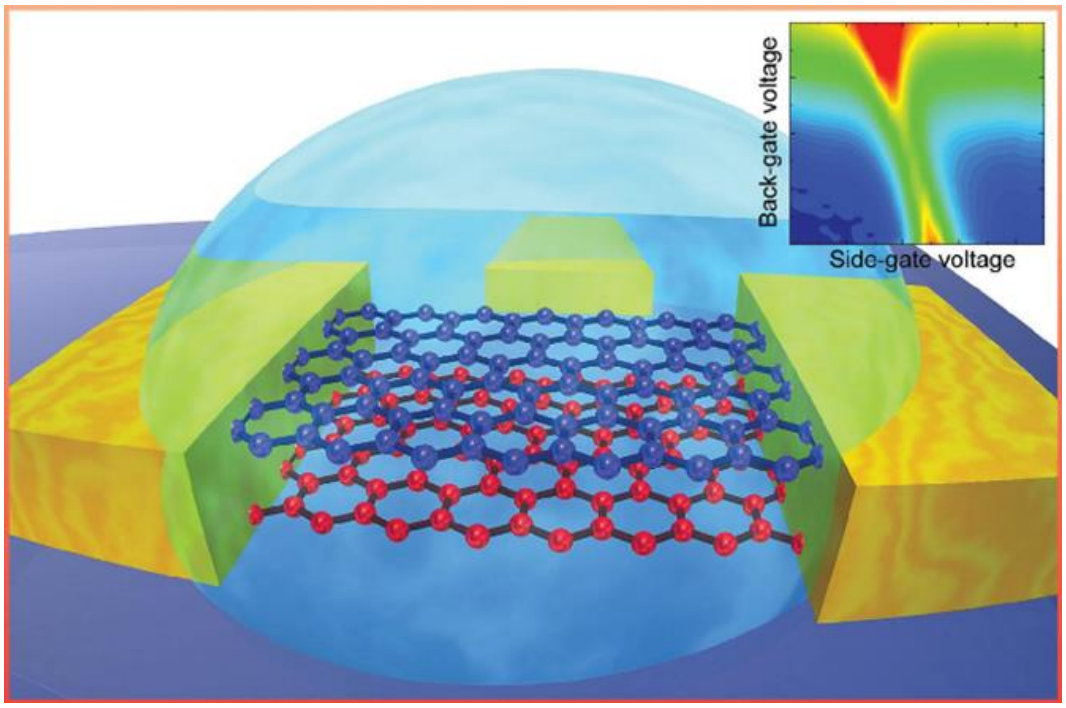

3.1 Introduction

In this chapter, the electrical characteristics of mono-, bi- and tri-layer graphene FETs in ionic liquid will be discussed. The electrical characteristics of ionic-liquid-gated bilayer G-FETs by applying an effective electric field shows different characteristics from monolayer and trilayer graphene because of a band gap creation. Furthermore, the band gap size was estimated by Arrhenius plots of a conduction.

3.1.1 Background

The band gap can be formed by applying a perpendicular electric field to bilayer graphene.[19-21] That approach does not require processes to etch or cut graphene unlike a graphene nanoribbon, and the band-gap energy can be controlled by changing the electric-field intensity. The electric field is generally applied across solid insulators with

top- and back-gate electrodes by controlling the potential of the graphene layers. The top gate electrodes need several steps to fabricate. Moreover, applying electric field is applied only under the top gate electrode. The inhomogeneous electric field will create different band gap energy and different potential by location, resulting to decrease effects of gate operation. We attempted to generate the band gap in a new simple method using electrolyte gate.

3.1.2 Electrolyte gate FETs

When a voltage is applied between two electrodes contacted with an electrolyte, electrical double layers are formed in an interface between electrolyte and electrodes. Figure 3-1(a) shows the structure of an electrolyte gated graphene FET and Fig.3-1(b) shows an expanded view of the surface. When a negative (positive) gate voltage is applied, negative (positive) ions move to graphene surface and positive (negative) charges are induced in graphene. At this time, an electrical double layer of 3~5 nm is formed. The all of applied gate voltage drops in the electrical double layer. In other words, an electric potential in bulk region of the electrolyte is constant even if gate voltage are applied except to the interface between the ionic liquid and conductors (e.g. graphene or electrodes) as shown in Fig.3-1(b). That is why, the electrical double layer acts as very thin insulator and makes it possible to apply effective electric field. The electrolyte-gate structure provides effective electric field with simple fabrication process relative to solid top gate structures. The simple process and high effective electric field seems well-adapted for applying electric field to generate band gap of bilayer graphene. However, no researches have been reported.

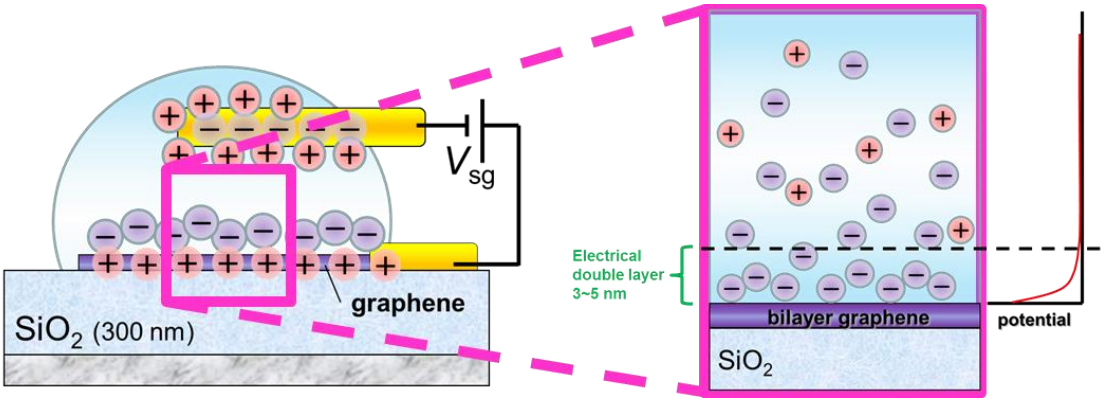

Figure 3-1. (a) Schematic of electrolyte gated FET and (b) an expanded view of the interface between the electrolyte and the FET channel.

1. Biosensor using electrolyte gate FETs

A channel material of nano carbon such as carbon nanotubes and graphene are often used for biosensor because of their high surface/bulk ratio and a strength for electrolysis reaction. Recently, we succeeded in operating electrolyte-gated FETs without solid insulators by using carbon nanotubes and graphene for biosensors[28-29]. Figure 3-2 shows the biosensing system with graphene channel. The GFETs were immersed in the electrolyte and a silicone rubber well was placed on the GFETs to allow the surface of the graphene channel to be filled with several buffer solutions and analyses for electrical measurement and sensing. A reference electrode which is used as the top-gate electrode forms an electrical double layer at the graphene/electrolyte interface serves as a thin insulator when bias voltage is applied. GFETs immersed in an electrolyte showed transconductances 30 times higher than those in a vacuum as shown in Fig. 3-2(b) and their conductances exhibited a direct linear increase with electrolyte pH, indicating their potential for use in pH sensor applications. Additionally, the liquid state allows for a homogeneous electric field to be applied over the entire surface of graphene, including regions near the source and drain electrodes.

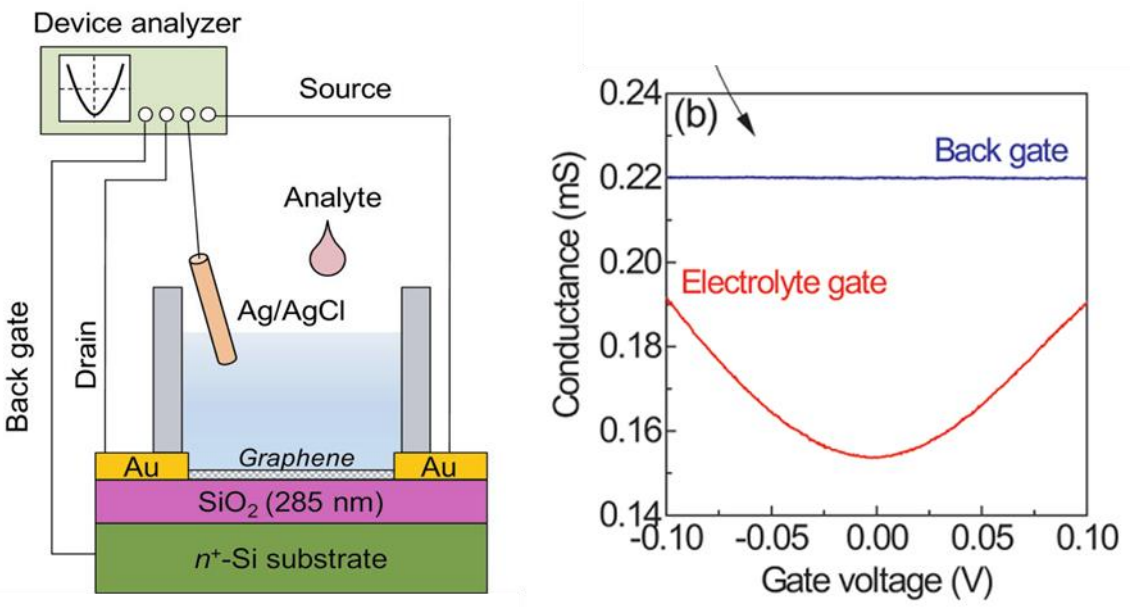

Figure 3-2. (a) Schematic illustration of the experimental setup for electrolyte-gated GFETs. (b) Back-gate and electrolyte-gate dependence of conductance.

2. Ionic-liquid gated FETs

The electrolyte consisting of water as described above is useful for sensors, however, its electrical strength of 0.1 V is too weak for applying electric field to generate band gap of bilayer graphene. In this study, we applied an electric field to graphene layers by using an ionic-liquid gate. Ionic liquid has several advantageous properties, such as zero vapor pressure, high relative permittivity, and high dielectric strength.[30] As these properties, the ionic liquid has already been utilized to induce a large amount of carriers in ZnO-based FETs.[31] Although the water electrolyte FETs as described above have high transconductance, the electrical breakdown of the electrolyte occur at the gate voltage of 0.1 V. On the other hand, the electrical breakdown in ionic liquid electrolyte occur at 3.0 V because of its strength in high electric field. Hence, a high effective and large electric field can be applied through the gate, owing to the electrical double layer that forms in the interface between graphene and ionic liquid.

3.2 Purpose of this study

In this study, we attempted to generate the band gap in bilayer graphene by using ionic liquid gate. The purpose of this study is creating the band gap and investigating the properties of the band gap by electrical measurements.

3.3 Experimental

The fabrication process are same as shown in chapter 2 except to fabricate side-gate electrode and to apply the ionic liquid. The side-gate electrodes were patterned at a distance of approximately 20 μm from the channels. *N*, *N*-Diethyl-*N*-methyl-*N*-(2-methoxyethyl)ammonium bis(trifluoromethanesulfonyl)imide ([DEME][TFSI]) ionic liquid was placed into the graphene channel and onto the side-gate electrode without any passivation films after the device was annealed at 300 °C for 1 hour in a hydrogen atmosphere to clean the surface of graphene. An optical micrograph and a schematic of an experimental setup of a G-FET with ionic liquid is shown in Fig. 3-3(a) and 3-3(b), respectively. The sample was annealed again in vacuum at 150 °C to dehydrate the ionic liquid before each measurement of electrical characteristics because the dehydrated ionic liquids have high electrical strength (3.0–4.0 V). The electrical characteristics were measured with a semiconductor parameter analyzer (B1500A, Agilent).

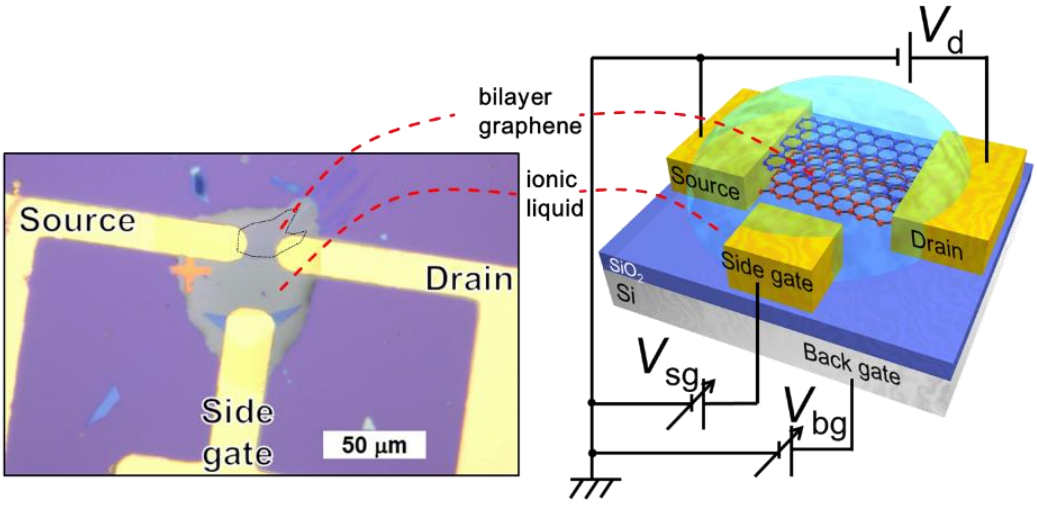

Figure 3-3. (a) Optical micrograph of typical G-FET with ionic liquid and (b) schematic of experimental setup.

3.4 Results and Discussion

The potential of graphene channel can be controlled by both back-gate voltage (V_{bg}) and side-gate voltage (V_{sg}). Figure 3-4(a-c) respectively shows resistance contour plots as functions of V_{bg} and V_{sg} in G-FETs with monolayer, bilayer and trilayer graphene at drain voltage of 5 mV at 300 K in vacuum. Red and blue regions correspond to higher and lower resistance in the G-FET, respectively. A ridge line corresponding to charge neutrality was clearly observed (dotted line in Fig. 3-4a, 3-4b, 3-4c). The carrier densities in graphene were held constant on the ridge lines because of the balance between the back- and side-gate voltages. As shown in Figs. 3-4(a) and (c), the resistance of monolayer and trilayer G-FETs along the dotted lines corresponding to charge neutrality was nearly constant. However, in the bilayer G-FET, the resistance changes to form a valley in the plot (Fig. 3-4b); that is, an increase in resistance was clearly observed as the magnitude of the electric-field intensity was increased. The increasing resistance of bilayer graphene was not caused by variation of the charge density in the bilayer graphene, because the potential in the bilayer graphene remained constant along the ridge lines. The results indicate that this resistance change was due to the formation of a band gap and a decrease in carrier density, which is consistent with previous reports.[32)]

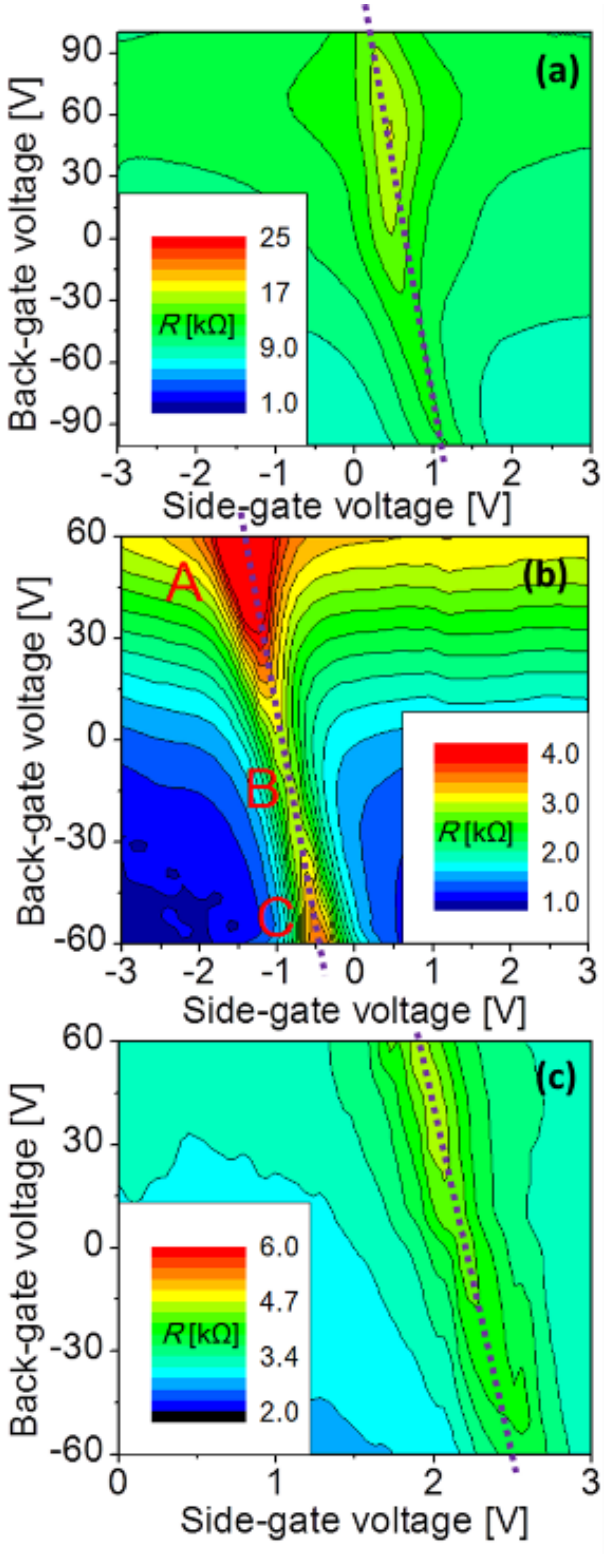

Figure 3-4. Resistance contour plots as a function of the back- and side-gate voltage (a) in monolayer, (b) bilayer, and (c) trilayer graphene.

Figure 3-5 shows the electric field dependence of the resistances in monolayer, bilayer, and trilayer G-FETs in ionic liquid at 300 K. The resistance at the charge neutrality point was plotted for each G-FET. The electric field in the horizontal direction was calculated by equation

$$E = \frac{1}{2}\left(\varepsilon_1 \frac{\Delta V_1}{d_1} - \varepsilon_2 \frac{\Delta V_2}{d_2}\right). \quad (3.1)$$

Where for gate insulator layer i (= 1 or 2), ΔV_i is the difference between the applied voltage and the charge neutrality voltage, ε_i is the relative permittivity, and d_i is the thickness. Charge neutrality voltage of back gate and side gate were determined by Fig. 3-4. The thickness of electrical double layer are derived by the slope of dotted line in Fig. 3-4. The detail of calculation will be described in chapter 5. Resistance curves in Fig. 3-5 were normalized by the resistance in zero field. Points A, B, and C in Fig. 3-5 correspond to those in Fig. 3-4(b) for the bilayer G-FET. In the monolayer and trilayer G-FETs, resistance slightly decreased as the magnitude of the electric field intensity was increased, which is consistent with a previous report[20]. In contrast, resistance increased in the bilayer G-FET, indicating that a band gap was created in the ionic-liquid-gated bilayer G-FET by the electric field.

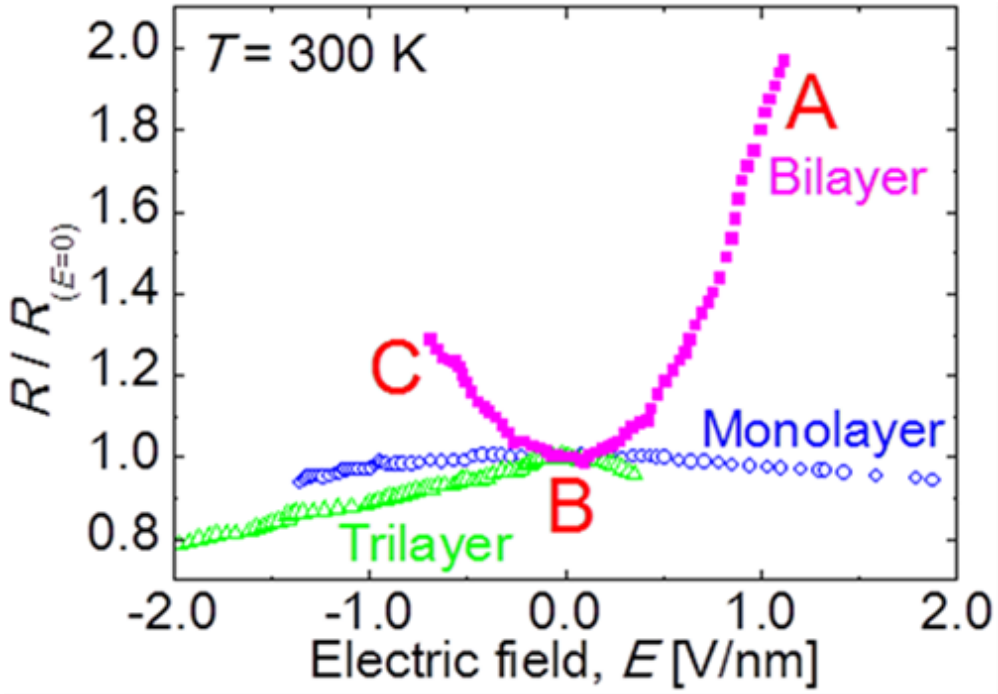

Figure 3-5. Resistance of monolayer, bilayer, and trilayer graphene in ionic liquid plotted against total electric field.

Lastly, a temperature dependences of conductance in the bilayer G-FET in ionic liquid are investigated with a four-probe method. A conduction in a semiconductor is affected by a thermally activated conduction described by

$$G_{\mathrm{a}} = G_{a0}\exp\left(-\frac{E_{\mathrm{g}}}{2k_{\mathrm{B}}T}\right), \qquad (3.2)$$

where G_{a0} is coefficient of conduction unit[20]. The band gap size E_{g} is derived as fitting parameter of temperature dependence. Figures 3-6(a) and (b) show Arrhenius plots for the bilayer G-FETs in electric fields of 0 and 2.5 V/nm, respectively. In zero field, a slight decrease in conductance was observed with decreasing temperature. On the other hand, a sharp drop in conductance in the low-temperature region was found for the bilayer G-FET in electric field of 2.5 V/nm. This drop results from the generation of the band gap in the bilayer G-FET. From the steep slope in the low-temperature region in Fig. 3-6(b), the band gap in the bilayer G-FET was estimated to be 235 meV at electric field of 2.5 V/nm, which was obtained by applying side-gate voltage of only -3.0 V in

the ionic liquid. While in the high-temperature region, the conductance was almost saturated. The phenomenon is not clear at present. In the high-temperature region, most electrons at the edge of the energy gap are considered to be already excited to the conduction band in the bilayer graphene since a singular enhancement of the density of state around the edge of the energy gap is obtained after applying electric field.[33] As a result, the conductance was almost saturated in the high-temperature region. The phenomenon is similar to the saturation range in impurity semiconductors.[34]

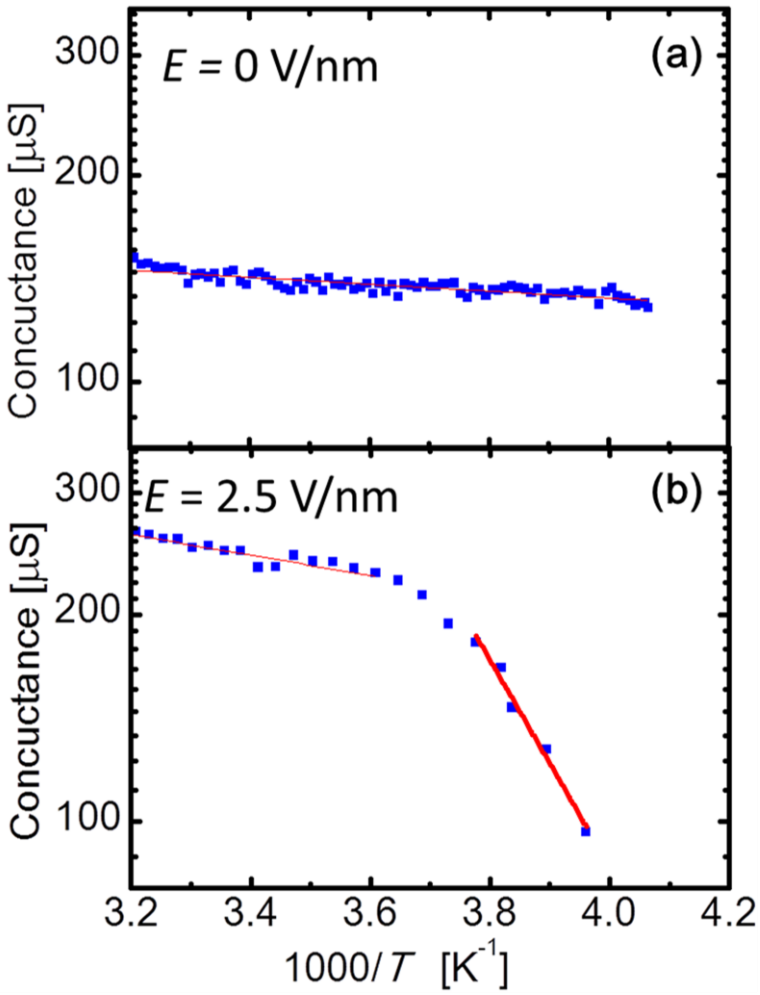

Figure 3-6. Arrhenius plots of conductance in bilayer graphene at electrical field of (a) 0 and (b) 2.5 V/nm.

From the Arrhenius plots at various electric-field intensities, the band-gap energy was plotted as a function of the electric-field intensity (Fig. 3-8). The solid curve shows the best fit of the low-energy approximation in the tight-binding model to the experimental

data.[35] These results are consistent with the previously reported value of the band-gap energy in bilayer graphene as observed by infrared microspectroscopy.[35] This indicates that the ionic-liquid gate generated the band gap in bilayer graphene by the electric field.

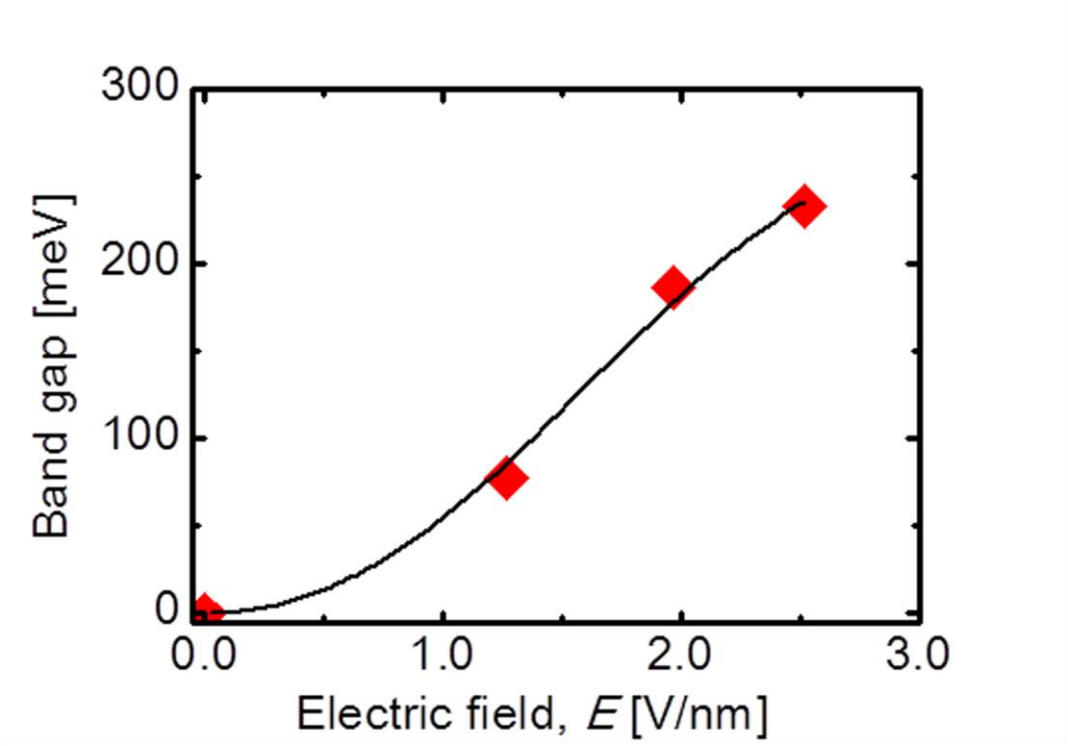

Figure 3-7. Electric field dependence of band gap in bilayer graphene. Solid curve shows the best fit to the experimental data.

3.5 Conclusions

We have fabricated ionic-liquid-gated G-FETs to create a band gap in bilayer graphene. Electrical measurements revealed that the resistance in the bilayer G-FET monotonically increased as the electric-field intensity was increased. In contrast, the resistance in the monolayer and trilayer G-FETs at the charge neutrality were nearly constant. These findings are attributable to a band gap forming in the bilayer graphene, but not the mono- or tri-layer graphene. A band gap of 235 meV in bilayer graphene was created at an ionic-gate-voltage of -3.0 V, as determined from Arrhenius plots. Ionic-liquid-gated structure should be useful in creating band gap of bilayer graphene.

Chapter 4 Electric-Field-Dependence of Raman Spectra in Bilayer Graphene

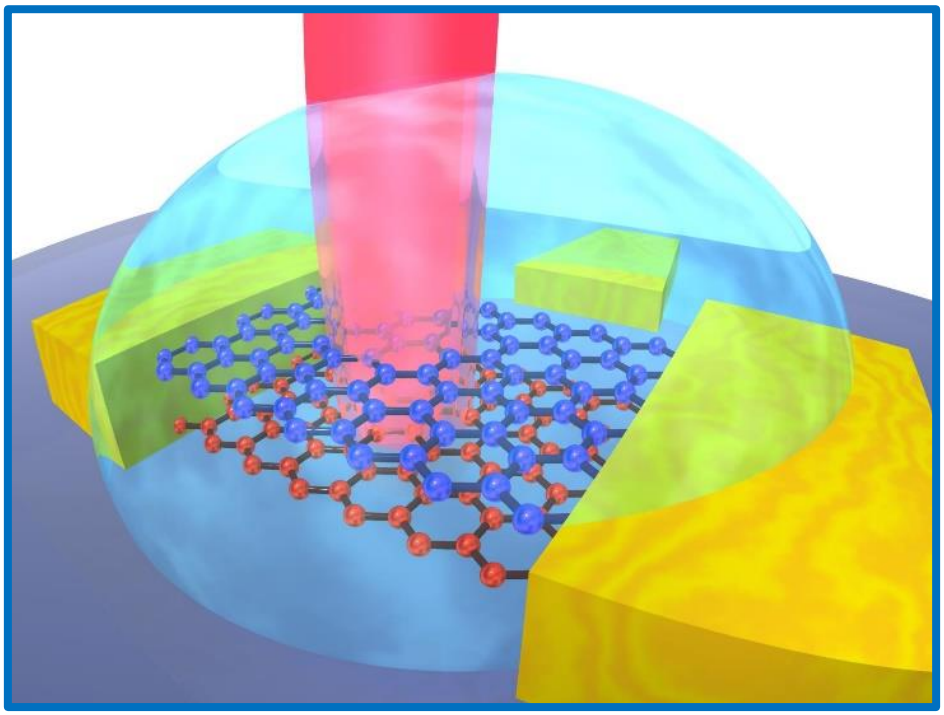

4.1 Introduction

In this chapter, electronic states and phonon energies in bilayer graphene were investigated by electrical and optical measurements under an external electric field. The electric field which controlled by applying bias voltage to a bottom-gate and a transparent ionic side-gate in a FET, opens band gap and affects Raman spectra. Symmetric and antisymmetric optical phonons were visible in the Raman scattering spectra. Their behavior was explained by a Kohn anomaly.

4.1.1 Background

The band gap is formed by the potential asymmetry between the two layers in the bilayer graphene, which arises from the electric field perpendicular to the surface. The effect of an external electric field on the electronic states in bilayer graphene is important

for graphene transistors. Therefore, the electrical properties was discussed when band gap of bilayer graphene was opened in the chapter 3. Optical measurements about band gap also should be discussed to understand the physical properties. To characterize the electric field dependences of the band structure and phonon vibrations, the effect of the band gap generation must be separated from that of the changes on carrier densities. Hence, two or more gate electrodes are required in the FET structures to control the carrier densities and electric field. A Si substrate covered with a SiO_2 layer under the graphene layer is generally used as a one gate electrode, and another gate is fabricated on the top of bilayer graphene from a thin insulator.[20,22] However, the top-gate electrode may prevent optical investigation of the device. In this study, we fabricated dual gate structures containing a back-gate and an ionic liquid side-gate[36] instead of the conventional top-gate. The ionic liquid was transparent in the visible range, making optical measurements possible under an external electric field (Fig. 4-1).

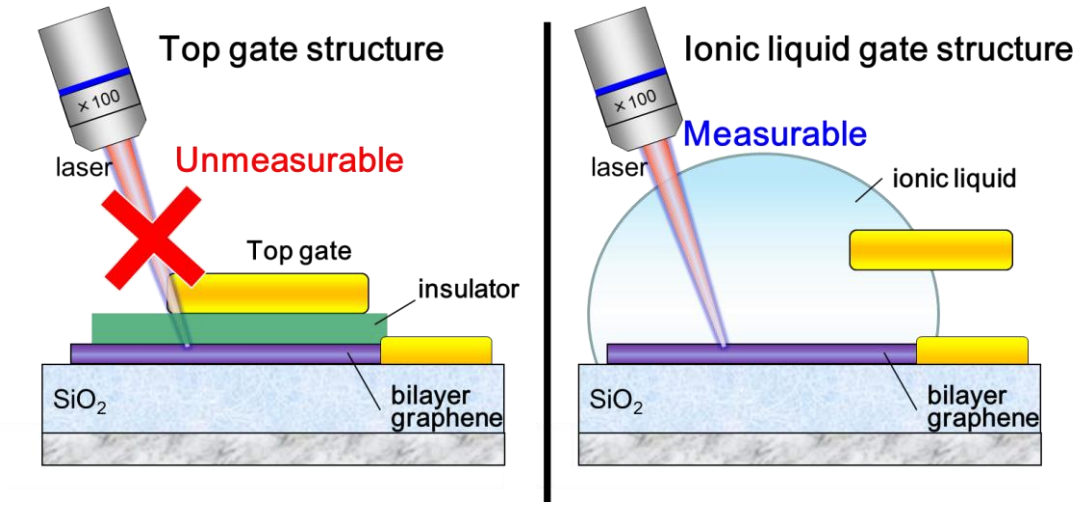

Figure 4-1. Schematics of top-gate structure and ionic-liquid-gate structure, which are irradiated by laser.

4.1.2 Kohn anomaly in Raman spectra of graphene

G-band of graphene shown in Raman spectra at ~1600 cm^{-1} indicates an optical phonon mode at the Γ point. An energy of G-band doesn't coincide with an eigen vibration of six-membered ring because the G-band energy consists of the sum of the eigen vibration and an electron-phonon (e-p) interaction energy.

$$\hbar\omega = \hbar\omega^{(0)} + \hbar\omega^{(2)} \tag{4.1}$$

where $\hbar\omega^{(0)}$ is the non-perturbative eigen vibration energy of six-membered ring, $\hbar\omega^{(2)}$ is the e-p interaction energy of second-order perturbation described by

$$\hbar\omega^{(2)} \propto -\sum_{eh} \frac{|\langle eh|V|n\rangle|^2}{E_{eh} - \hbar\omega^{(0)}}, \tag{4.2}$$

where E_{eh} is an electron-hole excitation energy. Because the second-order perturbation $\hbar\omega^{(2)}$ is negative value, the G-band energy measured in Raman is lower than $\hbar\omega^{(0)}$ of ~0.2 eV. The eigen vibration energy of six-membered ring depends on only binding force between carbon atoms. Thus, applying the gate voltage changes little the eigen energy. On the other hand, $\hbar\omega^{(2)}$ strongly depends on the gate voltage. Equation (4.2) indicates that electron-hole transitions with the excitation energy of ~0.2 eV enhances the $\hbar\omega^{(2)}$. The number of the transition of ~0.2 eV mainly determine the amount of $\hbar\omega^{(2)}$. Then, the number of the transition are changed by the gate voltage. The enhancement of the energy when E_{eh}= ~$\hbar\omega^{(0)}$ is called Kohn Anomaly.

1. Monolayer graphene

The band structure of mono layer graphene has one valence band and one conduction band. When Fermi level corresponds to Dirac point of mono layer graphene by adjustment of the gate voltage, all electron in valence band can transit to empty conduction band. On the other hand, when the positive gate voltage rises the Fermi level, Pauli' principle excludes the transition from valence band to filled conduction band shown in Fig. 4-2. When the negative voltage are applied also, the number of transition decreases because empty valence band can't transit to empty conduction band. That is why, $\hbar\omega^{(2)}$ depends on the gate voltage via changing the number of transition. Actually, G-band peak of mono layer graphene shift to low energy by applying positive or negative gate voltage.[37)]

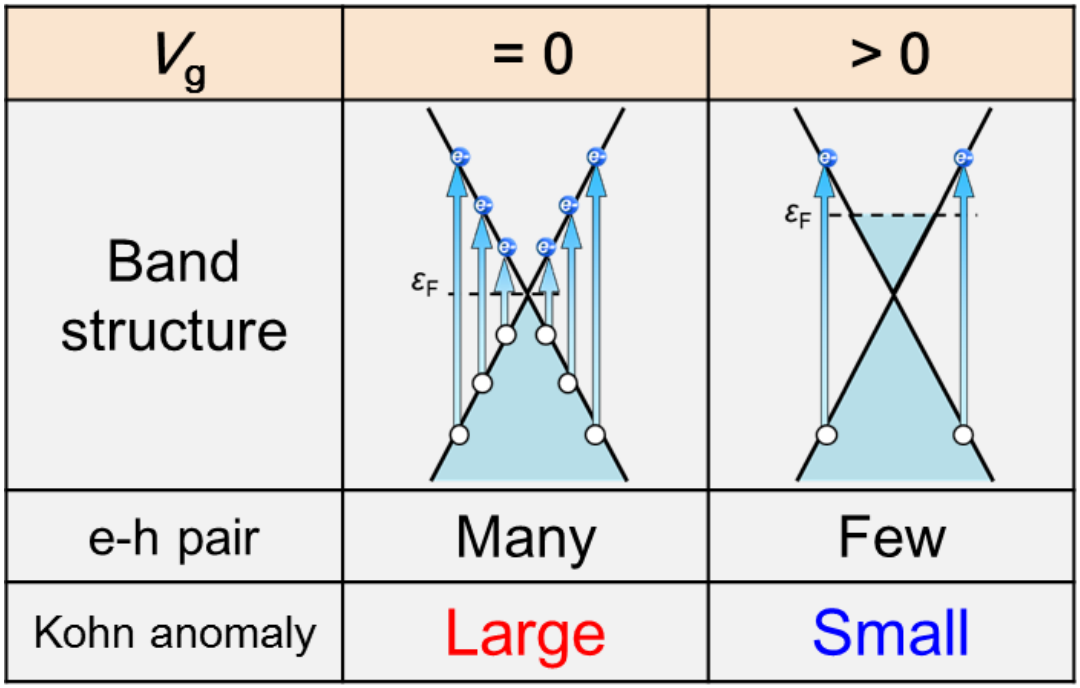

Figure 4-2. Band structures at Vg = 0 V and Vg > 0. The number of electron-hole pair is varied by applying gate voltage.

2. Bilayer graphene

G-band mode of bilayer graphene of only AB stacking will be discussed because AA-stacked bilayer graphene doesn't exist except to be artificially stacked. The AB-stacked structure of bilayer graphene has an inversion symmetry between upper and lower layers. Thus, two types of optical phonon modes at the Γ point with in-phase (IP) and out-of-phase (OP) vibrations are expected although mono layer graphene has only one mode as shown in Fig. 4-3.[38-39] IP mode corresponds to a symmetric Raman-active mode, and OP mode corresponds to an antisymmetric Raman-inactive mode while upper and lower layers keep the inversion symmtery in their emvironments. When the symmetry is broken in an external electric field, the IP and OP modes mix each other and form new two eigen vibrations. Both new peaks are observed in Raman measurements because new vibrations include Raman-active IP component.

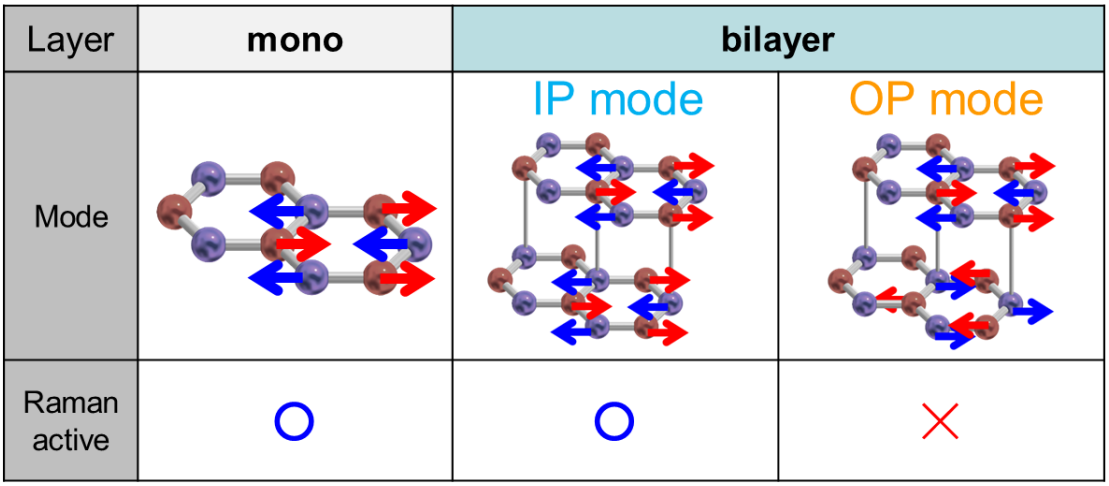

Figure 4-3 Raman activity of G band. Mono layer graphene and IP mode of bilayer graphene are Raman active.

The G_{IP} and G_{OP} band energies of bilayer graphene also obey the Eq. (4.1) and (4.2). The electronic band structure in AB-stacked bilayer graphene is that the two valence bands and two conduction bands at the K and K' points are close. The top of the valence band touches the bottom of the conduction band at the charge neutrality point. The four bands permit more transitions than the band of monolayer graphene. One is intra-band transition from upper valence band to lower conduction band. Other is inter-band transition between two valence bands or two conduction bands.

The transitions from the highest valence band to the lowest conduction band are responsible for the softening of the IP phonons. In contrast, the OP phonons are not coupled with the transitions between the conduction and the valence bands, but transition between two valence bands or two conduction band.[40] The transitions energy of intra and inter bands are strongly affected by the electrical band structure and Fermi level. Fermi level dependence are already reported in monolayer and bilayer graphene[37]. Figure 4-4 compares type of transitions and intensity of Kohn anomaly of IP mode to OP mode. In IP mode, applying gate voltage decrease Kohn anomaly because of a decrease of inter band transitions. On the other hand, in IP mode relating to intra band transition, applying gate voltage makes possible more transitions and enhance the effect of Kohn anomaly.

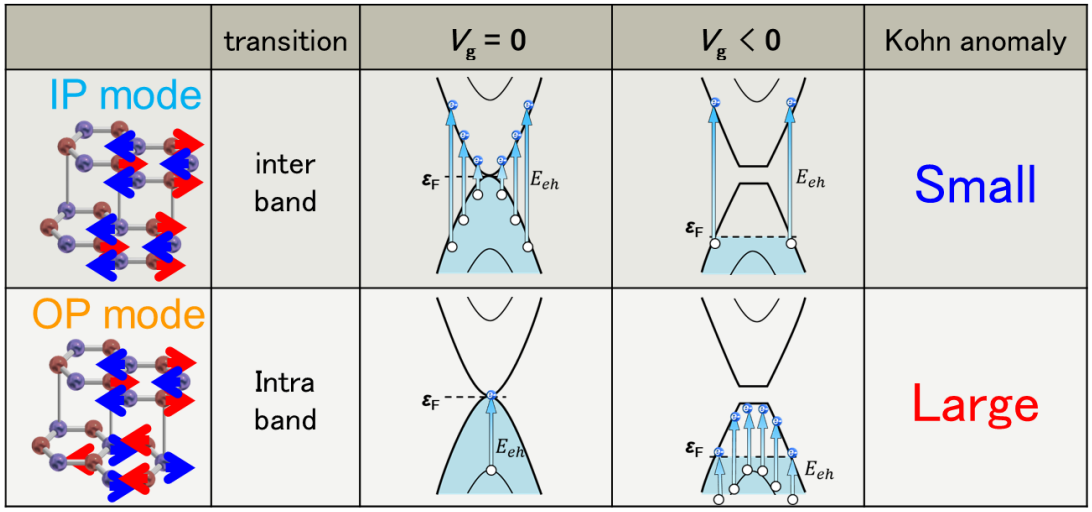

Figure 4-4. Kohn anomaly of IP and OP modes depend on gate voltage.

4.2 Purpose of this study

Applying electric field breaks an inversion symmetry of bilayer graphene and changes the band structure. Effects of the electric field are expected in the mixing of IP and OP, and in the Kohn anomaly. Purpose of this study is investigation of the effects of the change in carrier-density and the band-gap generation in bilayer graphene by Raman scattering and the electrical characteristics.

4.3 Experimental

A schematic of the bilayer graphene FET and the experimental setup are presented in Fig. 4-5(a). The fabrication process are same as shown in chapter 3. The side-gate electrodes were patterned at a distance of approximately 20 μm from the channels. The bilayer graphene FETs had been annealed before and after the ionic liquid were placed on the bilayer graphene. Needle probes could not be used for the electrical measurements because the objective lens for Raman measurements is located just above the bilayer graphene and electrode pads. Gold wire was used to connect the source, drain, back-gate, and side-gate electrodes to the printed-circuit board terminals which were connected by BNC cables to a semiconductor parameter analyzer (B1500A, Agilent). The printed circuit board was fixed to the stage of a Raman spectrometer (HR-800 UV, Horiba).

Laser light with a wavelength of 632.8 nm and a diameter of 1 μm was used to excite the Raman scattering. Electrical properties and Raman spectra were measured in air in this chapter. Thus, the electrical strength of the ionic liquid are decreased (1.0–2.0 V). Although the decreased electrical strength in air, the electrical double layer in ionic liquid can be used to change the carrier densities of bilayer graphene over a wide range, using a narrow range of side-gate voltages.

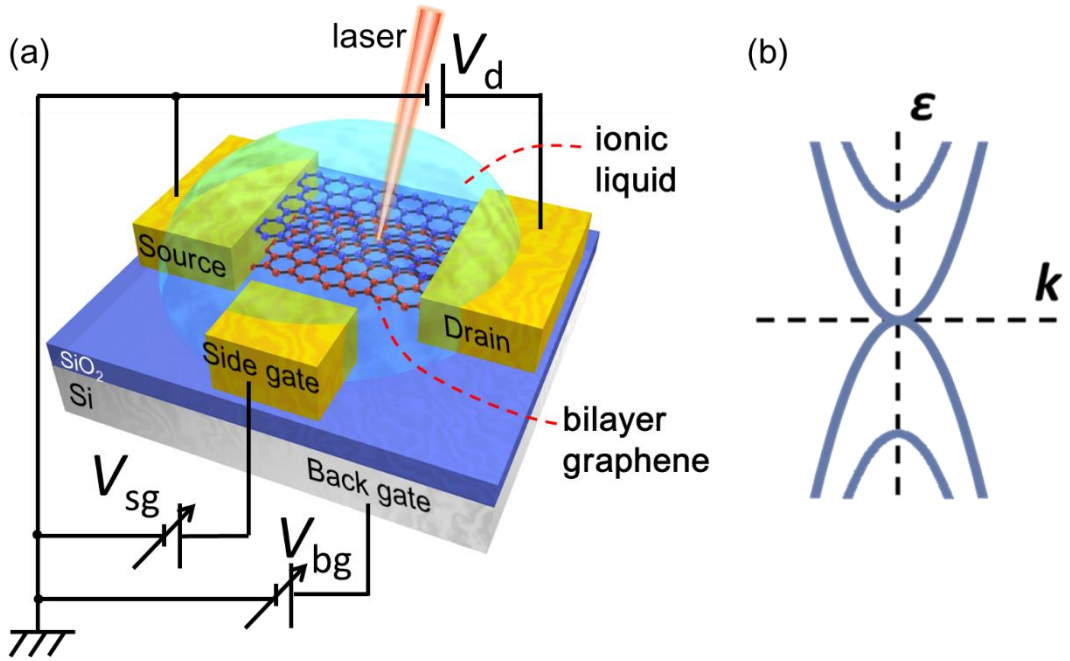

Figure 4-5. (a) Schematic of the experimental setup for the bilayer graphene FET with a transparent ionic liquid. (b) Electronic band structures of bilayer graphene around the K or K' point.

4.4 Results and Discussion

Figure 4-6 shows Raman spectra of the ionic liquid (DEME-TFSI), bilayer graphene and bilayer graphene with ionic liquid, respectively. Ionic liquid exhibit Raman peaks at lower energy than ~1500 cm^{-1}. G-band of ~1600 cm^{-1} and G'-band of ~1680 cm^{-1} don't overlap the peaks of ionic liquid, fortunately. Although only D-band energy of 1350 cm^{-1} overlap, defects of bilayer graphene are not discussed in this study. The intensity of bilayer graphene enough large even where bilayer graphene are covered with ionic liquid.

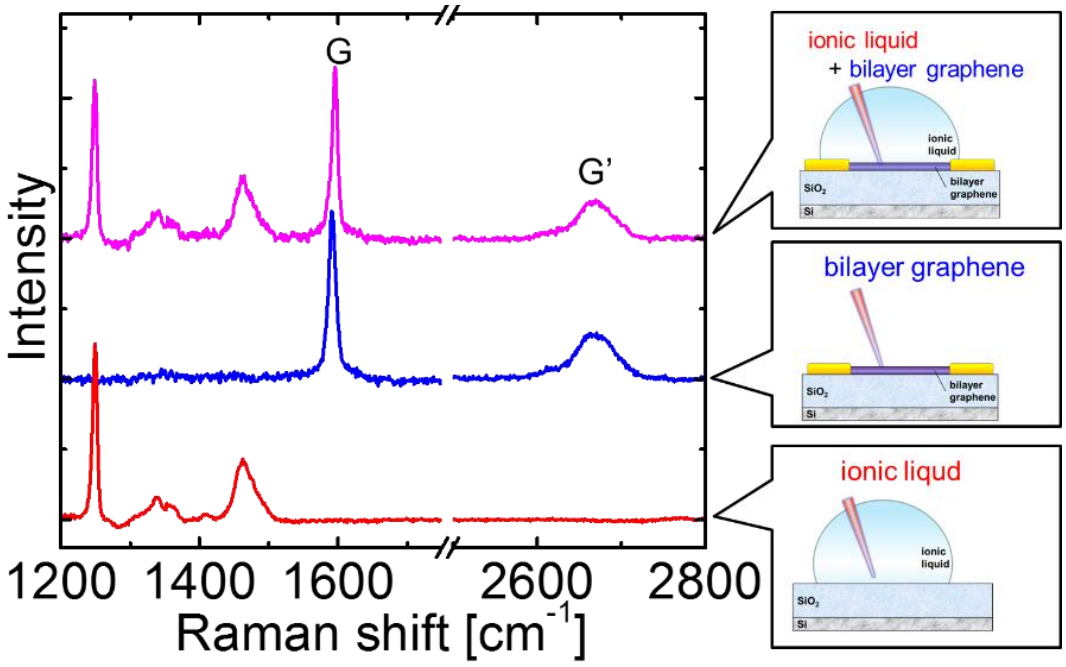

Figure 4-6. Raman spectra of ionic liquid, bilayer graphene, and bilayer graphene under the ionic liquid.

Mobile carriers are induced by applied gate bias voltages in the FET structure with bilayer graphene channels. Therefore, the electrical characteristics of the FETs shown in Fig. 4-5(a) were investigated before Raman measurements. Figure 4-7 shows the contour plots of the resistance of the bilayer graphene as a function of the back- and side-gate voltages at a drain voltage of 1 mV in air. Along the horizontal lines in the figure, the resistance changes depending on the side-gate voltage, V_{sg}, at a given constant back-gate voltage, V_{bg}. For example, along dashed line A, where V_{bg} = 0 V, the maximum resistance occurs at about V_{sg} = 1.0V. The maximum resistance indicates the Fermi energy in bilayer graphene coincides with the charge neutrality point of the electronic band structure (Fig. 4-5(b)). The charge neutrality point is similar to the Dirac point in monolayer graphene. The value of V_{sg} at the maximum point changes depending on V_{bg}, because the potential of the bilayer graphene is determined by the balance between V_{bg} and V_{sg}. For example, the maximum is at V_{sg} = 0.2 V along dashed line B, where V_{bg} = 60 V (Fig. 4-7). These maximum points produce inclined ridge line C.

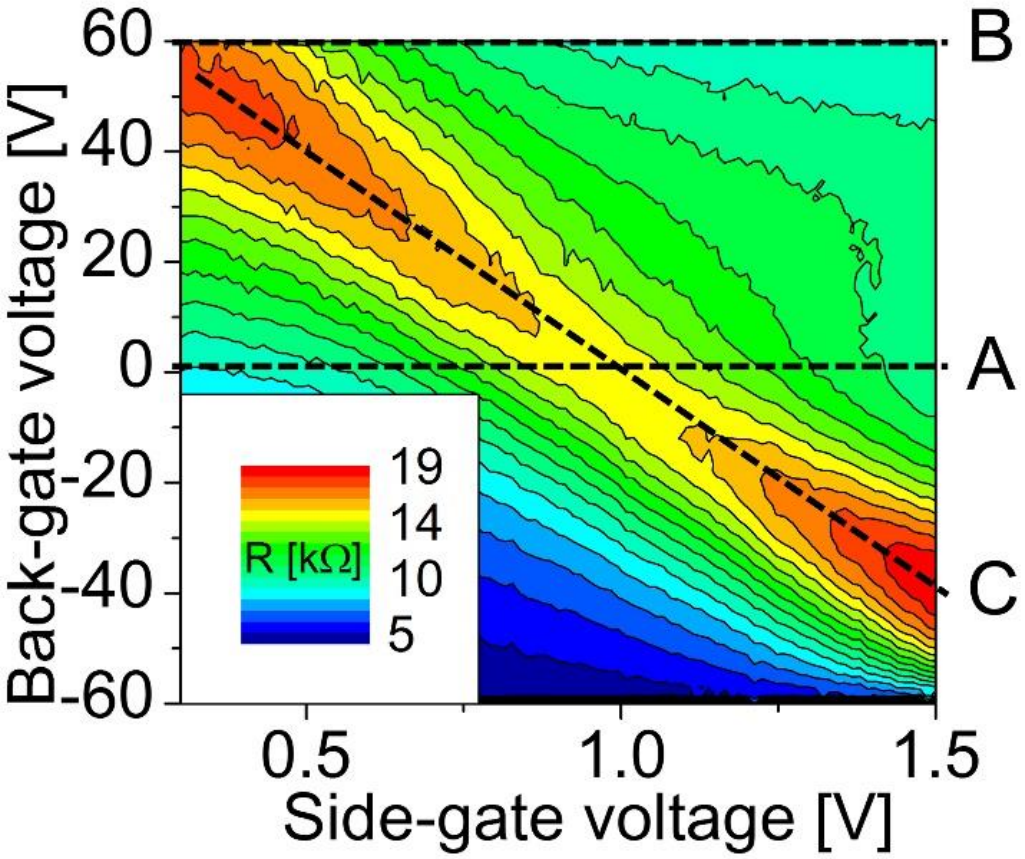

Figure 4-7. Contour plot of the channel resistance in the bilayer graphene FET as a function of two gate voltages, V_{bg} and V_{sg}. Red and blue areas correspond to areas of high and low resistance, respectively. The maximum resistance is observed at V_{sg} = 1.0 V on dashed line A at V_{bg} = 0 V and at 0.2 V on dashed line B at V_{bg} = 60 V. These maxima produce the inclined ridge line, C. Along line C, increases in resistance (red areas), caused by the generation of a band gap, are observed.

Given the potential of the bilayer graphene is constant at the charge neutral point along ridge line C, we can estimate the values of gate capacitance and the thickness of the electrical double layer from the slope of ridge line C, using the Helmholtz parallel plate model,[41)]

$$\frac{dV_{\mathrm{bg}}}{dV_{\mathrm{sg}}} = \frac{C_{\mathrm{sg}}}{C_{\mathrm{bg}}} = \frac{\varepsilon_{\mathrm{il}} d_{\mathrm{SiO2}}}{\varepsilon_{\mathrm{SiO2}} d_{\mathrm{edl}}}, \tag{4.3}$$

where C_{sg} is the capacitance of the electrical double layer, C_{bg} is the capacitance of the SiO_2 layer, ε_{il} is the relative permittivity of the ionic liquid, and ε_{SiO2} is the relative permittivity of the SiO_2 layer. Using the values $\varepsilon_{il} = 10$, $\varepsilon_{SiO2} = 3.9$, $d_{SiO2} = 300$ nm, and $dV_{bg}/dV_{sg} = 78$, d_{edl} is estimated to be 9.9 nm.

On ridge line C, where the Fermi energy coincides with the charge neutral point, the external electric field is applied depending on V_{bg} and V_{sg}, though the induced charges in the bilayer graphene are small. The change in resistance caused by the electric field is notable: increases in resistance (red areas) are observed on the upper left and lower right sides of ridge line C. As earlier study have been reported, the increases in the resistance are probably caused by the generation of a band gap in bilayer graphene.[19-20,22)] This is consistent with the constant resistance on the ridge line observed in monolayer and trilayer graphene.[32)] The layer number dependence of the electrical characteristics and the dependence of the width of the band gap in bilayer graphene on the electric field have been reported previously.[32)]

The minimum resistance is observed at $V_{bg0} = 0$ V and $V_{sg0} = 1.0$ V on ridge line C in Fig. 4-7, which indicates an external field of zero where the bilayer graphene has a band-gap energy of almost zero. The value of $V_{sg0} = 1.0$ V may arise from the contact potential between the side-gate and the ionic liquid. The external electric field can be estimated from the electrical double layer thickness. Along ridge line C, the electric field E is given by

$$E = \frac{1}{2}\left(\varepsilon_{\mathrm{SiO2}}\frac{V_{\mathrm{bg}} - V_{\mathrm{bg0}}}{d_{\mathrm{SiO2}}} - \varepsilon_{\mathrm{il}}\frac{V_{\mathrm{sg}} - V_{\mathrm{sg0}}}{d_{\mathrm{eld}}}\right). \qquad (4.4)$$

Figure 4-8 shows Raman spectra of bilayer graphene measured at $V_{bg} = 0$ V. The side-gate voltage, ΔV_{sg}, is calculated from V_{sgd} of 1.15 V, which corresponds to the maximum resistance position (charge neutrality point) along the horizontal constant V_{bg} lines (Fig. 4-7).

Figures 4-8(a)-(c) show the Raman spectra for three values of ΔV_{sg}, and Fig. 4-8(d) shows a series of spectra at side-gate voltages from +0.13 to -3.4 V. We investigated the hole-doped states, $\Delta V_{sg} < 0$, to avoid electrical breakdown of the ionic liquid. In all the spectra, two G-band peaks are visible which are fitted with two Lorentz functions. No extra peaks from the ionic liquid are present. The G-band peaks are provisionally identified as G^- on the lower energy side and G^+ on the higher energy side.[38)]

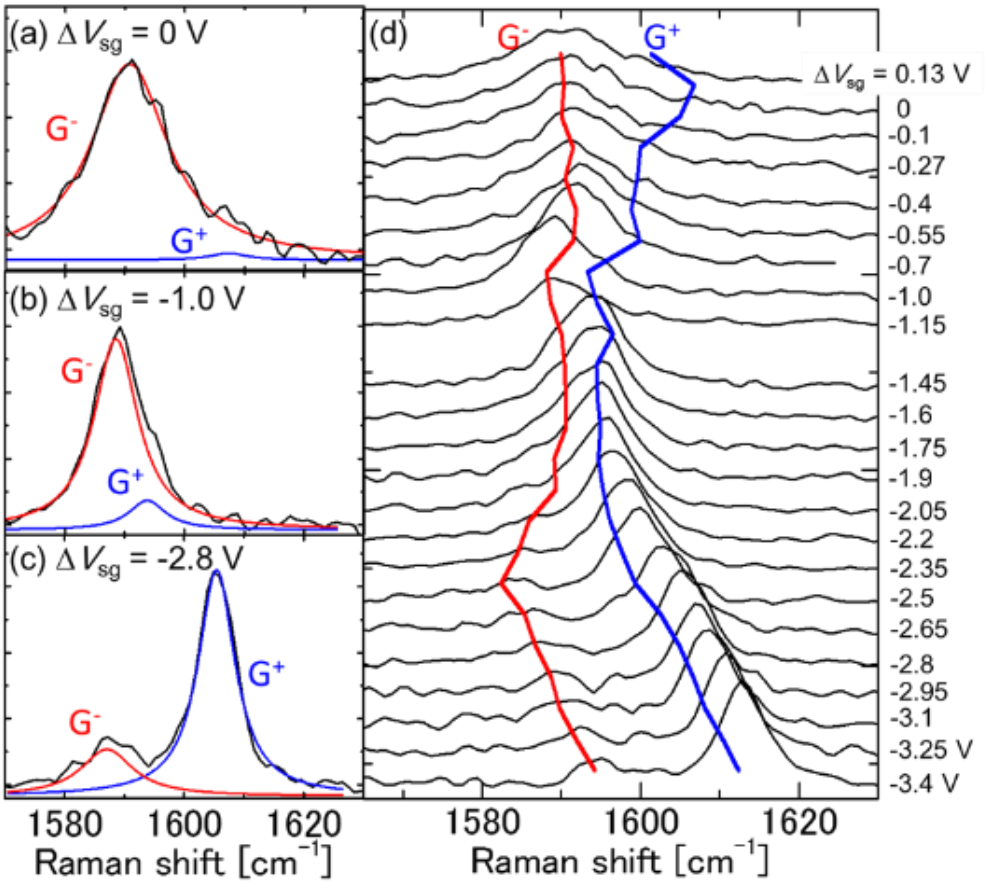

Figure 4-8. Typical Raman scattering spectra at V_{bg} = 0 V and at a ΔV_{sg}, of (a) 0.05 V, (b) -1.0 V, (c) -2.8 V, and (d) a series from ΔV_{sg} = +0.13 to -3.4 V. Traces of the Raman shifts of the G^- and G^+ peaks are indicated in (d) by the red and blue lines, respectively.

In Fig. 4-9, the positions and intensities of the two peaks as a function of ΔV_{sg} for V_{bg} = 0 V and for V_{bg} = 60 V are plotted. Although Fig.4-7 had indicated that charge neutral point is at V_{sgd} = 0.2 V along dashed line B, V_{sgd} were shifted toward high energy when the optical measurement were carried out probably because of some molecular adsorption from the atmosphere.[8] Thus, ΔV_{sg} in Fig.4-9(b) and (d) is calculated from V_{sgd} of 1.6 V. The intensity of the G^+ and G^- peaks swaps around ΔV_{sg} = -1.3 V. The intensity ratio of G^+ to G^- is about 4:1 at ΔV_{sg} = -3.0 V, whereas it is about 1:19 at ΔV_{sg} = 0 V (Fig. 4-9(a)). For V_{bg} = 60 V, the ratio is about 19:1 at ΔV_{sg} = -3.0 V, whereas it is about 1:19 at ΔV_{sg} = 0 V (Fig. 4-9(b)). This alternation of the intensity suggests that the characteristics of the phonons responsible for the two peaks swap over above and below ΔV_{sg} = -1.3 V.

The origin of the two peaks are assigned to the optical phonon modes at the Γ point with in-phase (IP) and out-of-phase (OP) vibrations of the two layers which form AB-stacked bilayer graphene. Because the bilayer graphene structure has an inversion symmetry, IP corresponds to a symmetric Raman-active mode, and OP to an antisymmetric Raman-inactive mode.[38-39] In the region where $\Delta V_{sg} > -1.0$ V, the G^- peak in the Raman spectra arises from IP vibrations, and the G^+ peak arises from OP, and vice versa in the region where $\Delta V_{sg} < -1.5$ V. The weak intensity of the Raman-inactive mode is explained by the small mixing of IP and OP vibrations induced by the partial breaking of the inversion symmetry. This is probably caused by the different environments of the bilayer graphene surfaces; the lower layer is in contact with the SiO_2 substrate, whereas the upper layer is in contact with the ionic liquid. The symmetry breaking is consistent with the lack of level crossing of the G^+ and G- lines in the transition region, $-1.5 < \Delta V_{sg} < -1.0$ (Figs. 4-9(c) and 4-9(d)).

The intensity ratio G^+: G^- in Fig. 4-9(b) of about 19:1 in the region $V_{sg} < -2.0$V for $V_{bg} = 60$ V is larger than the ratio of 4:1 in Fig. 4-9(a) for $V_{bg} = 0$ V. In the transition region, $-1.5 < \Delta V_{sg} < -1.0$, the change in intensity of G^+ and G^- occurs more abruptly for $V_{bg} = 60$ V than for $V_{bg} = 0$ V. Furthermore, the smallest splitting of the phonon energies of approximately 3 cm^{-1} for G^+ and G^- at $\Delta V_{sg} = -1.4$ V for $V_{bg} = 60$ V (Fig. 4-9(d)), is nearly half the splitting of 6 cm^{-1} for $V_{bg} = 0$ V (Fig. 4-9(c)). This indicates that the mixing of IP and OP for $V_{bg} = 60$ V is less than that for $V_{bg} = 0$ V, contrary to the prediction that the stronger electric field for $V_{bg} = 60$ V than for $V_{bg} = 0$ V should enhance the mixing, because the electric field induces the potential asymmetry in the two layers. The decoupling between the IP and OP phonons cannot be explained simply by this field effect, and probably relates to important electron-phonon interactions.

The phonon energies of the G^+ and G- peaks change considerably depending on ΔV_{sg} (Figs. 4-9(c) and (d)). There are sharp dips in the lowest G- lines at about $\Delta V_{sg} = -2.5$ V in Fig. 4-9(c), and at -2.1 and 0 V in Fig. 4-9(d). There is a shallow dip in the G^- line at about $\Delta V_{sg} = 0$ V in Fig. 4-9(c), which is visible because of the wide separation from the higher G^+ line. The softening of phonons in graphene has attracted much interest recently,[39-40,42-47] and has been interpreted in terms of the Kohn anomaly, where electron-phonon interactions play an important role.[46]

In the band structure in Fig. 4-5(b), the dispersion is mainly determined by the in-plane nearest neighbor transfer energy of electrons in the tight binding model, whereas the separation of the subband energies within the valence or conduction bands is mainly determined by the interlayer interactions.[48] The G-band optical phonon modes at the Γ point in bilayer graphene consist of the in-plane motions of the two layers.[49] Weak

interlayer interactions split them into IP and OP modes: a symmetric mode (IP), where the interlayer nearest neighbor atoms move in the opposite direction; and an antisymmetric mode (OP), where they move in the same direction. Because the in-plane electronic transfer energy is affected by the atomic motions of these phonons constructively (IP) or destructively (OP) for the two layers, the electronic states coupled to the two phonon modes are different. In the present study, the most important transition coupled to the IP mode is the transition from the higher valence subband to the lower conduction subband.[40] In contrast, the OP mode is coupled to the transition between two subbands in the valence band.[46] In the region $\Delta V_{sg} < 0$ V, where the Fermi energy is below the charge neutrality point, the higher subband states in the valence bands above the Fermi energy are empty. The electronic transitions from the lower valence subband to the higher valence subband may couple to the OP mode when the transition energies are close to the phonon energy. However, the IP phonons are barely affected by the inter-subband transitions in the valence bands. As the Fermi energy approaches the top of the lower valence subband, the number of the transitions may be maximized. Thus the dip in the lowest G- lines at $\Delta V_{sg} = -2.5$ V in Fig. 4-9(c) can be explained by the renormalization of the OP mode energy by the inter-subband transitions in the valence bands. Compared with the dip in Fig. 4-9(c), a larger dip is observed at $\Delta V_{sg} = -2.1$ V in Fig. 4-9(d) when the external field is applied. The external electric field creates the band gap at the K and K' points; therefore, the hole density of states is concentrated at the top of the valence band and the electron density of states is concentrated at the bottom of the conduction band. For this reason, the Kohn anomaly may become strong.

However, when ΔV_{sg} is around 0 V, the Fermi energy is near the charge neutral point. Instead of the inter-subband transitions in the valence bands, the transitions from the highest valence band to the lowest conduction band are dominant and responsible for the softening of the IP phonons. In contrast, the OP phonons are not coupled with the transitions between the conduction and the valence bands.[40]

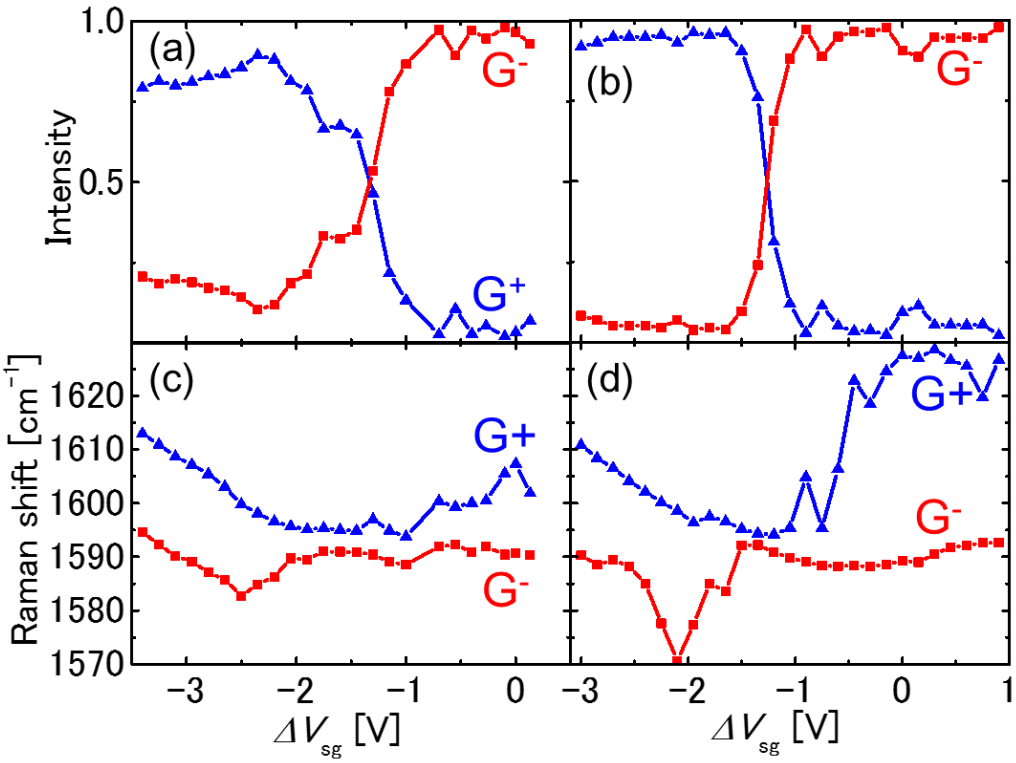

Figure 4-9. Raman intensities of the G^- and G^+ peaks as a function of ΔV_{sg} at a V_{bg} of (a) 0 V and (b) 60 V. The sum of the G^- and G^+ intensities is normalized to 1.0. The Raman shift of the G^- and G^+ peaks as a function of ΔV_{sg} at a V_{bg} of (c) 0 V and (d) 60 V. Red and blue lines correspond to the G^- and G^+ peaks, respectively.

The potential of the bilayer graphene is constant at the charge neutral point on ridge line C in Fig. 4-7. By choosing bias voltages of V_{bg} and V_{sg} on the ridge line C, the Raman spectra of bilayer graphene can be measured under the external electric field without changes in the carrier densities. We measured once again the contour plot of the channel resistance and obtained V_{bg0} of 0 V and V_{sg0} of 1.7 V. Additionally, I_d-V_{sg} characteristics at V_{bg} from -20 V to 50 V were measured to see the position of V_{sgd} just before each Raman measurement. Figure 4-10(a) shows Raman spectra at the each V_{bd} and the V_{sg} = V_{sgd}. The intensities, Raman shifts and FWHMs of the G^+ and G^- peaks are shown by Fig. 4-10(c-e). The horizontal axis corresponds to the external electric field estimated with Eq. (4-4). For comparison, Fig. 4-10(b) shows the band gap energy which is previously estimated from Arrhenius plots for another bilayer G-FET.[32] The band gap of bilayer graphene increases as the electric field is increased. The large dependence on electric field were not observed in the intensities. The most important feature is that the Raman

shift of G^+, which is assigned to the OP phonons, is almost constant at about 1620 cm^{-1} in the region of *E*, except for $E = 0$ where G^+ is shifted to a lower energy. When the valence bands are filled and the conduction bands are empty, major transitions that cause the Kohn anomaly of the OP phonons are forbidden. The exception is when $E = 0$, because the band gap energy is almost zero, some electrons at the top of the valence band can be thermally activated to the bottom of the conduction band at room temperature. The transitions from the occupied conduction band bottom states to empty higher conduction subbands, and the transitions from the lower subband of valence bands to some valence hole states, are possible and reduce the OP phonon energy by the Kohn anomaly. The FWHMs at $E = 0$ are consistently broad, although they are scattered because of the noise; the intensity of G^+ is very weak in this region. The position of the G^- peak, which is attributed to the IP phonons, is at 1590 cm^{-1} in range of *E*. This relatively low energy is explained by the Kohn anomaly caused by the transitions from the higher valence subband to the lower conduction band. A gradual increase in the FWHM of G^- is observed as *E* is increased. Eventually, the band gap energy approaches the phonon energies shown in Fig. 5(b). The concentration of the density of states accompanying the band-gap opening may strengthen the electron-phonon interactions and the excitation transitions. This may cause the broadening of the G^- peak.

In Fig. 4-9, the G^+ and G^- peaks for $V_{bg} = 60$ V mix far less than the peaks for $V_{bg} = 0$ V. Because the electronic transitions coupled to the IP and OP phonons are different, strong electron-phonon interactions separate the symmetry characteristics of IP and OP phonons and their energies. Thus, as the band-gap opening enhances the electron-phonon interactions, the mixing between the IP and OP phonons is probably reduced in the strong external electric field.

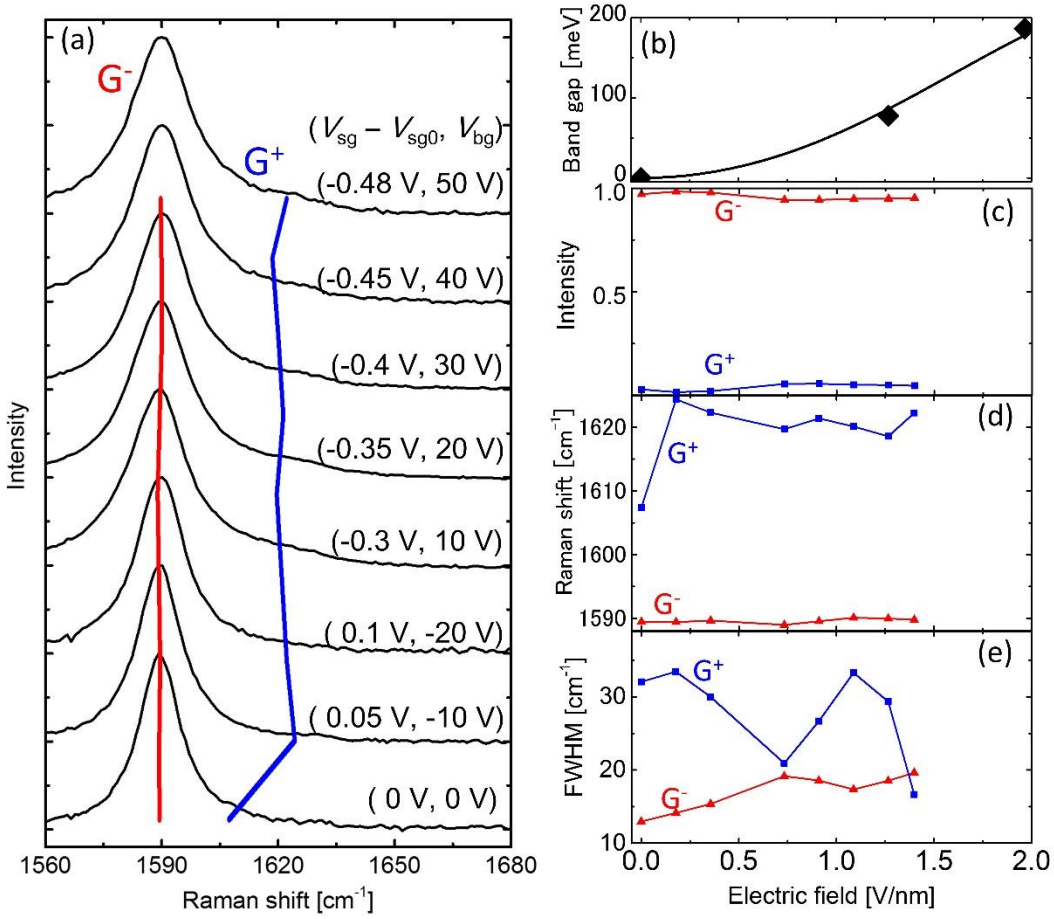

Figure 4-10. (a) A series of Raman scattering spectra from (V_{sg} - V_{sg0}, V_{bg}) = (0 V, 0 V) to (-0.48 V, 50 V). Red and blue lines indicate traces of the Raman shifts of the G- and G+ peaks, respectively. Electric field dependences of (b) band gap energies of a bilayer graphene FET, estimated from the Arrhenius plots, (c) the phonon energy, and (d) the FWHM of the Raman peaks. The potentials of bilayer graphene are kept at the charge neutral point.

4.5 Conclusions

Raman scattering spectra of bilayer graphene under a controlled electric field were measured through a transparent ionic liquid gate. Two G^+ and G^- peaks were observed in the G band Raman spectra, and their intensities and Raman shifts strongly depended on the applied electric field. The intense G^+ peak was assigned to the symmetric IP phonons, and the very weak G^- peak was assigned to the antisymmetric OP phonons in

the lower region of the side-gate voltage. When the side-gate voltage was increased to where the Fermi energy was close to the charge neutral point, the peak intensities swapped. In both regions, sharp dips were observed in a plot of the lowest G^- Raman shifts versus the side-gate voltage. These were caused by the Kohn anomaly; the IP and OP phonons were coupled with different electronic transitions near the K and K' points. The results show that the mixing between the IP and OP phonons is reduced under an external electric field, because of the enhancement of the electron-phonon interactions accompanied by the band gap opening.

Chapter 5 Floating-bridge structure of graphene with ionic-liquid gate

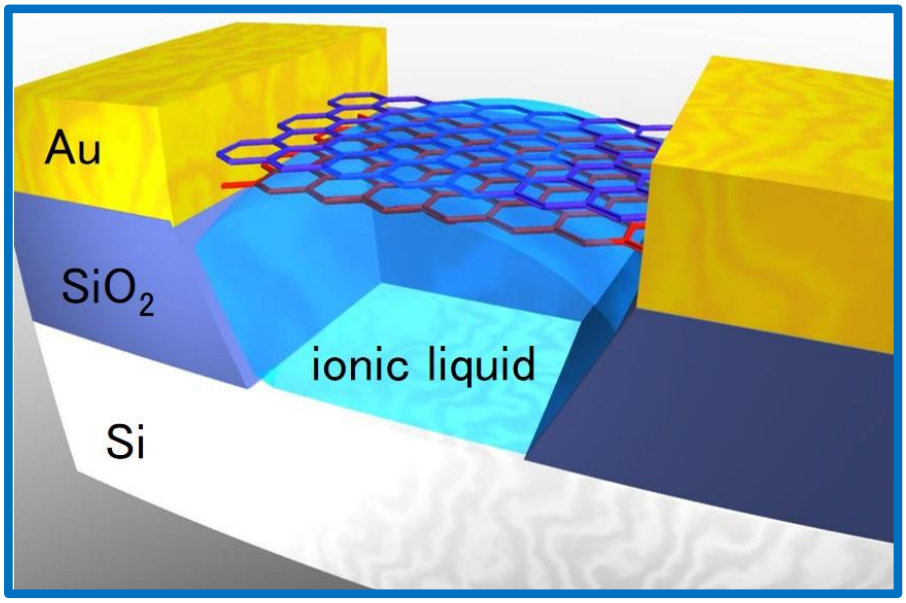

5.1 Introduction

The physical properties of the ionic-liquid-gated graphene FETs were investigated by electrical characteristics in chapter 3 and by optical measurements in chapter 4. This chapter shows applied studies for practical use. Floating-bridge structure of graphene, which is suspended graphene with the ionic liquid were fabricated. We attempt to improve the mobility and consumption power of graphene transistor by using the suspended structure and the floating-bridge structure.

5.1.1 Background

Graphene's extraordinary high mobility is expected to be used for a building block in next-generation electronics such as field-effect transistors (FETs),[50-51] high-frequency electronics,[4-5] transparent electrodes,[6-7] and high sensitivity sensors.[8-9,27] A large on/off ratio of electrical currents is essential to operate digital devices. However, graphene has low on/off ratio due to a zero-gap in graphene band structure.[1] Thus, several approaches have been attempted to create the band gap of graphene and establish that fabrication

process. Graphene nano ribbon is one of the well-known methods to generate the band gap.[15-17] However, the edge fluctuation in graphene nano ribbon is not controllable, and sensitively affects the band-gap energy of graphene.[15] Another method is to apply large electric field to bilayer graphene.[20,22,32,35] The band-gap energy can be controlled with the electric field, and the device structure is technologically easy to fabricate. However, when the band gap is created in bilayer graphene using electric field, the drain current is not switched off.[20] Figure 5-1 shows schematic of electrical characteristics of bilayer graphene and typical semiconductor. The strong dependence of drain current on gate voltage in bilayer graphene can be construction of high-frequency device or high-sensitivity devices. However, the non-off current causes high consumption devices.

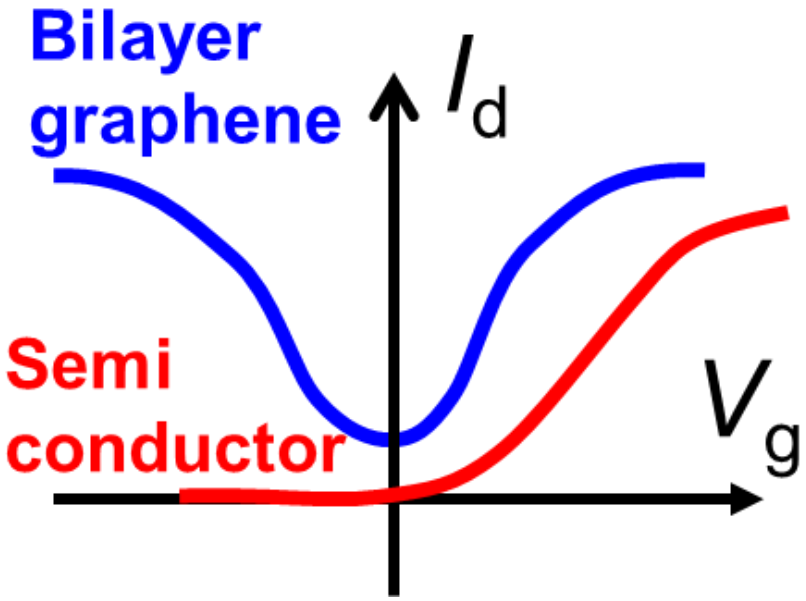

Figure 5-1 Schematic of Id vs Vg of n-type semiconductor and bilayer graphene FET.

5.1.2 Interaction between graphene and SiO_2 substrate

The too large off current despite existence of the band gap in bilayer graphene is considered to be caused by an interaction between graphene layer and Si substrate covered with SiO_2 layer. In general, charged impurities exist on the surfaces of silicon dioxide layers and create a charge puddles in graphene layer.[52-53] The charge puddle create impurity levels which allow a variable range hopping conduction in the band gap

(Fig. 5-2a and 5-2b).[20,52,54] For two dimensional conduction, it has a characteristic temperature dependence of

$$G_{\mathrm{h}} = G_0 \exp\left\{-\left(\frac{T_{\mathrm{h}}}{T}\right)^{1/3}\right\}, \tag{4.4}$$

where G_0 and T_{h} are coefficient of conduction and temperature units, respectively. When many impurity level are created in band gap, the variable range hopping conduction is as large as the thermally activated conduction which was described by Eq. (3.2). Because the variable range hopping has weaker dependence on the temperature than thermally activated conduction, the off current can't be switched off even at low temperature. As a result, the charge puddles induce the degradation of the on/off ratio in drain currents. Because the charge puddle in graphene also decrease carrier mobility, it is required to suppress the effects of interaction from SiO_2.

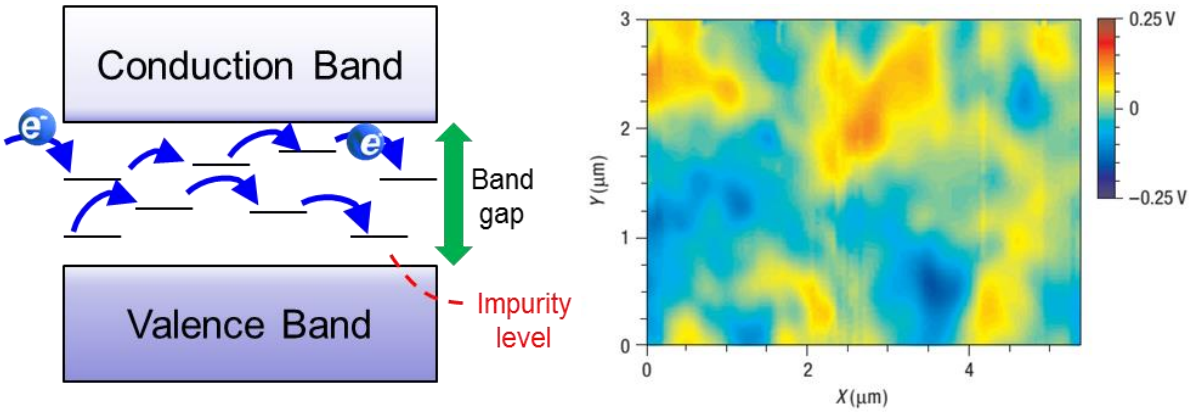

Figure 5-2 (a) Band structure of bilayer graphene with band gap. Carriers conduct through impurity levels. (b) Potential variations on the silicon oxide substrate.[52]

5.1.3 Suspended structure

Fabrication of the suspended structure is the most effective method to remove the influence from the substrate[36,55]. Actually, the highest mobility of 200,000 [cm^2/Vs] were exhibited in the suspended mono layer graphene. However, the back gate voltage must work against the vacuum owing to etching substrate surface. Hence, the relative permittivity decrease from 4 to 1, resulting in high-voltage operation devices.

5.1.4 Ionic liquid gate

When material physics were investigated in chapter 3 and 4, an electrical strength and a transparency of the ionic liquid were focused on. On the other hand, its very thin insulator is attractive for applications.

5.2 Purpose of this study

Three types of structures of graphene FETs were characterized as shown in Fig. 5-3. First is an ionic liquid gated graphene on Si/SiO_2, which is same to the device used in chapter 3. Second is a suspended graphene FET. Third is floating bridge structure bilayer graphene.

Although the suspended graphene shows high mobility and high on/off ratio, high gate voltages are demanded for operation because of low gate capacitance. Here, we have fabricated floating-bridge structures of bilayer graphene with ionic-liquid gate. After selectively removing silicon oxide layers under graphene channels, ionic liquid was introduced under the suspended graphene. Thus, owing to suppression of interaction from silicon oxide layers, graphene devices with higher performance are expected to be obtained. Moreover, electrical double layer formed in the interface between graphene and the ionic liquid makes possible a high effective electric field. The high effective electric field generates large band gap with low voltage, resulting in fabrication of low-power-consumption devices[32]. In this study, the suspended-graphene structures were observed using optical and scanning electron microscopes, and transfer characteristics were investigated in the floating-bridge structures of graphene with ionic liquid gate.

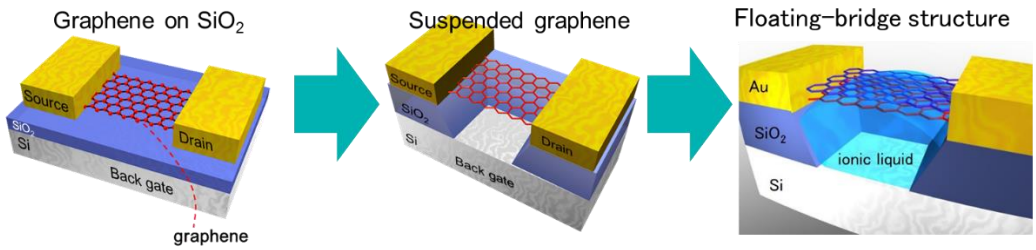

Figure 5-3 Schematics of graphene FET on SiO2, Suspended graphene, and Floating-bridge structure.

5.3 Experimental

The fabrication processes of the floating-bridge structure of graphene with ionic-liquid gate are shown in Fig. 5-4. Monolayer or bilayer graphene was prepared from bulk Kish graphite using mechanical exfoliation on a silicon substrate covered by a 300 nm thickness oxide layer. Ti/Au electrodes were formed using photolithography, electron beam lithography and metal deposition (Fig. 5-4a). The sample was covered by positive electron-beam resist, and a small hole of 0.7 μm in diameter was formed in the resist using electron-beam lithography. Subsequently, graphene at the lithographed region was removed by reactive ion plasma using oxygen (Fig. 5-4b). Then, buffered hydrofluoric acid was introduced through the hole, and the silicon dioxide layer under the graphene channel was etched for 30 minutes, resulting in fabrication of a suspended-graphene structure (Fig. 5-4c), which was observed after removing the resist by using an optical microscopy and scanning electron microscopy (SEM). Finally, the ionic liquid was dropped on the sample and was induced under the suspended graphene in vacuum (Fig. 5-4d). In this study, *N*, *N*-Diethyl-*N*-methyl-*N*-(2-methoxyethyl) ammonium bis (trifluoromethanesulfonyl) imide ([DEME] [TFSI]) was utilized as ionic liquid. The electrical characteristics of the sample were investigated using a semiconductor parameter analyzer (B1500A, Agilent).

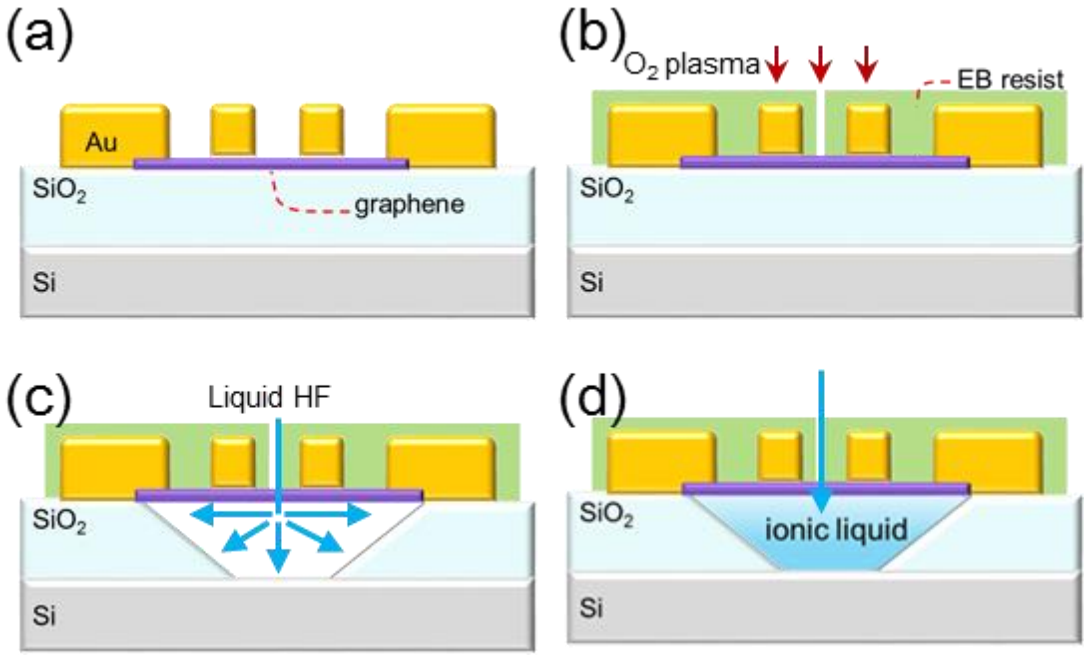

Figure 5-4. Schematics of fabrication process for floating-bridge structure of graphene with ionic liquid gate; (a) graphene FET on the Si/SiO_2 substrate, (b) dry etching process, (c) wet etching process, and (d) floating-bridge structure of graphene.

5.4 Results and Discussion

5.4.1 Ionic liquid gated graphene on SiO_2

First, the electrical characteristics of G-FETs with monolayer graphene channels in an ionic liquid were investigated. Figure 5-5(a) shows the resistance of the G-FET as a function of the back-gate voltage at 300 K in vacuum; the measurement was taken at drain and side-gate voltages of 5 and 0 mV, respectively. From the transfer characteristics, which were observed by sweeping the back-gate voltage between -100 and 100 V, ambipolar behavior was clearly observed. In addition, the resistance of the G-FET in ionic liquid was measured as a function of side-gate voltage at drain and back-gate voltages of 5 and 0 mV, respectively, at 300 K in vacuum (Fig. 5-5(b)). The inset shows an expanded view of the resistance in the ionic-gated G-FET plotted against the side-gate voltage, also showing that ambipolar characteristics were obtained. From Figs. 5-

5(a) and 5-5(b), the transconductance when using the side gate was much larger than that when using the back gate, owing to the formation of a very thin gate insulator.

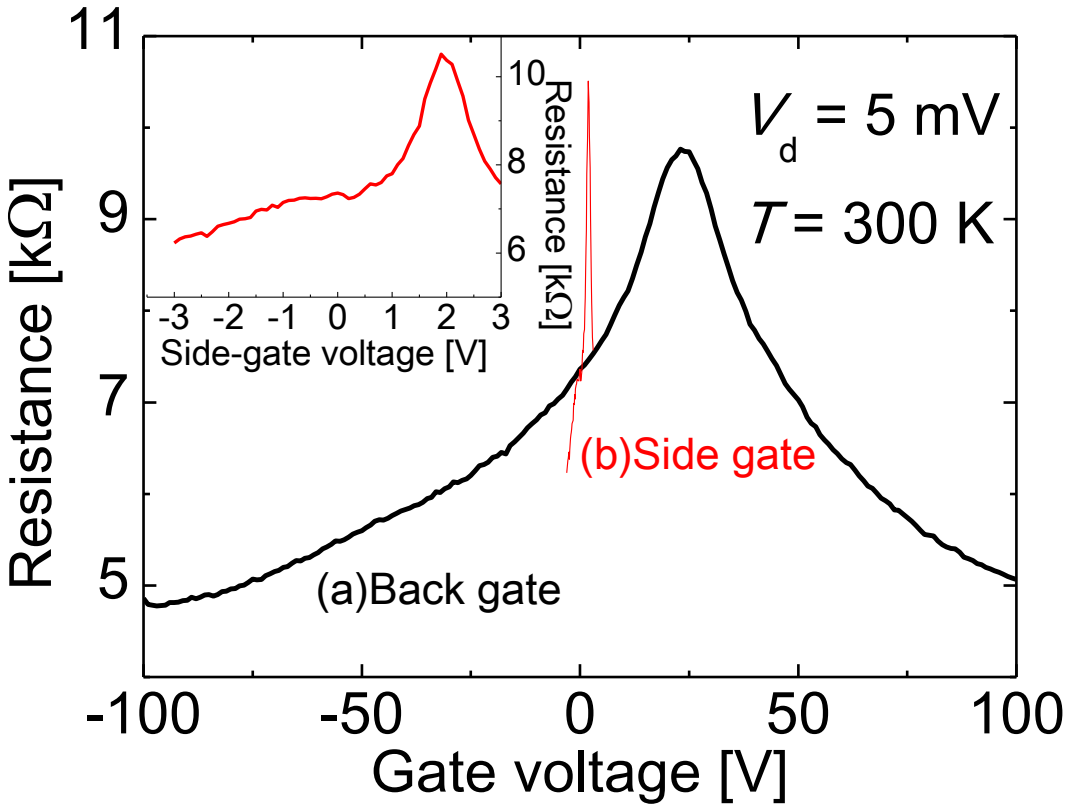

Figure 5-5. Resistance as a function of (a) back- and (b) side-gate voltages in vaccum. Inset shows expanded view of (b).

To investigate the effects of the ionic-liquid gate on the electrical characteristics in detail, resistance contour plots were constructed as a function of back- and side-gate voltages at drain voltage of 5 mV at 300 K in vacuum (Fig. 5-6). The carrier density of monolayer graphene were held constant on the dotted line because of the balance between the back- and side-gate voltages. The capacitance of the electric double layer, which was estimated from the slope of the dotted line in Fig. 5-6, was approximately 200-fold that of a 300-nm-thick SiO_2 layer. It should be noted that the effect of the electrical double layer on the side of bilayer graphene is considered to be negligible since the size of the bilayer graphene is much larger than thickness of the bilayer graphene. The thickness of the electrical double layer (d_{edl}) is calculated from the slope by using Eq.(4.3):

$$\frac{dV_{\mathrm{bg}}}{dV_{\mathrm{sg}}} = \frac{C_{\mathrm{sg}}}{C_{\mathrm{bg}}} = \frac{\varepsilon_{\mathrm{il}} d_{\mathrm{SiO2}}}{\varepsilon_{\mathrm{SiO2}} d_{\mathrm{edl}}}, \tag{4.3}$$

where C_{sg} is the capacitance of the electrical double layer, C_{bg} is the capacitance of the SiO_2 layer, ε_{il} is the relative permittivity of the ionic liquid, and ε_{SiO2} is the relative permittivity of the SiO_2 layer. For ε_{il} = 10, ε_{SiO2} = 3.9, d_{SiO2} = 300 nm, and dV_{bg}/dV_{sg} = 200, d_{edl} was estimated to be 3.85 nm, which corresponds to the length of the five ionic molecules used in this study.[56] This result is consistent with the thickness of a few nanometers previously reported for such an electrical double layer.[22]

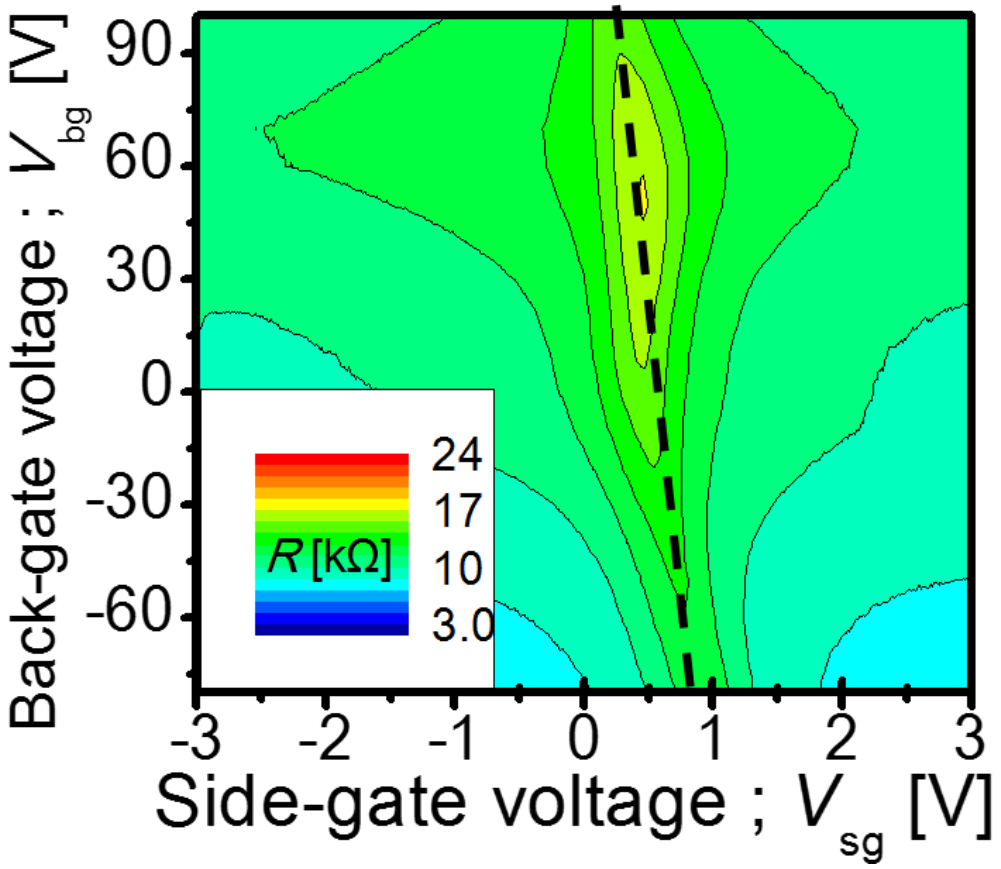

Figure 5-6 Resistance contour plots as a function of the back- and side-gate voltage in monolayer graphene

Then, the intensity of the electric field was calculated by using the electrical double layer thickness. For a dual-gate structure, the total electric field is given by

$$E = \frac{1}{2}\left(\varepsilon_1 \frac{\Delta V_1}{d_1} - \varepsilon_2 \frac{\Delta V_2}{d_2}\right). \qquad (5.1)$$

where, for gate insulator layer i (= 1 or 2), ΔV_i is the difference between the applied voltage and the charge neutrality voltage, ε_i is the relative permittivity, and d_i is the thickness. The total electric field applied to the ionic-liquid gate structure was estimated as 3.2 V/nm at side- and back-gate voltages of 2.0 and 100 V, respectively. Previously, Zhang et al. demonstrated a gate-controlled band gap in bilayer graphene, where their device structure had an amorphous Al_2O_3 top-gate insulator of 80 nm in thickness.[22] To obtain a total electric field of 3.2 V/nm by using their structure, top-gate voltage of 54 V must be applied to the Al_2O_3 top-gate insulator, which is 27-fold that in the present ionic-liquid G-FET. Therefore, the ionic-liquid G-FETs gate can generate a relatively large band gap by means of an effective electric field, which will be useful in fabricating low-power devices. Actually, 235 meV of band gap were obtained at only -3 V of side gate voltage as shown in chapter 3. Although large band gap were created in bilayer graphene, high on/off ratio in drain current were not achieved. Figure 5-7 shows side-gate dependence of a resistance at back gate voltage of -60 V in the same bilayer graphene FET to Fig.3-4 in chapter 3. When the V_{sg} of -0.5 V are applied, electric field of 0.6 V/nm are applied. The band gap is much larger than the energy of room temperature, however, the resistance are only 3.6 kilo ohm. The ratio of on and off current is 4. The electrical properties are strongly affected by charge puddles caused by interaction from SiO_2 substrate.

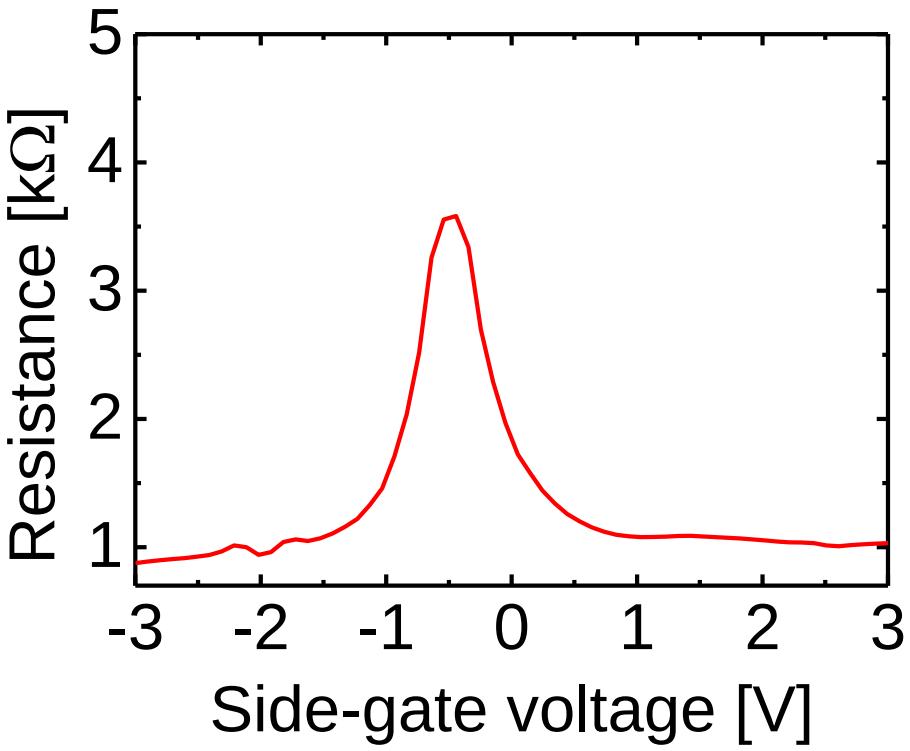

Figure 5-7 Resistance of bilayer graphene as a function of side-gate voltages.

5.4.2 Suspended structure

Figure 5-8(a) and 5-8(b) show optical-microscope images of graphene on SiO_2 layer and suspended graphene after removing the resist, respectively. The area enclosed with a dotted line in Fig. 5-8(a) corresponds to graphene. The etched regions are easily identified by the change in the color of the sample surface because the color of SiO_2 layer depends on the thickness of SiO_2 layer. The color-changed region in Fig. 5-8(b) corresponds to the shape of graphene in Fig. 5-8(a). The results indicate that the SiO_2 layer under the graphene channel was selectively etched by the buffered hydrofluoric acid. As shown in Fig. 5-8(b), the central region of the graphene has the color of white and the region around the center became dark blue. The results indicate that the SiO_2 layer under the central region of the graphene was almost removed as shown in Fig. 5-4(c).

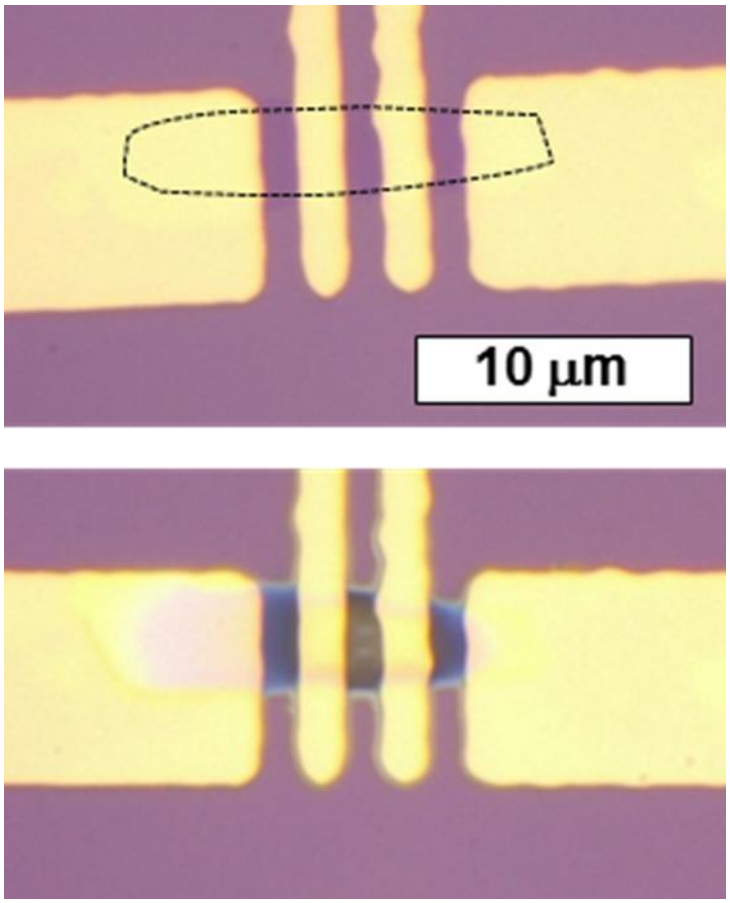

Figure 5-8 Optical micrograph images of graphene FET on SiO_2 layer and. suspended-graphene FET.

To characterize the surface and edge of graphene after etching process, the sample was observed using SEM, as shown in Fig. 5-9(a) and 5-9(b). The image in Fig. 5-9(a) reveals that the graphene channel with flat surface and the SiO_2 layer remain between the electrodes. Figure 5-9(b) shows the expanded area of the edge of the graphene channel. Any cracks, wrinkles or rolls of graphene were not observed. The results indicate that suspended structures of graphene were successfully fabricated using the process in Fig. 5-4.

Although hydrofluoric acid was introduced from the center of the graphene channel, the SiO_2 layer under the graphene channel was selectively etched. As shown in Fig. 5-9(b), the SiO_2 layer near the edge of the graphene channel was slightly etched; however, other SiO_2 region still has flat surfaces. This is considered to be attributed to anisotropic diffusion of hydrofluoric acid. It is assumed that hydrofluoric acid is easily diffused at the interface between the graphene channel and the SiO_2 layer. In conclusion, the process

in Fig. 1 is useful for fabrication of suspended structures of graphene.

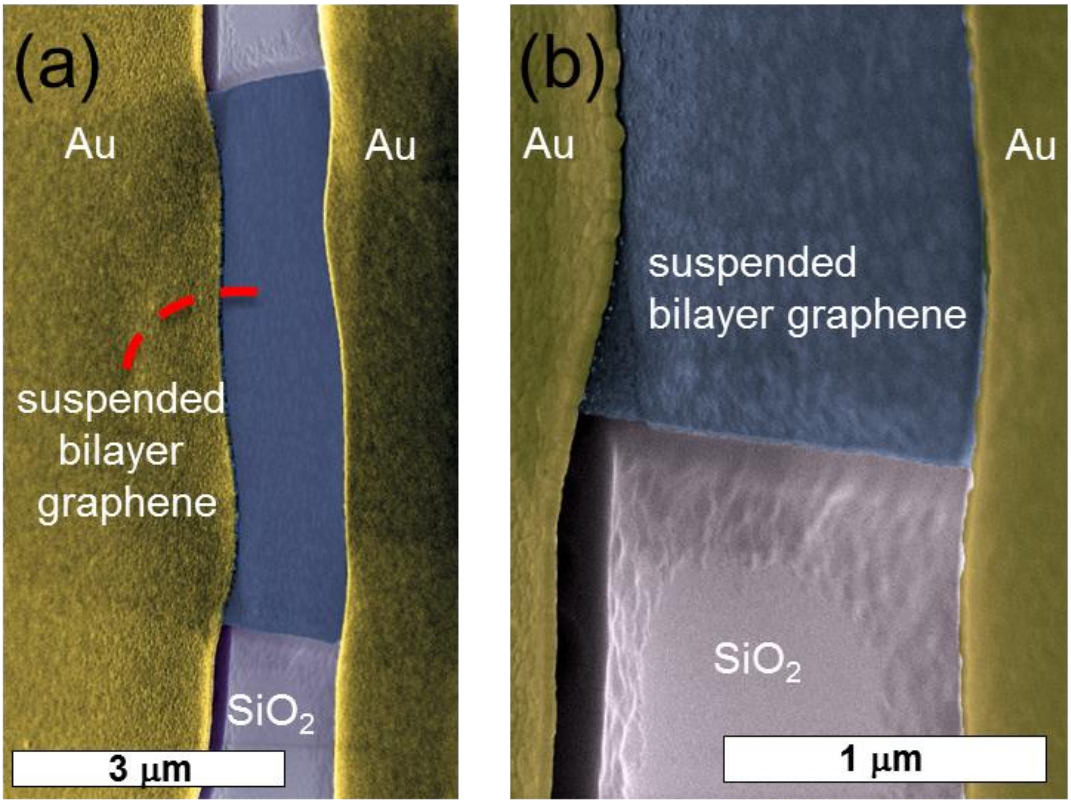

Figure 5-9 Scanning electron microscope image of suspended graphene (a) and its extended image of the edge (b).

5.4.3 Suspended monolayer graphene

The electrical characteristics of suspended-monolayer-graphene FETs were investigated using a semiconductor parameter analyzer. As shown in the inset of Fig. 5-10, the electrical characteristics were measured without removing the electron-beam resist in the experiments. Figure 5-10 shows the conductance as a function of back-gate voltage in the suspended monolayer-graphene FET without the ionic liquid. The measurement reveals that the device acted as a FET even though the SiO_2 layer under the graphene was removed. The space under the graphene channel can be regarded as the gate insulator. Since the distance between the graphene channel and the Si substrate is approximately 300 nm and the relative permittivity of the space is 1, the field-effect mobility is estimated to be 20,000 cm^2/Vs. In addition, the on/off ratio of the conductance becomes 10. In our typical graphene FETs on the SiO_2 layer using

mechanical exfoliation, mobility and on/off ratio are 3,000 – 5,000 cm^2/Vs and 3, respectively[26-27]. Therefore, the higher mobility and on/off ratio were obtained in suspended graphene owing to elimination of the charge doping from the SiO_2 layer. However, the device didn't achieve the mobility of 200,000 cm^2/Vs, which was already reported[36,57]. The electron-beam resist on the graphene may interact with graphene although not so much strong as SiO_2 layer. Additionally, etchant residues would also decrease the performance. Resist/etchant residues on the suspended graphene were not desorbed by annealing in this study because on/off ratios became worse during the annealing process. Fabrication of suspended graphene shows high performance; however, large gate voltage is necessary for operation of the device owing to the low relative permittivity of the back gate.

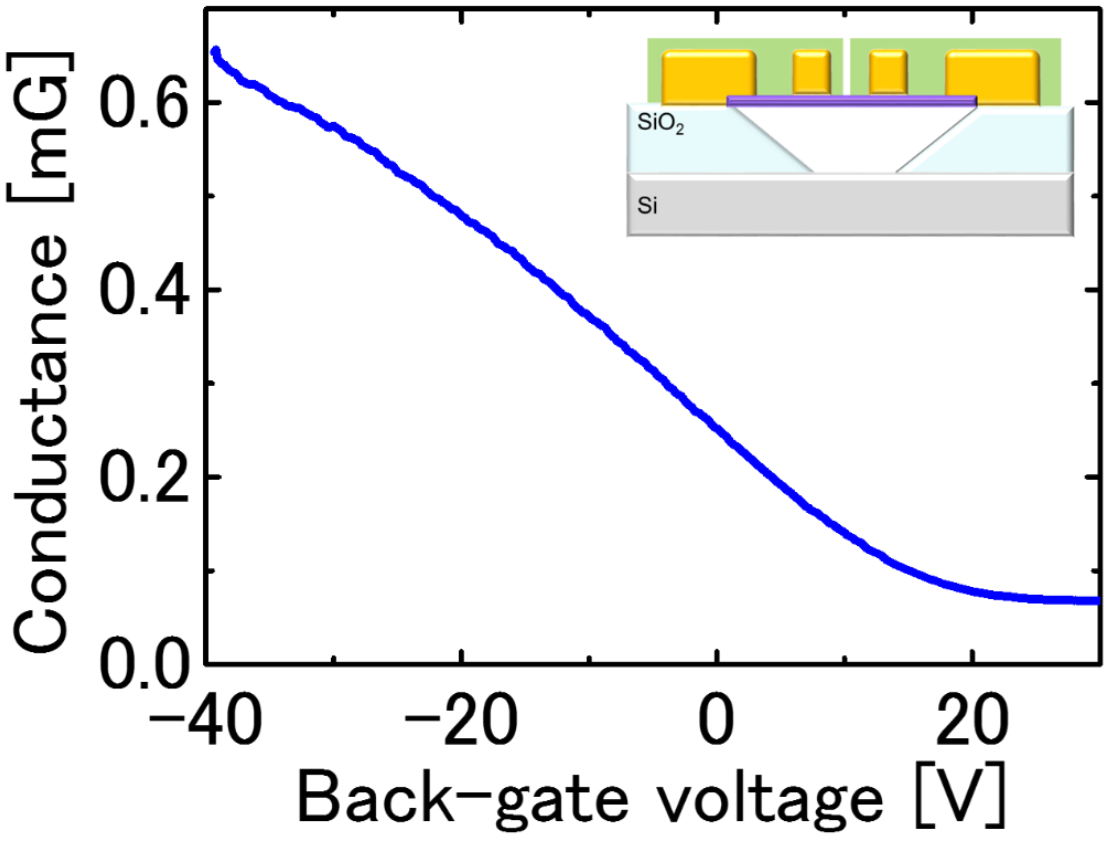

Figure 5-10. Conductance as a function of back-gate voltage of suspended monolayer graphene.

5.4.4 Floating-bridge structures

Finally, floating-bridge structures of bilayer graphene with ionic-liquid gate were fabricated. After etching the SiO_2 layer (Fig. 5-4c), the space under the graphene channel was filled with the ionic liquid as shown in the inset of Fig. 5-11. Dropped ionic liquid on channel easily goes through under the suspended bilayer graphene in a vacuum, resulting in formation of the floating-bridge structure of graphene with the ionic liquid gate. Figure 5-11 shows the back-gate dependence of the conductance in the suspended bilayer graphene device before and after introduction of the ionic liquid. The conductance before introduction of the ionic liquid becomes almost constant within a range of a few voltages because of the low gate capacitance. On the other hand, the conductance in the floating-bridge bilayer graphene with ionic-liquid gate strongly depends on the back-gate voltage. The on/off ratio was estimated to be 20, which was obtained by applying the back-gate voltage of only 2 V in the ionic liquid. When the back-gate voltage is applied, an electrical double layer forms at the graphene/liquid interface and acts as a thin back-gate insulator with a high dielectric constant. The back gate voltage of 2 V through ionic liquid corresponds to 300 V through 300-nm thick SiO_2. For this reason, large conductance was obtained with low voltage when introducing the ionic liquid. Because the upper surface of the graphene channel is masked by electron-beam resist, the electrical double layer forms at only bottom of the bilayer graphene. The asymmetrically applied electric field generate a potential difference between upper and lower graphene layers. As a result, the band gap is generated in bilayer graphene[35], thus, the off current was suppressed. Both effective electric field and generation of the band gap contribute to high on/off ratio as shown in Fig. 5-11.

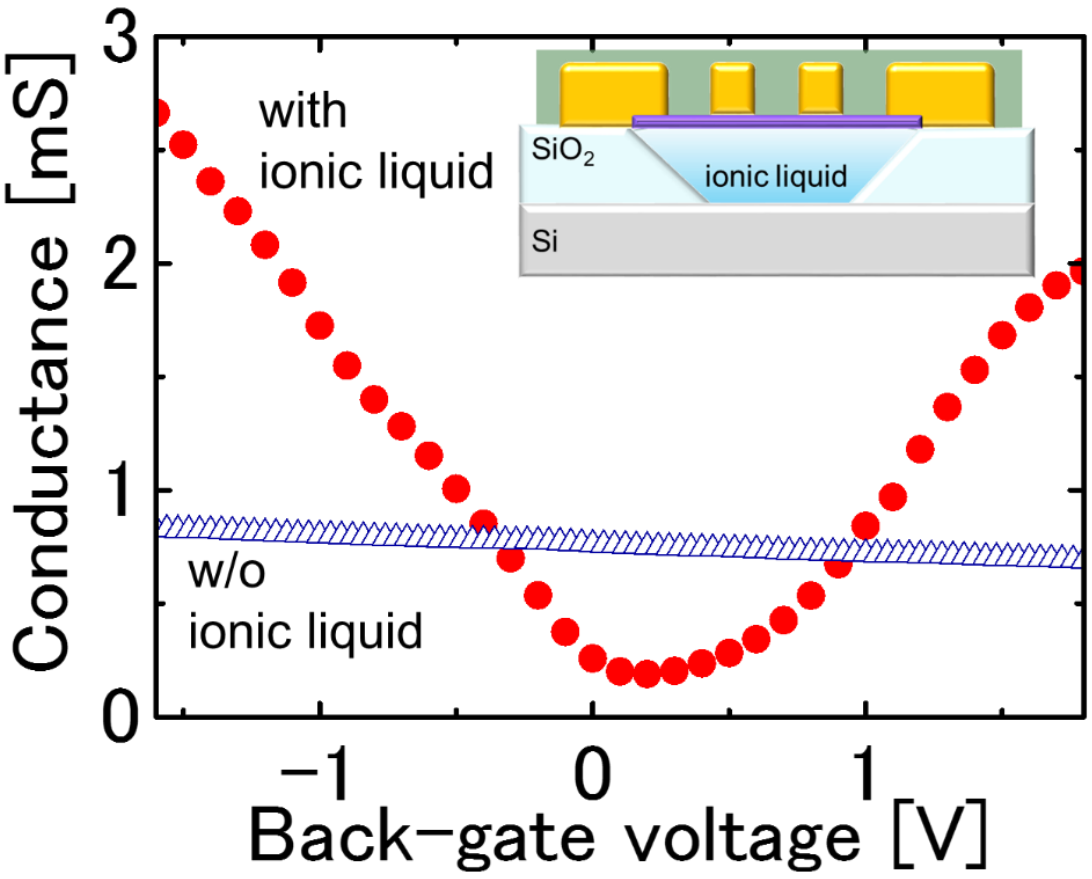

Figure 5-11. Conductance as a function of back-gate voltage of suspended bilayer graphene without and with ionic liquid.

5.5 Conclusions

Floating bridge structures of graphene with ionic liquid have been successfully fabricated. After selectively etching the SiO_2 layer under the graphene channel, the mobility of 20,000 cm^2/Vs was achieved in the suspended monolayer graphene, which is attributed to the suppression of the charge doping from SiO_2 layer. Floating bridge structures of bilayer graphene with the ionic-liquid gate have low-power operation and 20-fold on/off ratio in the conductance. The band gap is considered to be generated in the bilayer graphene. Therefore, floating bridge structures of graphene with the ionic-liquid gate are useful for fabricating high-peformance and low-power-consumption devices.

Chapter 6 Summaries

- Summaries of chapter 1

  The unique properties of graphene, method of band-gap creation, and purpose of this thesis were described in chapter 1.

- Summaries of chapter 2

  We have prepared graphene layers on Si/SiO_2 substrate by mechanical exfoliated method and fabricated graphene FETs. The number of graphene layer was identified by optical images and Raman spectra. Mobility and on/off ratio of graphene FETs on the SiO_2 layer were 3,000 – 5,000 cm^2/Vs and 3, respectively. We confirmed that atmosphere exposure decreases mobility of graphene and shifts the charge neutrality point because of absorption of oxygen and water molecules. In this chapter, fabrication process and characterization methods of graphene FETs without an ionic liquid were described.

- Summaries of chapter 3

  We have fabricated ionic-liquid-gated G-FETs to create a band gap in bilayer graphene. Electrical measurements revealed that the resistance in the bilayer G-FET monotonically increased as the electric-field intensity was increased. In contrast, the resistance in the monolayer and trilayer G-FETs at the charge neutrality were nearly constant. These findings are attributable to a band gap forming in the bilayer graphene, but not the mono- or tri-layer graphene. A band gap of 235 meV in bilayer graphene was created at an ionic-gate-voltage of -3.0 V, as determined from Arrhenius plots. Ionic-liquid-gated structure should be useful in creating band gap of bilayer graphene.

- Summaries of chapter 4

  Optical properties of bilayer graphene were investigated in chapter 4. Raman scattering spectra of bilayer graphene under a controlled electric field were measured through a transparent ionic liquid gate. Two G^+ and G^- peaks were observed in the G band Raman spectra, and their intensities and Raman shifts strongly depended on the applied electric field. The intense G^+ peak was assigned to the symmetric IP phonons, and the very weak G^- peak was assigned to the antisymmetric OP phonons in the lower region of the side-gate voltage. When the

side-gate voltage was increased to where the Fermi energy was close to the charge neutral point, the peak intensities swapped. In both regions, sharp dips were observed in a plot of the lowest G^- Raman shifts versus the side-gate voltage. These were caused by the Kohn anomaly; the IP and OP phonons were coupled with different electronic transitions near the K and K' points. The results show that the mixing between the IP and OP phonons is reduced under an external electric field, because of the enhancement of the electron-phonon interactions accompanied by the band gap opening.

- Summaries of chapter 5

  Floating bridge structures of graphene with ionic liquid have been successfully fabricated. After selectively etching the SiO_2 layer under the graphene channel, the mobility of 20,000 cm^2/Vs was achieved in the suspended monolayer graphene, which is attributed to the suppression of the charge doping from SiO_2 layer. Floating bridge structures of bilayer graphene with the ionic-liquid gate have low-power operation and 20-fold on/off ratio in the conductance. The band gap is considered to be generated in the bilayer graphene. Therefore, floating bridge structures of graphene with the ionic-liquid gate are useful for fabricating high-peformance and low-power-consumption devices.

- Summaries of this work

  We attempted to fabricate new structure of graphene FET by using ionic liquid gate. This work revealed that physical properties relating to band gap in bilayer graphene using ionic liquid and its excellent properties for an application to transistor.

Acknowledgement

I would like to express the sincerest gratitude to Professor Kazuhiko Matsumoto of ISIR, Osaka University for the thoughtful guidance, supports and discussion.

I am very grateful to two supervisors for this thesis, Professor Hirokazu Tada and Professor Hiroshi Yoshida, of Graduate School of Engineering Science, Osaka University.

I deeply express my gratitude to Associate Professor Koichi Inoue, Associate Professor Kenzo Maehashi and Associate Professor Yasuhide Ohno of ISIR, Osaka University for the guidance, advice on experiments, helpful discussion and continuous encouragement.

I would like to express my gratitude to Professor Mototsugu Ogura of ISIR, Osaka University.

I would like to express my gratitude to Assistant Professor Yasushi Kanai of ISIR, Osaka University for helpful discussion.

I thank to Mrs. Reiko Yamauchi of secretaries of Professor Matsumoto for supports in my study.

I wishes to express my thanks to Mr. Takashi Ikuta, Mr. Keisuke Koshida and Mrs. Nursakinah Binti Mohd Zaifuddin for the support on the experiments.

I would like to thank Mr. Takeshi Oe, Mr. Kohei Seike, Mr. Masatoshi Nakamura, Mr. Yusuke Ishibashi, and Mr. Masayuki Okano, of Matsumoto laboratory for assistance on the experiments.

I wish to express my thanks to Mr. Takahiro Ohori, Mr. Yasuhumi Hakamata, Mr. Hideto Onodera for constant encouragement and discussion.

I thank to Mr. Satoshi Okuda, Mr. Yasuyuki Sofue, Mr. Kenta Gumi, Mr. Yusuke Fuji, Mr. Shogo Okamoto for their kind encouragement.

Finally, I would like to express my deep thanks to my family for their support and warm encouragement.

Bibliography

1) A. K. Geim and K. S. Novoselov, Nat Mater 6 (2007) 183.

2) I. Meric, M. Y. Han, A. F. Young, B. Ozyilmaz, P. Kim, and K. L. Shepard, Nat Nano 3 (2008) 654.

3) D. Kondo, S. Sato, K. Yagi, N. Harada, M. Sato, M. Nihei, and N. Yokoyama, Appl. Phys. Express 3 025102.

4) L. Liao, Y.-C. Lin, M. Bao, R. Cheng, J. Bai, Y. Liu, Y. Qu, K. L. Wang, Y. Huang, and X. Duan, Nature 467 (2010) 305.

5) Y.-M. Lin, K. A. Jenkins, A. Valdes-Garcia, J. P. Small, D. B. Farmer, and P. Avouris, Nano Lett. 9 (2008) 422.

6) K. S. Kim, Y. Zhao, H. Jang, S. Y. Lee, J. M. Kim, K. S. Kim, J.-H. Ahn, P. Kim, J.-Y. Choi, and B. H. Hong, Nature 457 (2009) 706.

7) X. Wang, L. Zhi, and K. Mullen, Nano Lett. 8 (2007) 323.

8) F. Schedin, A. K. Geim, S. V. Morozov, E. W. Hill, P. Blake, M. I. Katsnelson, and K. S. Novoselov, Nat Mater 6 (2007) 652.

9) Y. Ohno, K. Maehashi, and K. Matsumoto, J. Am. Chem. Soc. 132 (2010) 18012.

10) Y. Sofue, Y. Ohno, K. Maehashi, K. Inoue, and K. Matsumoto, Jpn. J. Appl. Phys. 50 06GE07.

11) K. Bolotin, K. Sikes, Z. Jiang, M. Klima, G. Fudenberg, J. Hone, P. Kim, and H. Stormer, Solid State Communications 146 (2008) 351.

12) R. R. Nair, P. Blake, A. N. Grigorenko, K. S. Novoselov, T. J. Booth, T. Stauber, N. M. R. Peres, and A. K. Geim, Science 320 (2008) 1308.

13) A. A. Balandin, S. Ghosh, W. Bao, I. Calizo, D. Teweldebrhan, F. Miao, and C. N. Lau, Nano Lett. 8 (2008) 902.

14) M. Y. Han, J. C. Brant, and P. Kim, Phys. Rev. Lett. 104 (2010) 056801.

15) X. Li, X. Wang, L. Zhang, S. Lee, and H. Dai, Science 319 (2008) 1229.

16) M. Y. Han, B. Özyilmaz, Y. Zhang, and P. Kim, Phys. Rev. Lett. 98 (2007) 206805.

17) K. A. Ritter and J. W. Lyding, Nat Mater 8 (2009) 235.

18) Y. Yinxiao and R. Murali, Electron Device Letters, IEEE 31 (2010) 237.

19) J. B. Oostinga, H. B. Heersche, X. Liu, A. F. Morpurgo, and L. M. K. Vandersypen, Nat Mater 7 (2007) 151.

20) H. Miyazaki, K. Tsukagoshi, A. Kanda, M. Otani, and S. Okada, Nano Lett. 10 (2010) 3888.

21) E. McCann, Physical Review B (Condensed Matter and Materials Physics) 74 (2006).

22) Y. Zhang, T.-T. Tang, C. Girit, Z. Hao, M. C. Martin, A. Zettl, M. F. Crommie, Y. R. Shen, and F. Wang, Nature 459 (2009) 820.

23) P. Blake, E. W. Hill, A. H. Castro Neto, K. S. Novoselov, D. Jiang, R. Yang, T. J. Booth, and A. K. Geim, Appl. Phys. Lett. 91 (2007) 063124.

24) W. Ying Ying, G. Ren Xi, N. Zhen Hua, H. Hui, G. Shu Peng, Y. Huan Ping, C. Chun Xiao, and Y. Ting, Nanotechnology 23 (2012) 495713.

25) K. S. Novoselov, D. Jiang, F. Schedin, T. J. Booth, V. V. Khotkevich, S. V. Morozov, and A. K. Geim, Proceedings of the National Academy of Sciences of the United States of America 102 (2005) 10451.

26) S. Okamoto, Y. Ohno, K. Maehashi, K. Inoue, and K. Matsumoto, Jpn. J. Appl. Phys. 51 (2012) 06FD08.

27) Y. Sofue, Y. Ohno, K. Maehashi, K. Inoue, and K. Matsumoto, Jpn. J. Appl. Phys. 50 (2011) 06GE07.

28) K. Maehashi, T. Katsura, K. Kerman, Y. Takamura, K. Matsumoto, and E. Tamiya, Anal. Chem. 79 (2007) 782.

29) Y. Ohno, K. Maehashi, Y. Yamashiro, and K. Matsumoto, Nano Lett. 9 (2009) 3318.

30) T. Sato, G. Masuda, and K. Takagi, Electrochim. Acta 49 (2004) 3603.

31) H. Yuan, H. Shimotani, A. Tsukazaki, A. Ohtomo, M. Kawasaki, and Y. Iwasa, Adv. Funct. Mater. 19 (2009) 1046.

32) Y. Yamashiro, Y. Ohno, K. Maehashi, K. Inoue, and K. Matsumoto, J. Vac. Sci. Technol. B 30 (2012) 03D111.

33) T. Ohta, A. Bostwick, T. Seyller, K. Horn, and E. Rotenberg, Science 313 (2006) 951.

34) S. M. Sze and K. K. Ng, *Physics of Semiconductor Devices*, 3rd ed. (Wiley, New York, 2007).

35) H. Min, B. Sahu, S. Banerjee, and A. H. MacDonald, Phys. Rev. B 75 (2007) 155115.

36) K. I. Bolotin, K. J. Sikes, Z. Jiang, M. Klima, G. Fudenberg, J. Hone, P. Kim, and H. L. Stormer, Solid State Commun. 146 (2008) 351.

37) A. Das, S. Pisana, B. Chakraborty, S. Piscanec, S. K. Saha, U. V. Waghmare, K. S. Novoselov, H. R. Krishnamurthy, A. K. Geim, A. C. Ferrari, and A. K. Sood, Nat. Nanotechnol. 3 (2008) 210.

38) J. Yan, T. Villarson, E. A. Henriksen, P. Kim, and A. Pinczuk, Phys. Rev. B 80 (2009) 241417.

39) T. Ando, J. Phys. Soc. Jpn. 76 (2007) 104711.

40) L. M. Malard, D. C. Elias, E. S. Alves, and M. A. Pimenta, Phys. Rev. Lett. 101 (2008) 257401.

41) D. C. Grahame, Chem. Rev. 41 (1947) 441.

42) I. Milošević, N. Kepčija, E. Dobardžić, M. Mohr, J. Maultzsch, C. Thomsen, and M. Damnjanović, Phys. Rev. B 81 (2010) 233410.

43) F. de Juan and H. A. Fertig, Phys. Rev. B 85 (2012) 085441.

44) A. Allard and L. Wirtz, Nano Lett. 10 (2010) 4335.

45) D. L. Mafra, L. M. Malard, S. K. Doorn, H. Htoon, J. Nilsson, A. H. Castro Neto,

and M. A. Pimenta, Phys. Rev. B 80 (2009) 241414.

46) T. Ando and M. Koshino, J. Phys. Soc. Jpn. 78 (2009) 034709.

47) A. Das, B. Chakraborty, S. Piscanec, S. Pisana, A. K. Sood, and A. C. Ferrari, Phys. Rev. B 79 (2009) 155417.

48) E. McCann, Phys. Rev. B 74 (2006) 161403.

49) A. C. Ferrari and D. M. Basko, Nat. Nanotechnol. 8 (2013) 235.

50) I. Meric, M. Y. Han, A. F. Young, B. Ozyilmaz, P. Kim, and K. L. Shepard, Nat. Nanotechnol. 3 (2008) 654.

51) D. Kondo, S. Sato, K. Yagi, N. Harada, M. Sato, M. Nihei, and N. Yokoyama, Appl. Phys. Express 3 (2010) 025102.

52) J. Martin, N. Akerman, G. Ulbricht, T. Lohmann, J. H. Smet, K. von Klitzing, and A. Yacoby, Nat Phys 4 (2008) 144.

53) X. Y. Fan, R. Nouchi, and K. Tanigaki, J Phys Chem C 115 (2011) 12960.

54) N. F. Mott, in *Festkörperprobleme 9*, edited by O. Madelung (Springer Berlin Heidelberg, 1969), Vol. 9, pp. 22.

55) X. Du, I. Skachko, A. Barker, and E. Y. Andrei, Nature nanotechnology 3 (2008) 491.

56) Y.-J. Kim, Y. Matsuzawa, S. Ozaki, K. C. Park, C. Kim, M. Endo, H. Yoshida, G. Masuda, T. Sato, and M. S. Dresselhaus, J. Electrochem. Soc. 152 (2005) A710.

57) S. V. Morozov, K. S. Novoselov, M. I. Katsnelson, F. Schedin, D. C. Elias, J. A. Jaszczak, and A. K. Geim, Phys. Rev. Lett. 100 (2008) 016602.

Publication list

Scientific Journals – first author –

1) [5]**Yusuke Yamashiro**, [4]Yasuhide Ohno, [3]Kenzo Maehashi, [2]Koichi Inoue, and [1]Kazuhiko Matsumoto,
"Electric-field-induced band gap of bilayer graphene in ionic liquid",
J. Vac. Sci. Technol. B **30**, 03D111 (2012).

2) **Yusuke Yamashiro**, Yasuhide Ohno, Kenzo Maehashi, Koichi Inoue, and Kazuhiko Matsumoto,
"Floating-bridge structure of graphene with ionic-liquid gate",
Phys. Status Solidi C **10**, 1604 (2013).

3) **Yusuke Yamashiro**, Koichi Inoue, Yasuhide Ohno, Kenzo Maehashi, and Kazuhiko Matsumoto,
"Electric field-dependence of optical phonons in Raman scattering spectra of bilayer graphene",
Journal of the Physical Society of Japan (2013). (accepted)

Scientific Journals – co-author –

1) Yasuhide Ohno, Kenzo Maehashi, **Yusuke Yamashiro**, and Kazuhiko Matsumoto,
"Electrolyte-Gated Graphene Field-Effect Transistors for Detecting pH and Protein Adsorption",
Nano Lett. **9**, 3318 (2009).

International Conferences

[Oral]

1) Yusuke Yamashiro, Yasuhide Ohno, Kenzo Maehashi, Koichi Inoue, and Kazuhiko Matsumoto, "Electric-field-induced band gap of bilayer graphene in ionic liquid", *International Conference on Solid State Devices and Materials 2011*, K-9-2, Nagoya (2011).

2) Yusuke Yamashiro, Yasuhide Ohno, Kenzo Maehashi, Koichi Inoue, and Kazuhiko Matsumoto, "Band-gap Generation by using Ionic-Liquid Gate in Bilayer Graphene", *AVS the 58th International Symposium & Exhibition*, 415, Nashville (2011).

3) Yusuke Yamashiro, Yasuhide Ohno, Kenzo Maehashi, Koichi Inoue, and Kazuhiko Matsumoto, "Generating band gap of bilayer graphene in ionic liquid", *TOKIMEKI2011*, 24-SO-8, Osaka (2011).

4) Yusuke Yamashiro, Takashi Ikuta, Yasuhide Ohno, Kenzo Maehashi, Koichi Inoue, and Kazuhiko Matsumoto, "Ionic-liquid-Gate Control of Bilayer Graphene", *International Conference on Nanoscience + Technology 2012*, 947, Paris (2012).

[Poster]

1) Yusuke Yamashiro, Yasuhide Ohno, Kenzo Maehashi, Koichi Inoue, and Kazuhiko Matsumoto, "Electric-field dependence of G-band spectra in bilayer graphene", *International Conference on Solid State Devices and Materials 2012*, PS-13-17, Kyoto (2012). (Late News)

5) Yusuke Yamashiro, Yasuhide Ohno, Kenzo Maehashi, Koichi Inoue, and Kazuhiko Matsumoto, "Ionic-liquid-gated bilayer graphene FETs for generating band gap", *International Workshop on Quantum Nanostructures and Nanoelectronics*, P-18, , Tokyo (2011).
6) Yusuke Yamashiro, Yasuhide Ohno, Kenzo Maehashi, Koichi Inoue, and Kazuhiko Matsumoto, "Bilayer Graphene FET with Ionic-Liquid Electrolyte", *7th Handai Nanoscience and Nanotechnology International Symposium*, PII-12, Osaka (2011).

7) Yusuke Yamashiro, Yasuhide Ohno, Kenzo Maehashi, Koichi Inoue, and Kazuhiko Matsumoto, "Electrical Field Dependence of Bilayer Graphene in Ionic-liquid", *The 15th SANKEN International Symposium 2012*, P18, Osaka (2012).

8) Yusuke Yamashiro, Masatoshi Nakamura, Yasuhide Ohno, Kenzo Maehashi, Koichi Inoue, and Kazuhiko Matsumoto, "G-band spectra of bilayer graphene with dual gate structure", *8th Handai Nanoscience and Nanotechnology International Symposium*, Osaka (2012).

9) Yusuke Fujii, Yusuke Yamashiro, Kohei Seike, Takafumi Kamimura, Yasuhide Ohno, Kenzo Maehashi, Koichi Inoue, and Kazuhiko Matsumoto, "Improvement of Retention Characteristics of Carbon Nanotube NVM", *8th Handai Nanoscience and Nanotechnology International Symposium*, Osaka (2012).

10) Takashi Ikuta, Yusuke Yamashiro, Yasuhide Ohno, Kenzo Maehashi, Koichi Inoue, and Kazuhiko Matsumoto, "Synthesis of calcium-intercalated multi-layer graphene", *8th Handai Nanoscience and Nanotechnology International Symposium*, Osaka (2012).

11) Yusuke Yamashiro, Masatoshi Nakamura, Yasuhide Ohno, Kenzo Maehashi, Koichi Inoue, and Kazuhiko Matsumoto, "G-band Spectra of Bilayer Graphene in Ionic Liquid", *The 16th SANKEN International Symposium 2012*, P54, Osaka (2013).

12) Yusuke Yamashiro, Yasuhide Ohno, Kenzo Maehashi, Koichi Inoue, and Kazuhiko Matsumoto, "Transistor Operation of Bilayer Graphene with Ionic Liquid Based Electrolyte", *MRS*, 17p-PM1-13, Kyoto (2013).

13) Yusuke Yamashiro, Yasuhide Ohno, Kenzo Maehashi, Koichi Inoue, and Kazuhiko Matsumoto, "Floating-Bridge Graphene Devices on Ionic Liquid", *26th International Microprocesses and Nanotechnology Conference*, 149, Hokkaido (2013).

Domestic Conferences

[Invited Presentations]

1) 山城祐介, 大野恭秀, 前橋兼三, 井上恒一, and 松本和彦, "Electric-field-induced band gap of bilayer graphene in ionic liquid", *第12 回関西コロキアム電子デバイスワークショップ*, Session I-2, 大阪 (2012).

[Oral Presentations]

1) 山城祐介, 大野恭秀, 前橋兼三, 井上恒一, and 松本和彦, "イオン液体から高効率電界を印加した二層グラフェンのバンドギャップ生成", *第 72 回応用物理学会学術講演会*, 31a-K-11, 山形 (2011).

2) 山城祐介, 大野恭秀, 前橋兼三, 井上恒一, and 松本和彦, "イオン液体電解質を用いた二層グラフェン FET の電界印加特性", *特定領域研究「カーボンナノチューブナノエレクトロニクス」*, P12, 東京 (2011).

3) 山城祐介, 大野恭秀, 前橋兼三, 井上恒一, and 松本和彦, "イオン液体を用いた二層グラフェンラマン分光特性の電位電界依存特性", *第 59 回応用物理学関係連合講演会*, 16a-B2-10, 東京 (2012).

4) 山城祐介, 大野恭秀, 前橋兼三, 井上恒一, and 松本和彦, "二層グラフェンにおける G バンドの電界依存性", *第 73 回応用物理学会学術講演会*, 12p-C2-14, 愛媛 (2012).

5) 山城祐介, 大野恭秀, 前橋兼三, 井上恒一, and 松本和彦, "架橋二層グラフェントランジスタのイオン液体ゲート特性 ", *第60 回応用物理学関係連合講演会*, 28a-G10-2, 神奈川 (2013).

Fellowships

1) 平成 25 年度日本学術振興会特別研究員-DC2

Scientific awards

1) 2012 IEEE EDS Kansai Chapter MFSK Award

Other

1) Cover of “J. Vac. Sci. Technol., B”, Volume 30, Issue 3 (2012)
2) The Virtual Journal of Nanoscale Science & Technology, April 30, 2012